Title

The immortality mechanism of TERT promoter mutant cancers is self-reinforcing and reversible by targeted degradation

Author

Stevers, Nicholas Oliver

Publication Date

2024

The immortality mechanism of TERT promoter mutant cancers is self-reinforcing and reversible by targeted degradation

by
Nicholas Oliver Stevers

DISSERTATION
Submitted in partial satisfaction of the requirements for degree of
DOCTOR OF PHILOSOPHY

in

Biomedical Sciences

in the

GRADUATE DIVISION
of the
UNIVERSITY OF CALIFORNIA, SAN FRANCISCO

Approved:

DocuSigned by:
William Weiss
1EF6E77D125647B...

William Weiss
Chair

DocuSigned by:
Joseph Costello
DocuSigned by:
Allan Balmain
DocuSigned by:
David Raleigh
7A381335D7C9402...

Committee Members

Dedication

Glory be to God; through You I have achieved much.

To my wife, Meredith. Being a graduate student yourself, you comprehend the journey I have faced, and the trials and tribulations involved. You have redefined the definition of love in my mind and heart. Even when times are tough, you always greet me with a smile and a heart of joy.

To my parents, my family, and friends - Thank you for your support. I could not have achieved this without you.

To my grandmother – Thank you for helping raise me and helping me become the man who I am. I wish you were here to see it.

To my mentor, my friend, and my ally through these last 6 years, the bond we have formed and the time we have had together has changed my life forever. I am endlessly thankful for all your support and all that you have taught me, Joe.

To my mentees, Olivia Lenzo, Samuel Wu, Nadia Grishanina, Yu Jin Lee, Joshua Wu, and Oli Doyle: You each hold the future of our world in your hands, and I couldn't be happier. I cannot wait to watch each of you grow as you progress along your journeys in life.

To Jay, Dan, and Darwin: Thank you for your friendship and all the fellowship we shared in. You have helped me greatly through the ups and downs of graduate school.

To Chibo: Thank you for being such a great person and for always watching out for me over these many years. You have supported me so much spiritually and emotionally. I am forever grateful that we shared these years together.

The immortality mechanism of *TERT* promoter mutant cancers is self-reinforcing and reversible by targeted degradation

Nicholas O. Stevers

Abstract

Activating mutations in the Telomerase Reverse Transcriptase (*TERT*) promoter are prevalent in cancer and enable limitless cell division characteristic of immortal cells[1-12]. Solving the immortality mechanism represents a major step towards selective reversal in cancer cells. *TERT* promoter mutations create a *de novo* E26 transformation specific (ETS) transcription factor binding motif. Here, we analyzed fifty-three cell lines representing sixteen cancer types and six recurrent *TERT*p mutations and found that the GA-binding protein (GABP) tetramer is responsible for promoter activation in all cases, extending prior studies on a few cancers and two hotspot mutations. Surprisingly, *TERT* expression is maintained after tetramer depletion. Further investigation revealed an underlying network of auto-suppression, the release from which drives *TERT* maintenance via upregulated GABP dimers or a paralogous tetramer. To target all three complexes, we used AlphaFold2 to design a biological proteolysis-targeting chimera to specifically degrade GABPA protein. *TERT* expression was abolished in a promoter mutation-specific manner, shortening telomeres and improving survival in a GBM xenograft model. The GABPB1L tetramer is, therefore, a pan-cancer, pan-mutation activator of the mutant *TERT* promoter, but it is replaceable. Domains shared by the three GABP complexes, rather than solely the B1L tetramer, are mutation-specific vulnerabilities.

Table of Contents

List of Figures

List of Tables

Chapter 1: Introduction

Tumor cells can achieve replicative immortality through reactivation of telomerase reverse transcriptase (*TERT*)[1-6,13]. A heterozygous point mutation in the *TERT* promoter reactivates *TERT* expression to overcome the strict limits on cellular lifespan[7,9]. In the absence of *TERT* activation, activated oncogenes drive cells into senescence or death instead of producing tumors. *TERT* promoter mutations are the most common non-coding mutation in cancer, and *TERT* is the third most mutated gene behind *TP53* and *RAS*[7,10,11]. The exceptionally high frequency of the mutations underscores a potentially strong selective pressure for their acquisition in the earliest stages of tumor evolution[14].

Understanding how the promoter mutations lead to *TERT* reactivation and immortality is a central question in cancer research with major therapeutic implications[15,16]. However, a cadre of regulators of the mutant *TERT* promoter have been proposed or predicted. The two hotspot mutations generate identical *de novo* E26 transformation specific (ETS) transcription factor binding motifs largely shared by the 28 family members[7,10,12]. If multiple ETS factors are the main regulators, they could represent regulatory redundancy and hence, intractability of therapeutic targeting[17,18]. In silico, 23 to 25 of the ETS factors are predicted to bind the hotspot mutations[19]. Furthermore, ELF1, ELF2, ETV6[20]; ELK4, ELF4, ETV1[21]; ETS1, ETS2[17,18,22]; and GABP[20,23-32] have been shown to activate the mutant *TERT* promoter in tumor cells, albeit with different assays and in different cellular contexts. Further adding to the complexity, each promoter mutation may recruit its own unique factors[17,18]. *TERT* promoter mutations exhibit positive selection in over fifty cancer types and occur at many promoter locations[7,10,11], but their activating mechanism(s) remain unresolved.

Chapter 2: A pan-cancer and pan-mutation mechanism of *TERT* activation

2.1 Results

More than a dozen recurrent mutations have been reported throughout the *TERT* promoter, but it is not known if or how they reactivate the promoter[10,33]. Like the G228A and G250A hotspot mutations, four of the uncharacterized mutations (prevalence: T161G = 3.0-4.1%, G228T = 0.15-2.2%, GG228/229AA = 0.1-4.1%, GG242/243AA = 0.5%-5.7%) also create ETS motifs, suggesting their potential to recruit one or more of the ETS transcription factors (**Fig. 1A-B, S1A**)[10,11,33-37]. To determine if these promoter mutations activate *TERT* expression, we conducted luciferase promoter reporter assays, which revealed that each recurrent mutation stimulated promoter activity to a level comparable to the hotspot mutations (**Fig. 1C**)[11,12,23,38]. While the less frequent G242A and G243A mutations have been individually observed in a few tumors[10], neither one alone creates an ETS motif nor increases *TERT* promoter activity to a similar level as the hotspot mutations (**Fig. S1B**). In contrast, the ETS motif created by the GG242/243AA double mutation significantly increased promoter activity. Each of these mutations therefore shares a feature with the hotspot mutations: the critical need for a *de novo* ETS site to reactivate *TERT* expression (**Fig. 1C**).

Twenty-four members of the ETS transcription factors bind sequences like those created by the six mutations we tested[39]. However, 8 are not consistently expressed across tumor samples or cell lines from cancer types that acquire *TERT* promoter mutations. In contrast, GABPA and GABPB1 are among the widely expressed ETS factors (**Fig. S1C-D**)[40-43]. GABP is the only multimeric ETS factor, requiring a heterodimer or heterotetramer form composed of the DNA-binding GABPA and the transactivating GABPB. GABPB is encoded by either *GABPB1* (*B1*)—expressed as a dimer forming

GABPB1S (*B1S*) and tetramer forming *GABPB1L* (*B1L*)—or its paralogue *GABPB2* (*B2*)[26,27,42,44-54]. All six recurrent mutations are positioned roughly full helical turns from the native ETS-195 site or overlapping ETS-200 site, a required configuration for recruitment of the GABP tetramer to the hotspot mutant *TERT* promoter in glioblastoma (GBM) (**Fig. 1B**)[23,24]. The ETS factor expression pattern and the spacing of the native and *de novo* ETS motifs shared among the six mutations suggest a mechanistic convergence on the GABP tetramer for *TERT* promoter activation. In support of this hypothesis, abolishing the native ETS motifs reduced the activity of each mutant *TERT* promoter to near wildtype levels (**Fig. 1C**), suggesting both ETS sites are necessary. Furthermore, knockdown of *GABPA* abrogated the increased promoter activity for all six mutations in both the bladder cancer and GBM cells with little to no effect on wildtype promoter activity (**Fig. 1D, S1E**). Therefore, the increased promoter activity of all six mutations is GABP-dependent, in two different epigenetic and genetic backgrounds.

These observations and the inferred strong positive selection for ETS site-generating mutations across dozens of cancers led us to ask whether GABP plays a universal role in the immortality of *TERT* promoter mutant cancers. Knockdown alone cannot distinguish between direct and indirect effects. Therefore, we first tested for direct effects by assessing GABP recruitment. We conducted a total of 212 independent chromatin immunoprecipitation (ChIP) reactions on 53 cancer cell lines representing 16 cancer types and all six mutations. GABPA was enriched at the *TERT* promoter in all mutant cell lines, whereas *TERT* promoter wildtype cell lines exhibited little to no enrichment (**Fig. 1E, S1F**). Furthermore, sequencing of the GABPA-immunoprecipitated

DNA revealed GABPA selectively bound to the mutant promoter in all cases, highlighting consistent cancer cell specificity across cancer types (**Fig. S1G**).

The pan-cancer GABPA occupancy could be opportunistic due to chromatin made accessible by another factor, or it may be required for *TERT* expression. To resolve these possibilities and determine which GABPA transactivation partner is involved, we examined *TERT* expression following knockdown of *GABPA*, *B1*, or *B2* in 38 cancer cell lines with mutant *TERT* promoter specific GABPA occupancy, yielding a total of 456 knockdowns and 4560 gene expression measurements. *GABPA* knockdown reduced *TERT* expression significantly—75% reduction on average—in 37 of the 38 cell lines (**Fig. 1F, S1H, S2A, table 1**) representing the six mutations (**Fig. S2B**). Knockdown of *B1*, which includes the tetramer-forming B1L and dimer-restricted B1S isoforms, significantly reduced *TERT* by 63% on average, in 33 of the 38 lines (**Fig. S2C, table 1**), whereas knockdown of the dimer and tetramer competent *B2* modestly reduced *TERT* by 40% on average, in 11 of the 38 cell lines (**Fig. S2D, table 1**).

In summary, we observe remarkably consistent and mutation-selective binding of GABPA across diverse cancer and mutation types (**Fig. 1E**), a shared positional configuration of the six recurrent *TERT* promoter mutations relative to the native ETS sites (**Fig. 1B**), requirement for both the native and *de novo* ETS sites for promoter activity (**Fig. 1C**), and dependence on GABPA and B1 for mutant promoter activation (**Fig. 1D-F, S2C**). Together these data suggest B1L tetramers may mediate a pan-cancer and pan-mutation mechanism of mutant *TERT* promoter activation, the rate-limiting step in converting cells with a finite lifespan to an immortal state.

2.2 Main Figures

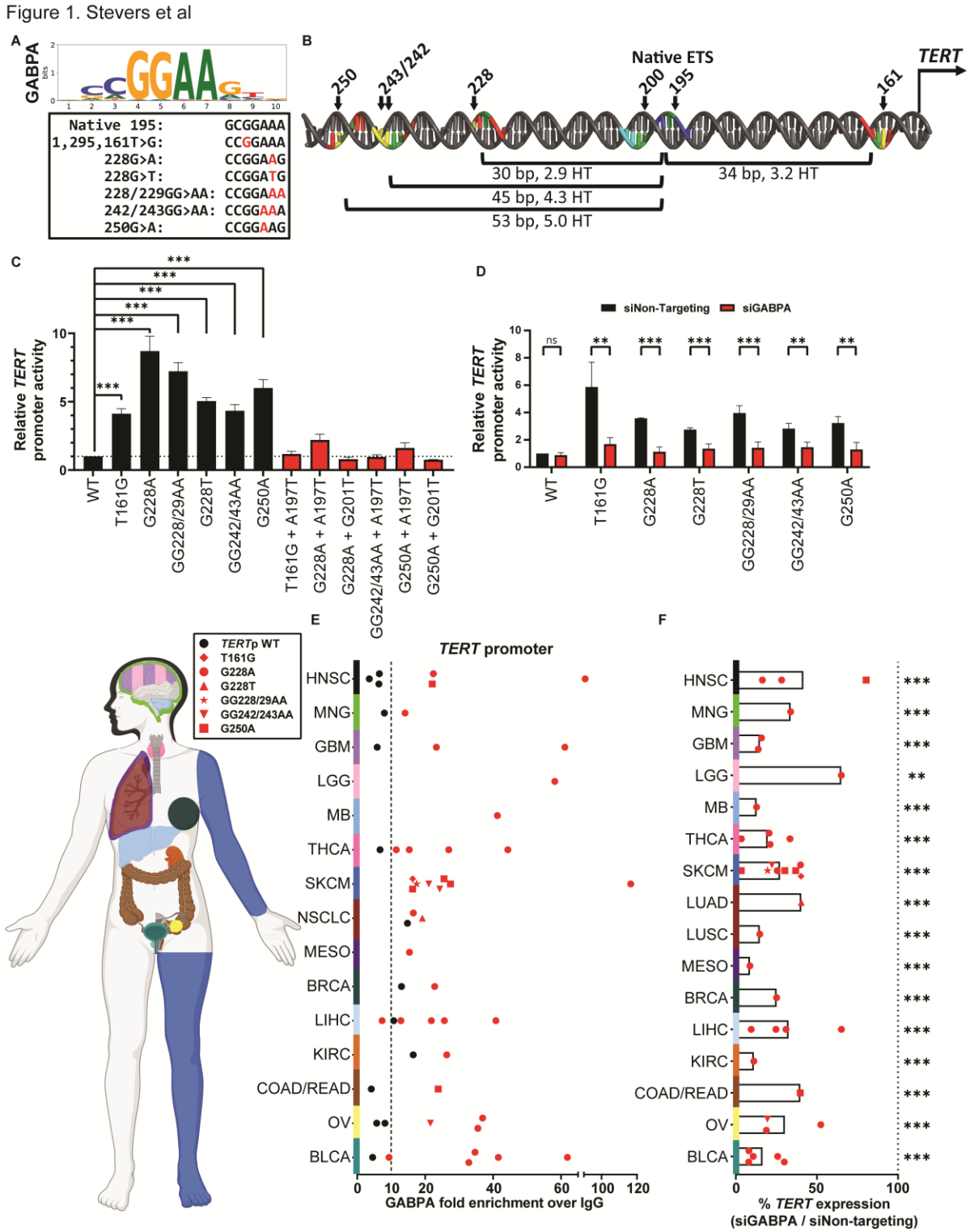

Fig. 1. A GABP tetramer regulates the mutant *TERT* promoter in 16 cancer types and six different mutations. (Figure caption continued on the next page.)

(Figure caption continued from the previous page.)

A. (Top) Sequence logo of GABPA binding motif learned by the convolutional neural network (CNN) trained to classify GABPA chromatin immunoprecipitation sequencing (ChIP-seq) peak regions in the *TERT* promoter mutant A-375 melanoma cell line (Methods). (Bottom) The six most common ETS motif-generating *TERT* promoter mutations in cancer and their nucleotide position (hg19 coordinates).
B. The *TERT* promoter showing the position of common *de novo* ETS motif-generating mutations (yellow) and the distance between each *de novo* ETS and the stronger of the two native ETS motifs (ETS-195) in base pairs and helical turns (HT), calculated from the center (GG|AA) of the respective ETS motifs. Yellow = mutation, red = *de novo* ETS motif, green = GG of each ETS motif, cyan = native 200 ETS motif, and blue = native 195 ETS motif. Figure created in PyMOL.
C. Activity of each mutant *TERT* promoter relative to the wildtype promoter in bladder cancer cells (UM-UC-3). Native ETS 195 or 200 were abolished with mutation of A197T or G201T respectively and effect on each *TERT* promoter variant measured (red bars). Results are a mean + standard deviation (SD) of three independent experiments.
D. Wildtype or mutant *TERT* promoter activity following siRNA-mediated GABPA knockdown in UM-UC-3 cells. Results are a mean + SD of four independent experiments.
E. GABPA occupancy at the *TERT* promoter in a total of 53 *TERT* promoter wildtype (black) and *TERT* promoter mutant (red) cell lines by quantitative ChIP-qPCR. Each dot represents one cell line. Data from 212 ChIP reactions and 636 PCR reactions are presented. Results from the two Immunoglobulin G (IgG) or two GABPA antibodies were averaged, and GABPA fold enrichment over IgG at the *TERT* promoter was calculated. A 10-fold or greater enrichment of GABPA IP signal over IgG negative control was considered enriched. BLCA = Bladder Urothelial Carcinoma; GBM = Glioblastoma multiforme; LGG = Brain Lower Grade Glioma; THCA = Thyroid carcinoma; SKCM = Skin Cutaneous Melanoma; LIHC = Liver hepatocellular carcinoma; HNSC = Head and Neck squamous cell carcinoma; KIRC = Kidney renal clear cell carcinoma; MB = Medulloblastoma; OV = Ovarian serous cystadenocarcinoma; MESO = Mesothelioma; NSCLC = LUAD (Lung adenocarcinoma) and LUSC (Lung squamous cell carcinoma); COAD/READ = Colon adenocarcinoma/Rectum adenocarcinoma; BRCA = Breast invasive carcinoma; MNG = Meningioma.
F. *TERT* expression following siRNA-mediated knockdown of *GABPA* in the 38 *TERT* promoter mutant cell lines. For each cell line, *TERT* expression is normalized to *GUSB* expression and plotted relative to siNon-Targeting control. Each point represents one cell line tested in biological triplicate.

(C-D), Two-tailed, unpaired Student's *t*-test. (F), Linear mixed-effects model. **P* < 0.05, ***P* < 0.01, ****P* < 0.001, ns, no significance.

2.3 Supplemental Figures

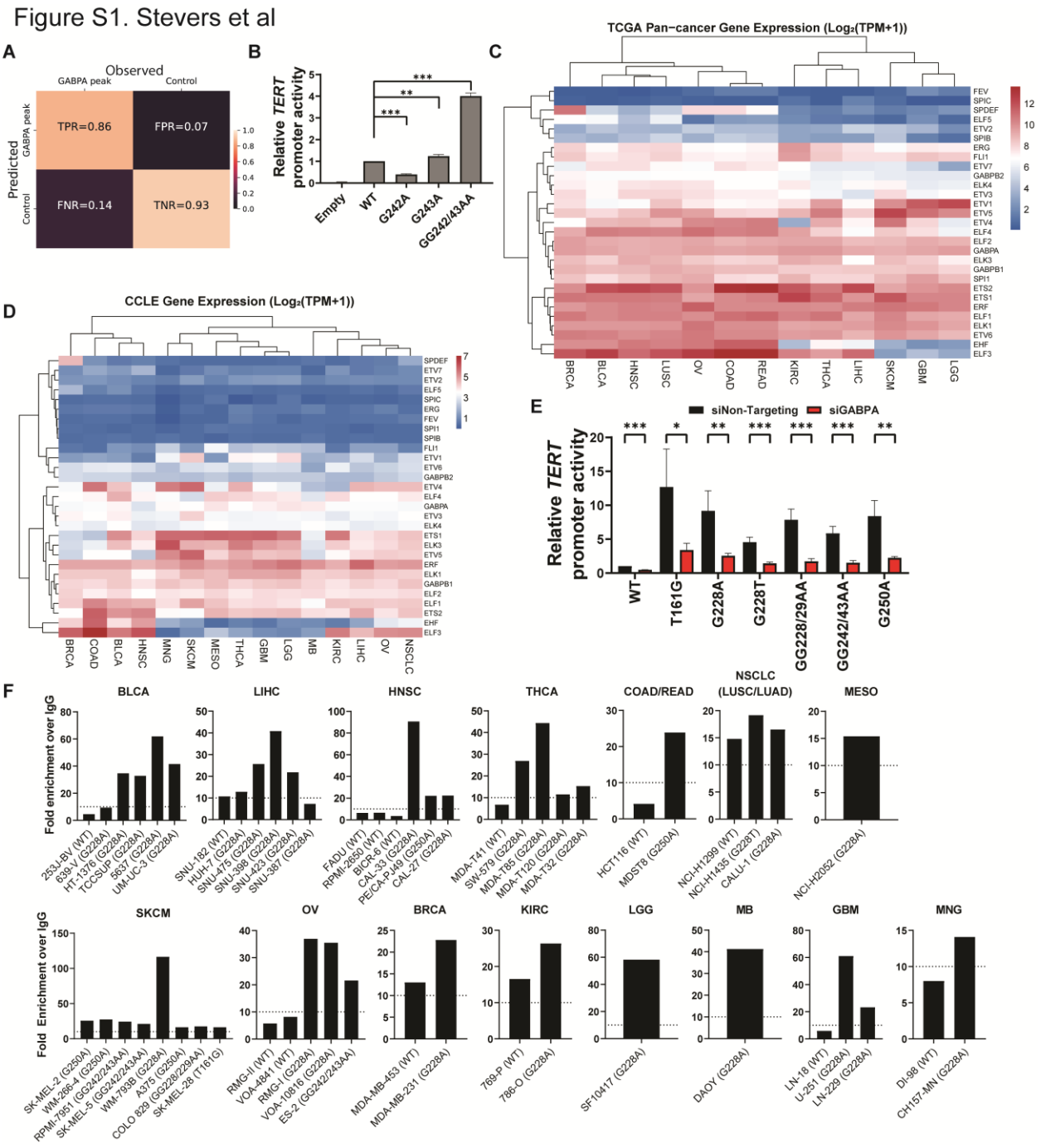

Fig. S1. GABP binding to the *TERT* promoter is mutant allele specific in 16 cancer types.

Figure S1 cont. Stevers et al

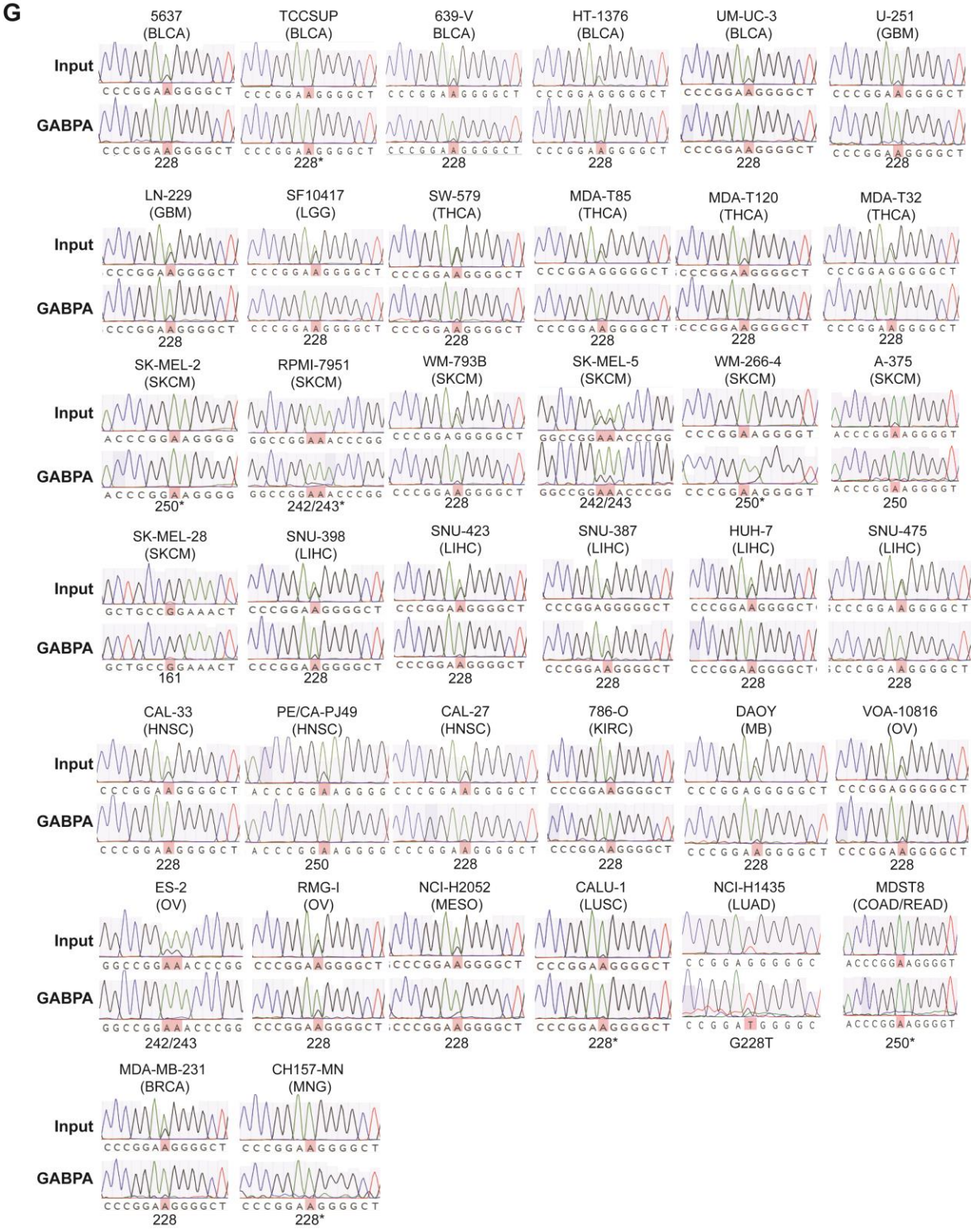

Fig. S1 (cont). GABP binding to the *TERT* promoter is mutant allele specific in 16 cancer types.

Figure S1 cont. Stevers et al

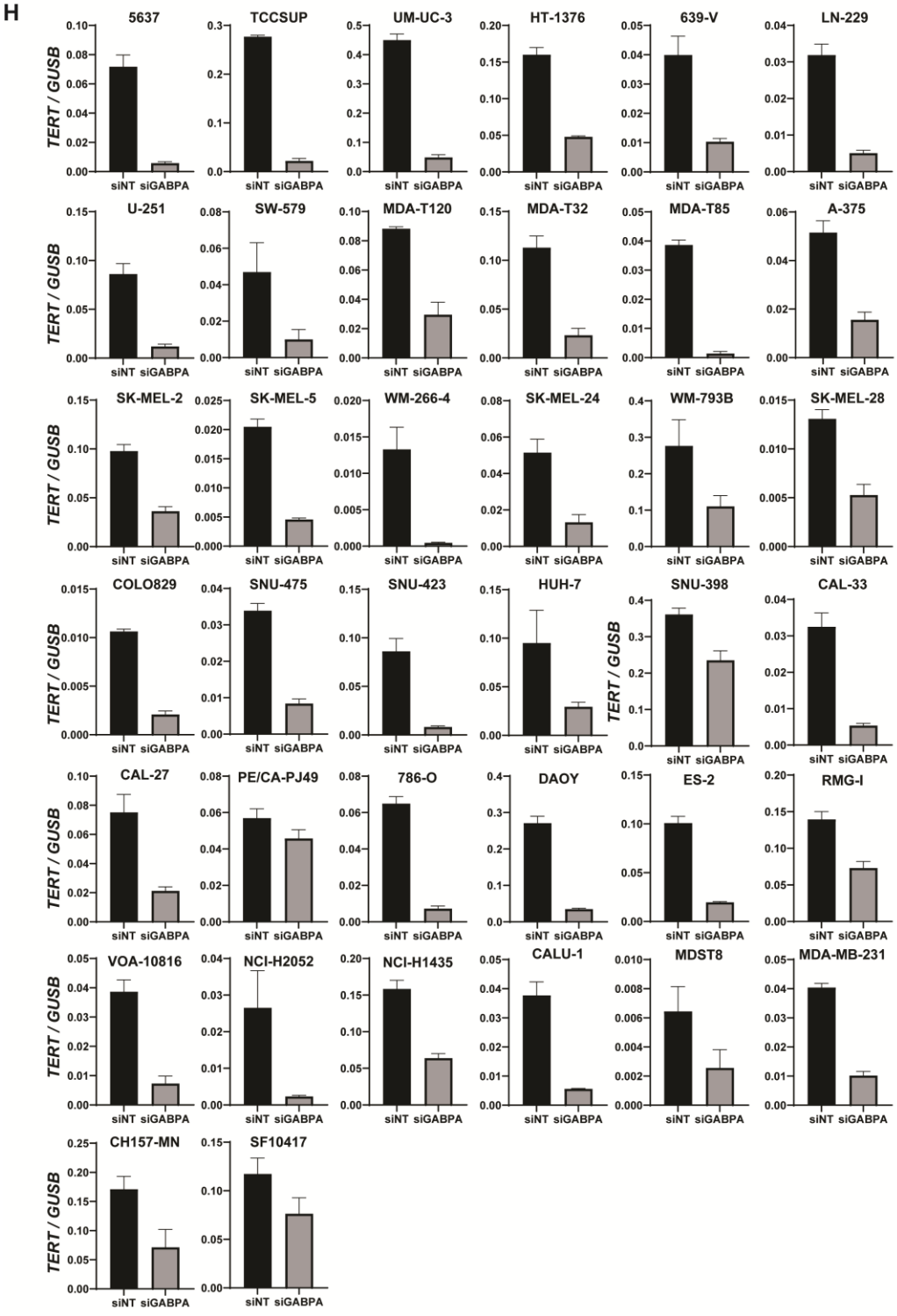

Fig. S1 (cont). GABP binding to the *TERT* promoter is mutant allele specific in 16 cancer types. (Figure caption continued on the next page.)

(Figure caption continued from the previous page.)

A. Confusion matrix for the CNN's prediction of GABPA binding regions on a test set. The test set consisted of 303 sequences from GABPA ChIP-seq peaks and corresponding 303 negative control sequences constructed by randomly permuting the nucleotides in each peak sequence. TPR: true positive rate, FPR: false positive rate, FNR: False negative rate, TNR: true negative rate. The overall accuracy of the CNN on the test set was 89.6% (Methods).
B. Effect of G242A or G243A single mutations or GG242/243AA double mutation on *TERT* promoter reporter activity in UM-UC-3 bladder cancer cells. The results are a mean + SD of three independent experiments.
C. Heat map of ETS transcription factor expression in tumor samples from different cancer types (data sourced from The Cancer Genome Atlas (TCGA)).
D. Heat map of ETS transcription factor expression in cancer cell lines from different cancer types (data sourced from the Cancer Cell Line Encyclopedia (CCLE)).
E. Wildtype or mutant *TERT* promoter activity following siRNA-mediated GABPA knockdown in LN-229 (GBM) cells. Results are a mean + SD of four independent experiments.
F. ChIP-qPCR results from **Figure 1E** presented by cancer type and by cell line.
G. ChIP-PCR Sanger sequencing of the *TERT* promoter in the *TERT* promoter mutant cell lines from the pan-cancer ChIP-qPCR. Cell line names are listed above their respective traces and results are shown with the Sanger trace for the input sample above the Sanger trace for the respective GABPA ChIP sample. Across cancers there are interesting trends in *TERT* promoter allelic ratios. Amongst the G228A cell lines: 10 cell lines had more mutant than wildtype alleles, 3 cell lines had no wildtype alleles, 1 cell line had more wildtype than mutant alleles, and 13 cell lines had an approximately equal number of mutant and wildtype alleles. Amongst the G250A cell lines: 1 cell line had more mutant than wildtype alleles and 3 cell lines had no wildtype alleles. Amongst the GG242/243AA cell lines: 1 cell line had more mutant than wildtype alleles, 1 cell line had no wildtype alleles, and 1 cell line had an approximately equal number of mutant and wildtype alleles. The T161G cell line (SK-MEL-28) did not have a detectable wildtype allele. * = Cell lines with homozygous *TERT* promoter mutation status (as determined by Sanger sequencing performed on *TERT* promoter PCR products generated from gDNA)
H. Individual *TERT* expression following siRNA-mediated knockdown of *GABPA* in the 38 *TERT* promoter mutant cell lines representing 16 cancer types and six different mutations. For each cell line, *TERT* expression is normalized to *GUSB* expression and plotted relative to siNon-Targeting control. Each one cell line tested in biological triplicate.

(B, E), Two-tailed, unpaired Student's *t*-test. *$P < 0.05$, **$P < 0.01$, ***$P < 0.001$, ns, no significance.

Figure S2. Stevers et al

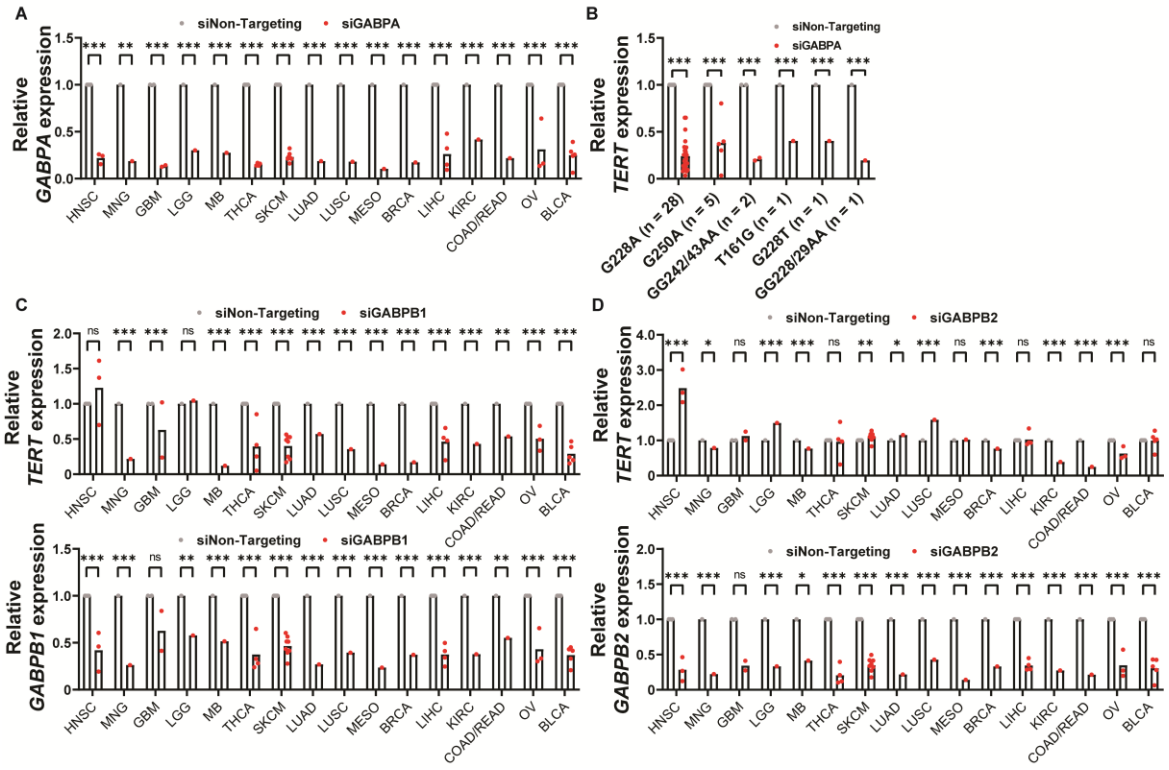

Fig. S2. The B1L tetramer activates the mutant *TERT* promoter across 16 cancers.

A. *GABPA* expression following siRNA-mediated knockdown of *GABPA* in the 38 *TERT* promoter mutant cell lines representing 16 cancer types. Each point represents one cell line tested in biological triplicate.

B. *TERT* expression following siRNA-mediated *GABPA* knockdown in the 38 *TERT* promoter mutant cell lines, with data presented by location of the mutation in the *TERT* promoter. Each point represents one cell line tested in biological triplicate.

C. *TERT* (top) and *B1* (bottom) expression following siRNA-mediated knockdown of *B1* in the 38 *TERT* promoter mutant cell lines representing 16 cancer types. Each point represents one cell line tested in biological triplicate.

D. *TERT* (top) and *B2* (bottom) expression following siRNA-mediated knockdown of *B2* in the 38 *TERT* promoter mutant cell lines representing 16 cancer types. Each point represents one cell line in biological triplicate.

E. mRNA level validation of the LN-229, UM-UC-3, and A-375 B1LKO CRISPR clones via RT-qPCR. *B1L* expression is normalized to *GUSB* expression.

F. *B1L* expression in UM-UC-3, A-375, and LN-229 with stable integration of a mirE-based shRNA targeting controls, *B1L*, or *B1S*.

G. *B1S* and *B2* expression in cells with stable integration of a mirE-based shRNA targeting controls or *B1S*.

(A-D), Linear mixed-effects model. (F-G), Two-tailed, unpaired Student's *t*-test. **P* < 0.05, ***P* < 0.01, ****P* < 0.001, ns, no significance. (A-D) For each cell line, target gene expression is normalized to *GUSB* expression and plotted relative to siNon-Targeting control. (F-G) target gene expression is normalized to *GUSB* expression and presented as a mean where each point represents an independent shRNA.

Chapter 3: *TERT* expression is maintained by alternative GABP complexes in the absence of the GABPB1L tetramer

3.1 Results

Given prior results in GBM[24], the B1L tetramer occupancy of the mutant *TERT* promoter across 16 cancers (**Fig. 1**), the consistent spacing of the *de novo* and native ETS sites, and decreased *TERT* in GABPA and B1 knockdowns, we expected the tetramer subunit B1L would be necessary to maintain *TERT* expression. A total of 40 clonal CRISPR-Cas9-mediated knockouts were generated, comprised of 16 control clones and 24 *B1L* tetramer knockout clones in the three cancer types that most frequently acquire *TERT* promoter mutations[55]. Unexpectedly, *TERT* expression was not consistently decreased in *B1L* knockout compared to control clones (**Fig. 2A, S3A**)[56]. The notable clone-to-clone fluctuations in *TERT* expression level may reflect heterogeneity within tumor cell populations[57]. Given the variable effect on *TERT* expression in the complete *B1L* knockout clones, yet highly consistent *TERT* reduction in the *GABPA* and *B1* short-term knockdown experiments in nearly all *TERT* promoter mutant cell lines, we explored these potentially discordant results in depth. We generated 36 cultures by transducing cancer cells from three cancer types, each with twelve different microRNA-adapted short hairpin RNAs (shRNA-mir) constructs, four selectively targeting *B1L* (**Fig. S3B**), *B1S* (**Fig. S3C**), and four negative controls. While *TERT* expression was modestly reduced in the GBM cell line (**Fig. 2B**), consistent with our prior results in this line[24,27], *TERT* was again maintained in bladder cancer and melanoma cells despite strongly reduced *B1L* expression (**Fig. 2B**).

In these experiments, *TERT* expression may have been reduced initially but then rapidly rebounded, as the knockdown and knockout approaches required days or weeks, respectively, of selection and growth. Therefore, we developed isoform-specific, transient

knockdown tools to examine *TERT* regulation more immediately following B1L reduction. To create a splice switching antisense oligonucleotide (ASO) to inhibit *B1L* production we investigated the mechanism controlling isoform generation for *B1*. First, we determined that *B1* isoforms are regulated by alternative polyadenylation (**Fig. S4A-C**), not alternative splicing as previously speculated[49,58,59]. Exploiting this knowledge, we designed a splice-switching ASO to prevent *B1L* production by enforcing early polyadenylation (**Fig. 2C**). Treatment of GBM cells with the ASO resulted in a dose-dependent reduction of B1L, a conspicuous and significant increase in B1S (**Fig. 2D**), but with *TERT* expression largely unaffected (**Fig. 2E**). Treatment of three cell lines with either this ASO or a derivative showed similar results including the significant increase in *B1S* (**Fig. 2F, S4D**).

This was surprising considering our prior study[24] showing that an mRNA-degrading gapmer ASO (UTR1) targeting *B1L* reduced *TERT* expression but, interestingly, did not increase *B1S.* At that time, this data led us to conclude that UTR1 was selective for B1L and that B1L tetramers were, therefore, necessary for mutant *TERT*p activation. However, the consistent *B1S* upregulation after B1L knockdown by B1L-ASO1, B1L-ASO2, and shRNAs, and after knockout prompted us to reassess this subunit following UTR1 treatment. We first confirmed *B1L* and *TERT* reduction with UTR1 (**Fig. S4E**)[24]. In contrast to the *B1L* knockout and multiple knockdown approaches reported here, UTR1 does not increase *B1S* (**Fig. S4E**), which may explain why UTR1 is the only B1L perturbation that uniquely reduces *TERT* expression. Indeed, while B1L-ASO1 reduces *TERT* when combined with shB1S, UTR1 does not (**Fig. S4F**), presumably because *B1S* is already reduced by UTR1. Following this logic, we reasoned that UTR1 reduces both *B1L* and *B1S* mRNA and found an imperfect UTR1 binding sequence in exon 7 shared

by *B1L* and *B1S* (**Fig. S4G-I**). In agreement with this prediction, UTR1 decreases *B1S* mRNA in a *B1L* knockout cell line (**Fig. S4J**). These new results demonstrate consistency across the multiple knockdown approaches here and from our prior study and show that UTR1 is equivalent to B1 knockdown and not specific for B1L as we previously thought.

One possibility is that alternative GABP complexes maintain *TERT* activation in the absence of B1L. In agreement, simultaneous knockdown of B1L tetramers and B1S dimers reduced *TERT* in 97% of the *TERT* promoter mutant cell lines (**Fig. S2C, table 1**). Knockdown of GABPA, which is common to all three GABP complexes, also consistently reduced *TERT* mRNA (**Fig. 1F**). Collectively, these data support a revised model whereby B1S dimers, and conceivably B2 tetramers (**Fig. S2D, table 1**), maintain *TERT* activation in the absence of B1L tetramers. Importantly, *B1S*, not *B2*, was significantly upregulated in *B1L* knockout (**Fig. 2G**) and *B1S* was upregulated more consistently and to a much greater extent than *B2* in knockdown cells (**Fig. 2H**). While B1L tetramers are present, reduction of B1S dimers and B2 tetramers does not consistently decrease *TERT* expression (**Fig. 2B, S2D**); however, in the absence of B1L, their increased expression may enable binding to and activation of the mutant *TERT* promoter (**Fig. 3A**). In fact, GABPA occupancy of the *TERT* promoter shows little change in *B1L* knockout cells (**Fig. 3B**). These data suggest a potentially critical contribution of B1S upregulation for *TERT* maintenance in the absence of B1L. In support, knockdown of *B1S*, but not *B2*, in B1L knockout clones consistently and significantly reduced *TERT* expression (**Fig. 3C**). To further test this hypothesis, we generated 8 clonal knockouts of *B1* from exon 2 to exon 9 in bladder cancer and melanoma cells (**Fig. S5A-D**). Such a large deletion has the potential to collaterally remove unannotated coding or regulatory elements within this

locus, so we additionally generated 18 clonal knockouts of the second exon of *B1*, which contains the translation start site (**Fig. S5B-D**). *TERT* expression was reduced in *B1* knockouts in *TERT* promoter mutant but not wildtype cells, strongly supporting that targeting total B1 is necessary to reduce *TERT* because B1S maintains *TERT* in the absence of B1L (**Fig. 3D**).

To more widely explore how the transcriptional program of cancer cells is affected by *B1* knockout, we conducted RNA sequencing. *TERT* was among the top 3% of downregulated genes, and *B2* was among the top 3% of upregulated genes in both melanoma (**Fig. 3E, S5D**) and bladder cancer cells (**Fig. 3F**). Knockdown of *GABPA* or *B1* also significantly increased *B2* in 33 and 34 of the 38 cancer cell lines, respectively (**Fig. S5E, table 1**). Notably, the increase of *B2* expression was greater in bladder compared to the melanoma cells, which we verified via RT-qPCR (**Fig. 3G**). The greater *B2* upregulation and residual *TERT* expression in these bladder cancer cells suggests intriguing additional complexity, with upregulated B2 tetramers potentially weakly activating the mutant *TERT* promoter in the absence of B1S dimers and B1L tetramers (**Fig. 3A, F, G**). Knockdown of either *GABPA* or *B2* in the *B1* knockout bladder cancer cells reduced *TERT* expression approximately 50% beyond the already significantly reduced state (**Fig. 3D, H**). These data suggest that if B2 tetramers are sufficiently upregulated they can maintain a minimal level of *TERT* expression in the absence of the B1L tetramer and B1S dimer.

In summary, *B1S* is robustly upregulated upon *B1L* targeting, and *B2* is modestly upregulated after total *B1* targeting. These results suggest tiered occupation and activation of the mutant *TERT* promoter entirely by GABP complexes with seemingly little

or no involvement of other ETS family members. Furthermore, because the B1S and B2 upregulations are rapid, the replacement mechanism is likely intrinsic rather than adaptive. Previous work demonstrated that B1L knockdown by the mRNA degrading gapmer, UTR1, was sufficient to decrease *TERT* expression, however, UTR1 targets both B1L and B1S. While B1L KD or KO alone is insufficient to reduce *TERT* expression, total B1 knockout is sufficient to decrease *TERT* expression, replicating the results of prior GABPA[23] and total B1[24] KD. Taken together with our prior data, the data presented here reveals a consistent relationship between B1S upregulation and *TERT* maintenance. These were the first clues to understanding why B1L is not essential to maintain *TERT* as previously thought, and what replaces it at the mutant *TERT*p.

3.2 Main Figures

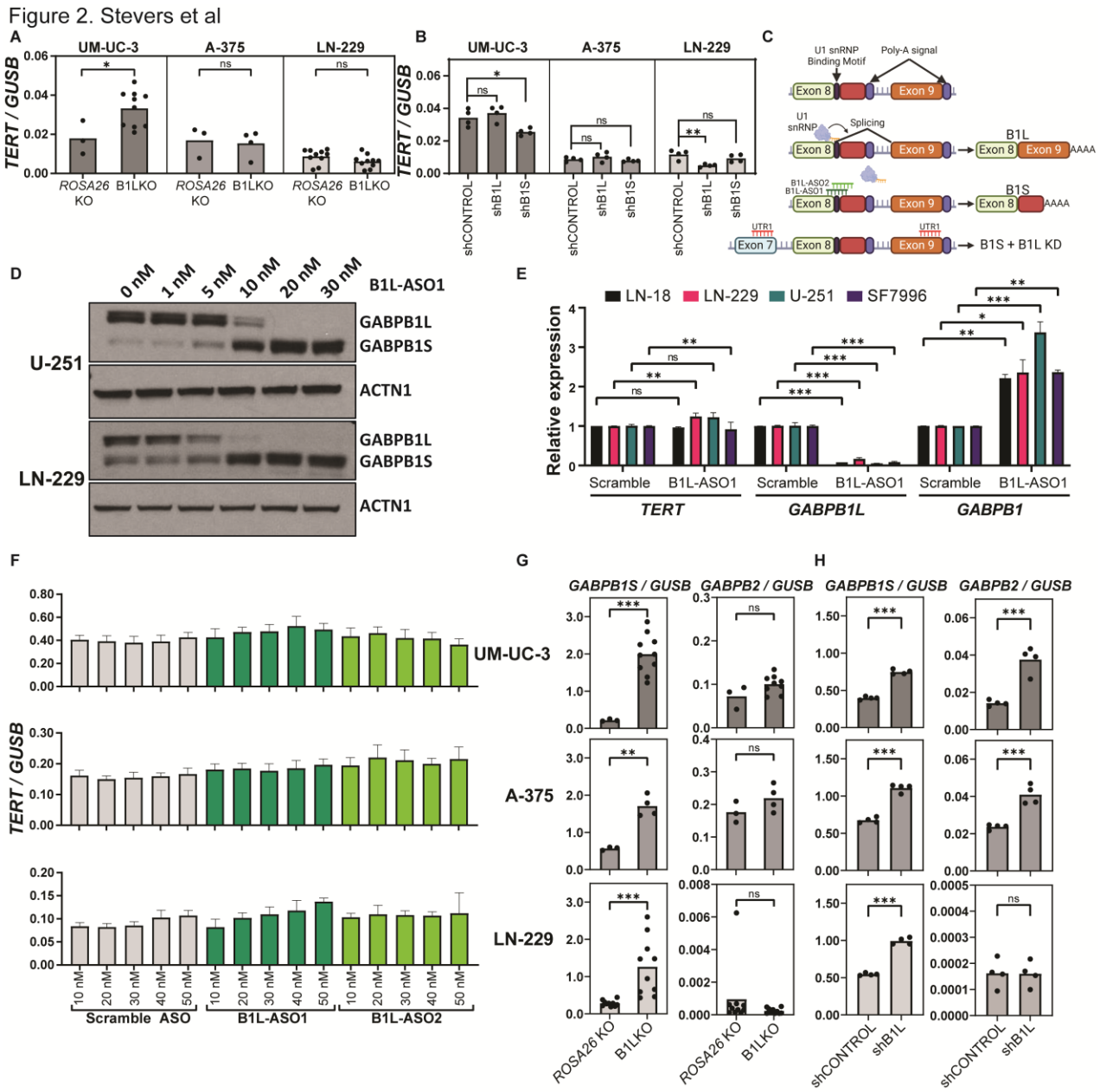

Fig. 2. *TERT* expression is unperturbed by *B1L* tetramer targeting.

A. *TERT* expression in control (*ROSA26*) and B1L knockout (B1LKO) clones in UM-UC-3 (bladder cancer), A-375 (melanoma), and LN-229 (GBM). *TERT* expression presented as a mean where each point represents an independent knockout clone.

(Figure caption continued on the next page.)

(Figure caption continued from the previous page.)

B. *TERT* expression in cells with stable integration of a mirE-based shRNA system targeting negative controls (shPPP1R12C-1, shPPP1R12C-2, shFirefly, shRenilla), *B1L* (shB1L-6, shB1L-7, shB1L-9, shB1L-10), or *B1S* (shB1S-2, shB1S-3, shB1S-4, shB1S-8). *TERT* expression presented as a mean where each point represents an independent shRNA.

C. B1L-ASO1 and derivative ASO2 bind the *B1L* producing splice site, enforcing *B1S* production by inducing early polyadenylation. RNAse-H activating UTR1 binds to both exon 7 and 9, inducing degradation of *B1S* and *B1L* encoding mRNA.

D. Immunoblot analysis of the effects of different B1L-ASO1 concentrations on B1L and B1S protein levels in U-251 and LN-229 72 hours post transfection. Alpha-Actinin (ACTN1) is the loading control.

E. Relative gene expression in *TERT* promoter wildtype (LN-18) and mutant (LN-229, U-251, and SF7996) GBM cell lines treated with 30 nM scramble ASO or B1L-ASO1 for 72 hours. Results are a mean + SD of at least two independent experiments.

F. *TERT* expression with increasing doses of scramble ASO, B1L-ASO1, or B1L-ASO2 at the indicated concentration. Results are a mean + SD of at least two biological replicates.

G. *B1S* and *B2* expression in control and B1LKO clones in UM-UC-3, A-375, and LN-229. Target gene expression presented as a mean where each point represents an independent knockout clone.

H. *B1S* and *B2* expression in cells with stable integration of a mirE-based shRNA targeting four different negative controls or *B1L*. Target gene expression presented as a mean where each point represents an independent shRNA.

(A-B, E, G-H), Two-tailed, unpaired Student's *t*-test. **P* < 0.05, ***P* < 0.01, ****P* < 0.001, ns, no significance.

Figure 3. Stevers et al

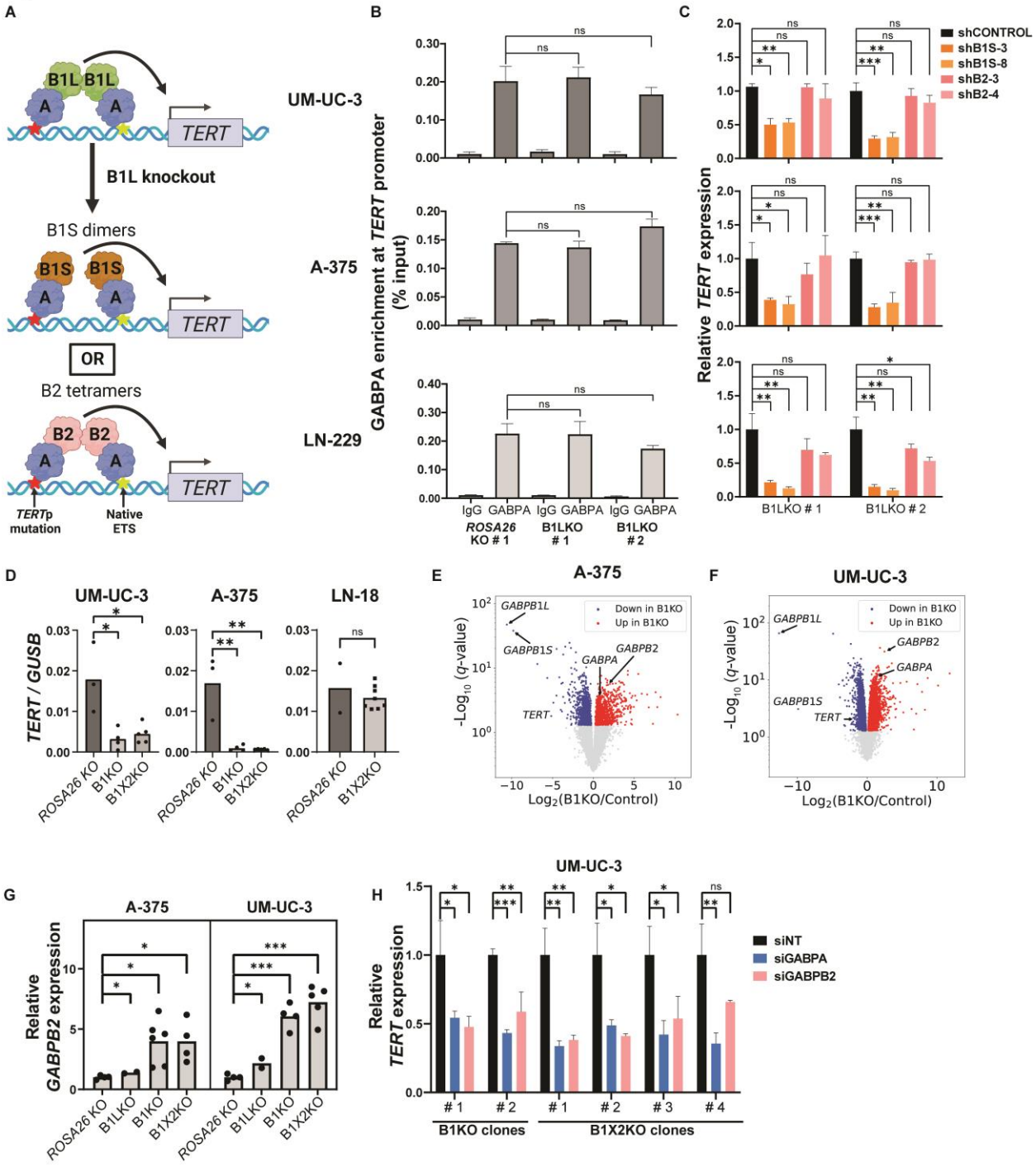

Fig. 3. Other GABP complexes drive *TERT* expression in the absence of B1L tetramers. (Figure caption continued on the next page.)

(Figure caption continued from the previous page.)

A. B1L tetramer regulation of the mutant *TERT* promoter (top) and the hypothetical binding of alternative GABP complexes, B1S dimers (middle) and B2 tetramers (bottom), in the absence of the B1L tetramer.
B. GABPA occupancy at the *TERT* promoter in control knockout or B1LKO clones. Each clone was subjected to ChIP for IgG or GABPA. The results are a mean + SD of three independent experiments.
C. *TERT* expression in B1LKO clones transduced with two independent mirE-based shRNAs targeting a negative control, *B1S* (shB1S-3, shB1S-8), or *B2* (shB2-3, shB2-4). The results are a mean + SD of at least two independent experiments, with *TERT* expression normalized to *GUSB* expression and plotted relative to shCONTROL (shPPP1R12C-1).
D. *TERT* expression in control knockout, B1KO (exon 2 through 9), and B1X2KO (exon 2 only) clones in UM-UC-3, A-375, and LN-18. *TERT* expression presented as a mean where each point represents an independent knockout clone.
E. Differential expression between B1KO and control samples in the A-375 cell line. Significantly differential expressed genes at a *q*-value threshold of 0.05 are shown in red and blue.
F. Same as in (E), but for the UM-UC-3 cell line.
G. Effect of B1LKO, B1KO, or B1X2KO on *B2* expression. *B2* expression is normalized to *GUSB* expression and presented as a mean relative to control knockouts, where each point represents an independent knockout clone.
H. Effect of *GABPA* or *B2* knockdown (KD) on *TERT* expression in the UM-UC-3 B1X2KO clones. *TERT* expression normalized to *GUSB* expression and plotted relative to siNon-targeting control. Results are a mean + SD of three biological replicates.

(B-D, G-H), Two-tailed, unpaired Student's *t*-test. **P* < 0.05, ***P* < 0.01, ****P* < 0.001, ns, no significance.

3.3 Supplemental Figures

Figure S3. Stevers et al

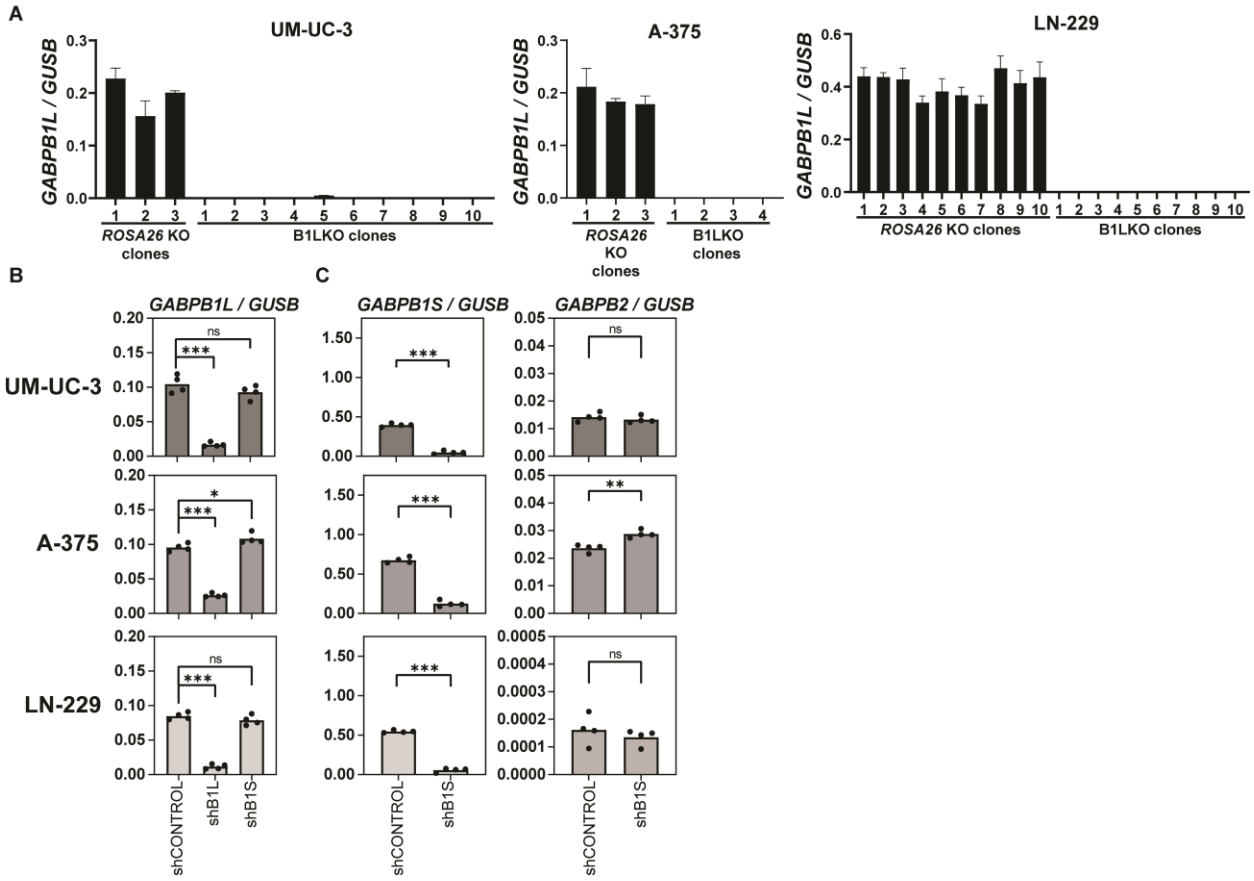

Fig. S3. Characterization of B1L knockouts and knockdowns.

A. mRNA level validation of the LN-229, UM-UC-3, and A-375 B1LKO CRISPR clones via RT-qPCR. *B1L* expression is normalized to *GUSB* expression.

B. *B1L* expression in UM-UC-3, A-375, and LN-229 with stable integration of a mirE-based shRNA targeting controls, *B1L*, or *B1S*.

C. *B1S* and *B2* expression in cells with stable integration of a mirE-based shRNA targeting controls or *B1S*.

(B-C), Two-tailed, unpaired Student's *t*-test. **P* < 0.05, ***P* < 0.01, ****P* < 0.001, ns, no significance. (B-C) target gene expression is normalized to *GUSB* expression and presented as a mean where each point represents an independent shRNA.

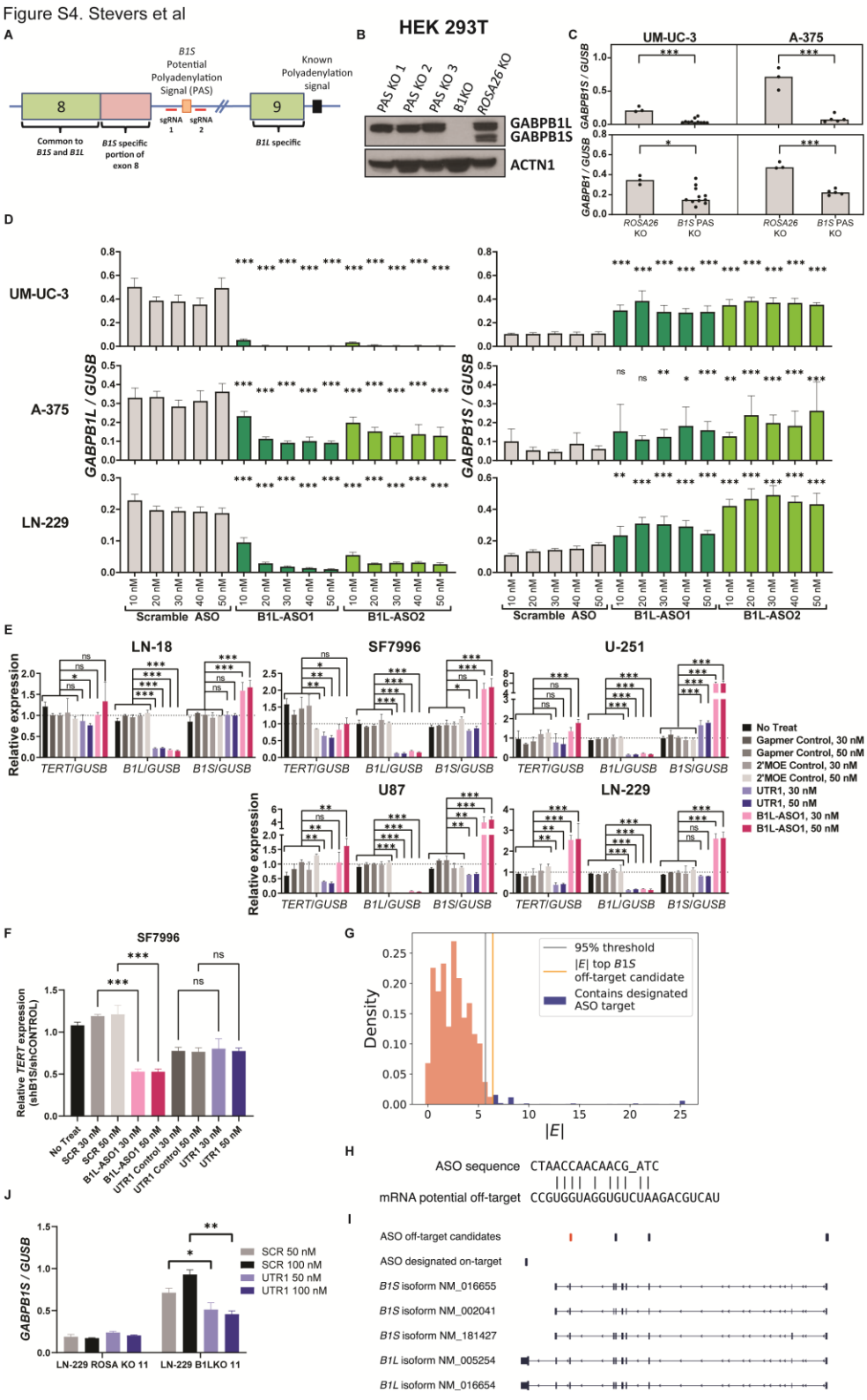

Fig. S4. Alternative polyadenylation produces the two isoforms of the *B1* transcript and can be targeted by ASOs designed to selectively reduce production of the B1L isoform. (Figure caption continued on the next page.)

(Figure caption continued from the previous page.)

A. Diagram of *B1*, region of exon 8 and exon 9.
B. Immunoblot showing the levels of B1S and B1L protein in HEK 293T cells with CRISPR-Cas9 engineering to knockout the polyadenylation sequence for *B1S*, exons 2 through 9 of *B1,* or a control knockout clone. ACTN1 serves as the loading control.
C. *B1S* (top) and *B1* (bottom) mRNA expression in A-375 and UM-UC-3 cells with the *B1S* polyadenylation sequence knockout (*B1S* PAS KO). Total *B1* and *B1S* expression are normalized to *GUSB* expression and presented as a mean where each point represents an independent knockout clone.
D. *B1L* (left) and *B1S* (right) expression in UM-UC-3, A-375, LN-229 cells treated with scramble ASO, B1L-ASO1, or B1L-ASO2 at the indicated final concentration. *B1L* and *B1S* expression are normalized to *GUSB* expression. Results are a mean + SD of at least two biological replicates. Two-tailed, unpaired Student's *t*-test applied to compare the B1L targeting treatments to control treatments.
E. Treatment of *TERT* promoter mutant (SF7996, U-251, LN-229, U-251) and *TERT* promoter wildtype (LN-18) GBM cell lines with the LNA-gapmer type ASOs (Gapmer Control or UTR1 used in Mancini et al, 2018) and the 2'-MOE based splice-switching ASOs (2'MOE Control or B1L-ASO1). Results are a mean + SD of at three biological replicates. *TERT*, *B1L*, and *B1S* expression are normalized to *GUSB* expression and values presented relative to controls. Two-tailed, unpaired Student's *t*-test applied to compare each of the B1L targeting treatments (UTR1 or B1L-ASO1) to control treatments (No treat, ASO control 1, and ASO control 2).
F. B1L-ASO1 reduces *TERT* expression in SF7996 cells stably expressing a mirE-based shRNA targeting *B1S*, but UTR1 does not. Results are a mean + SD of three biological replicates.
G. Histogram of the absolute value of predicted optimal hybridization energies $|E|$ of UTR1 to 25 bp sliding windows in the *B1* isoforms. The grey vertical line represents the threshold for the upper 5% of the empirical distribution of $|E|$, and the orange vertical line represents the window containing the top UTR1 off-target sequence with the largest $|E|$ among all windows in *B1S* isoforms (Methods). The blue bars represent the windows containing a portion of the designated UTR1 on-target site.
H. Computed optimal hybridization of UTR1 and the top candidate mRNA off-target site (**Figure S4G**). The vertical lines between the two sequences represent Watson-Crick base pairs, and the horizontal dash represents a gap in the alignment between UTR1 and its complementary mRNA.
I. Locations of the UTR1 on-target and candidate off-target sites (**Figure S4G**) in *B1S* isoforms NM_002041, NM_016655, and NM_181427. The orange bar denotes the top candidate off-target site.
J. *B1S* expression decreases in B1LKO cells following UTR1 treatment. Results are a mean + SD of at least two biological replicates.

(C-F, J), Two-tailed, unpaired Student's *t*-test. **P* < 0.05, ***P* < 0.01, ****P* < 0.001, ns, no significance.

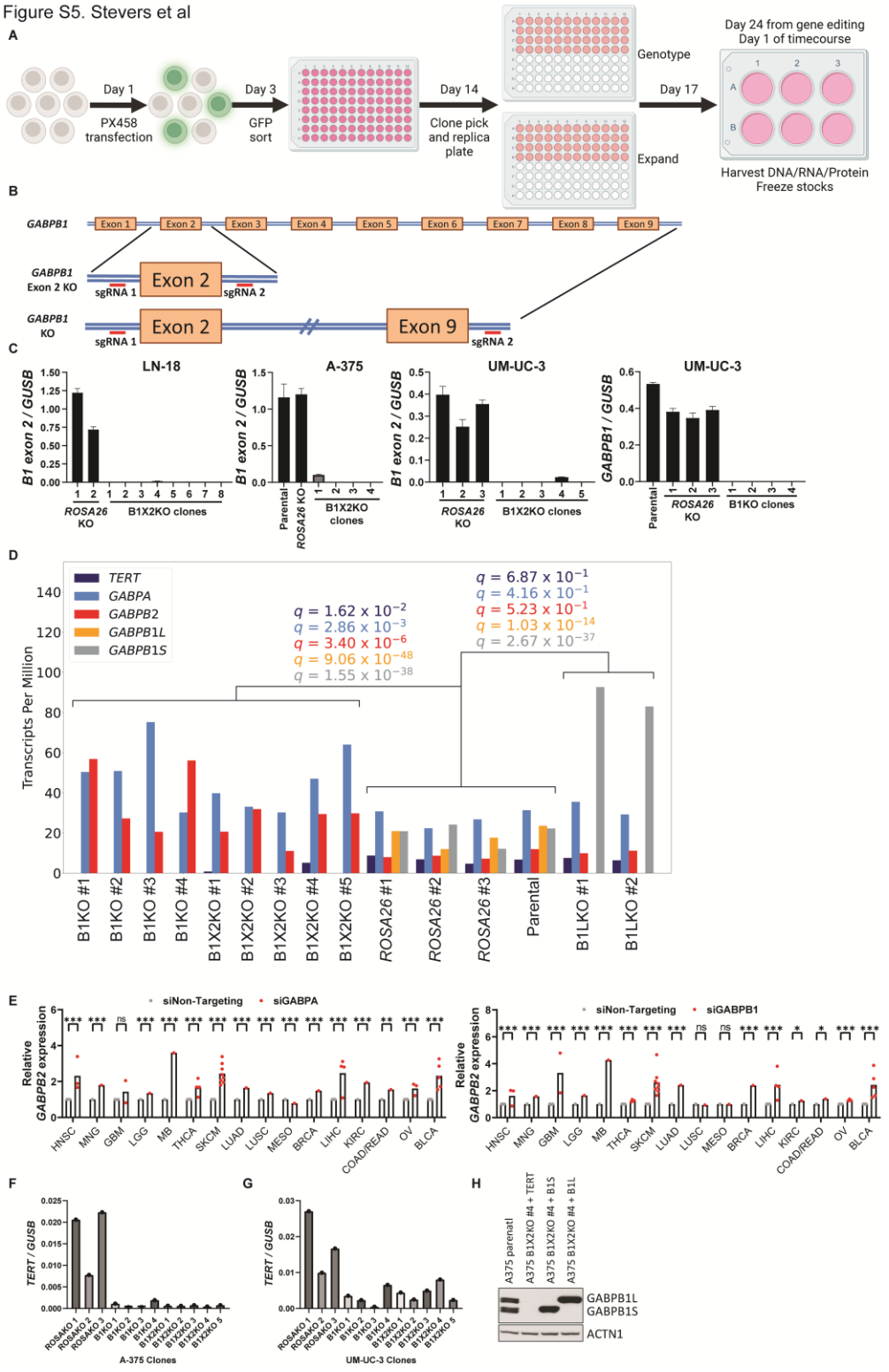

Fig. S5. Generation of CRISPR-Cas9 mediated *B1* knockout clones and *B2* upregulation following *B1* knockdown or knockout. (Figure caption continued on the next page.)

(Figure caption continued from the previous page.)

A. Diagram of the CRISPR knockout clone generation pipeline, from transfection of plasmids (day 1) to single cell sorting (day 3) to replica plating (day 14) and clone genotyping (day 17) through expansion and population doubling time course start (day 24, day 1 of time course).
B. Diagram of the two strategies for CRISPR-Cas9-mediated knock out of *B1*, either through targeted deletion of exon 2 (top) or deletion of *B1* from exon 2 to exon 9 (bottom).
C. mRNA level validation of the LN-18 B1X2KO, A-375 B1X2KO, UM-UC-3 B1X2KO, and UM-UC-3 B1KO CRISPR clones via RT-qPCR for the target of the knockout.
D. Transcription levels from RNA-seq. The leftmost, middle, and rightmost brackets represent the samples corresponding to A-375 *B1* knockout (B1KO and B1X2KO), controls (parental and ROSA26 knockouts), and B1LKO groups, respectively. Gene-wise *q*-values for differential expression relative to the control group are shown for the B1KO and B1LKO groups (Methods).
E. *B2* expression following siRNA-mediated knockdown of *GABPA* (left) or *B1* (right) in the 38 *TERT* promoter mutant cell lines representing 16 cancer types. For each cell line, *B2* expression is normalized to *GUSB* expression and plotted relative to siNon-Targeting control. Each point represents one cell line tested in biological triplicate.
F. *TERT* expression for each A-375 B1KO and B1X2KO clone.
G. *TERT* expression for each UM-UC-3 B1KO and B1X2KO clone.
H. Immunoblot analysis of the rescues of A-375 B1X2KO clone #4 compared to A-375 parental.

(E), Linear mixed-effects model. **P* < 0.05, ***P* < 0.01, ****P* < 0.001, ns, no significance.

Chapter 4: Release from negative feedback protects *TERT*

4.1 Results

Given the redundancy of ETS factor binding motifs, it is not clear why only GABP complexes play a role at the mutant *TERT* promoter. Understanding the mechanism of B1S and B2 upregulation may offer clues. *B1S* upregulation may be due to shunting of transcript production from both *B1S* and *B1L* to *B1S* only, or to an increase in *B1* transcription. The increase in total *B1* mRNA following *B1L* reduction suggested the latter possibility (**Fig. 2E**). GABP complexes possess transcriptionally activating and repressing functions depending on the promoter[60,61]. *B1* promoter activity increased following B1L knockout (**Fig. 4A**), suggesting the tetramer could be suppressing the *B1* promoter. In direct support, first we found that GABPA is bound to the *B1* promoter (**Fig. S6A-B**). The strongest GABPA occupancy occurs in a nucleosome-depleted region of the *B1* promoter and is lost upon knockout of the start codon containing second exon of *B1* (**Fig. S6C**). GABPA occupancy is conserved across individuals and cancer types (**Fig. 4B**). Second, total *B1* expression was significantly upregulated in the *TERT* promoter mutant cell lines following *GABPA* knockdown (**Fig. 4C-D, table 1**). Additionally, *B1L* knockout increased *B1* expression (**Fig. 4E**) and decreased GABPA occupancy at the *B1* promoter (**Fig. 4F**). Third, if B1L tetramers mediate a negative feedback loop, then targeting B1S dimers should not increase *B1* transcription. Indeed, reduction or elimination of B1S dimers decreased total *B1* expression (**Fig. S6D, S4C**). Fourth, GABPA occupancy of the *B1* promoter is restored by reintroducing B1L, but not B1S (**Fig. 4G**). Fifth, overexpression of *B1L* repressed B1S expression in GBM (**Fig. 4H, S6E**), melanoma, and bladder cancer cells (**Fig. 4I**). Sixth, inducible expression of *B1L* revealed a dose-dependent regulation over a brief timescale (**Fig. S6F-G**), whereas subsequent knockdown of GABPA

abrogated the *B1* promoter repression and increased B1S expression (**Fig. 4H-I**). These multi-level data solidly reveal the negative feedback loop whereby B1L tetramer occupancy causes *B1* promoter suppression.

Like B1S upregulation, *B2* upregulation following *B1* knockout may also be due to disengagement of a GABP-mediated repression. GABPA is in fact bound to the *B2* promoter in a nucleosome-free region in parental cells and occupancy is lost upon *B1* knockout (**Fig. S6H**). In distinction from the B1L tetramer-specific suppression of the *B1* promoter, reintroduction of either B1S dimers or B1L tetramers reduced *B2* expression to control levels (**Fig. 4J**). These data reveal a second conserved negative feedback loop underlying replacement of the B1L tetramer at the mutant *TERT* promoter, thereby protecting this widely utilized tumor cell immortality mechanism.

4.2 Main Figures

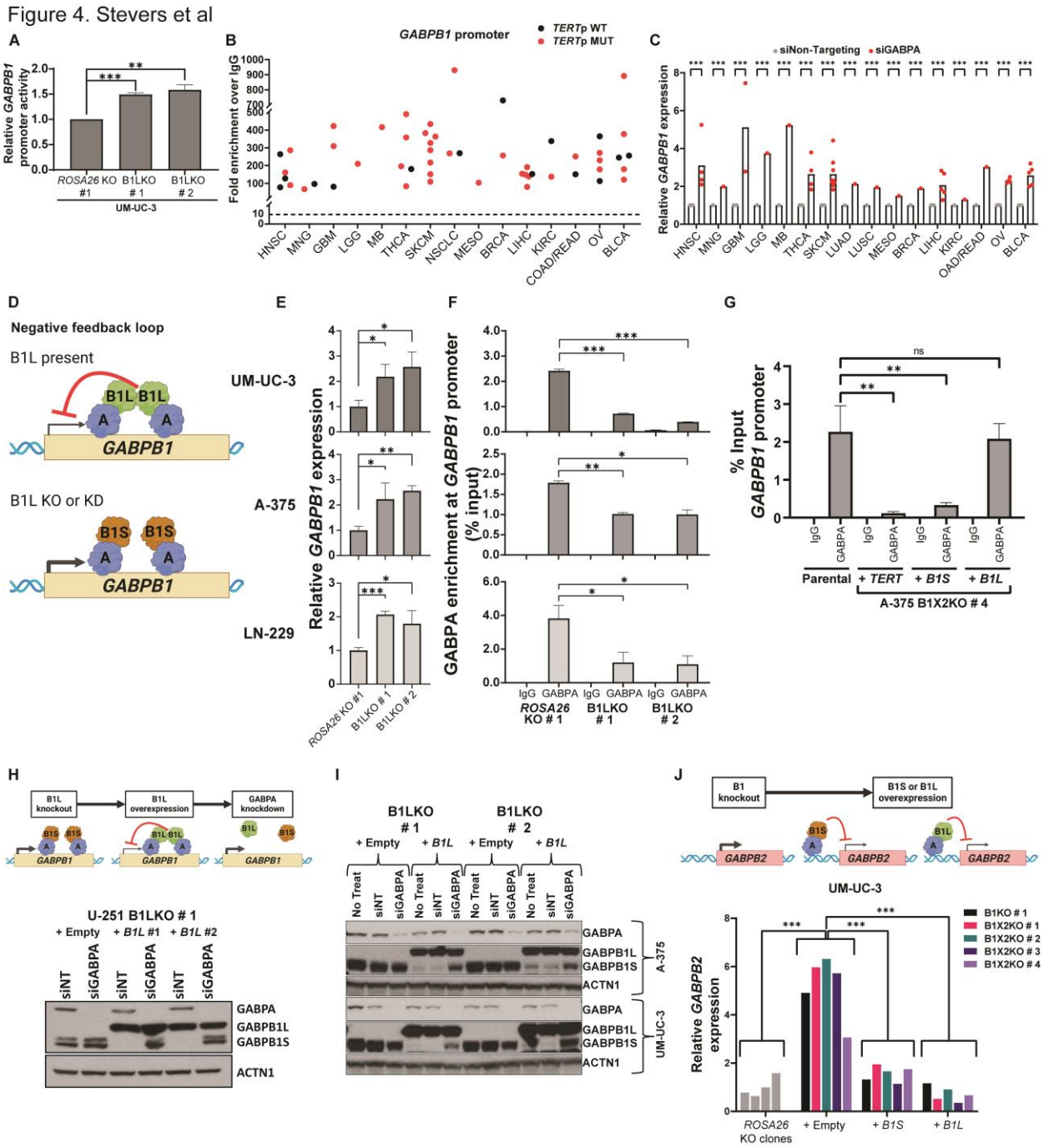

Fig. 4. Disengagement of GABP-mediated negative feedback loops upregulates GABP subunits. (Figure caption continued on the next page.)

(Figure caption continued from the previous page.)

A. *B1* promoter activity in control knockout or B1LKO UM-UC-3 cells 48 hours after transfection. Results are a mean + SD of four independent experiments, and within each experiment, the *B1* promoter activity of each B1LKO was normalized to control knockout cells before averaging over all experiments.
B. GABPA occupancy at the *B1* promoter in 14 *TERT* promoter wildtype (black) and 39 *TERT* promoter mutant (red) cell lines determined by ChIP-qPCR. Each point represents an independent cell line. ChIP was conducted with two IgG and two GABPA antibodies per cell line. Results from the two IgG or two GABPA antibodies were averaged, and GABPA fold-enrichment over IgG at the *B1* promoter was calculated. A 10-fold or greater enrichment of GABPA IP signal over IgG negative control was considered enriched.
C. *B1* expression following siRNA-mediated knockdown of GABPA in 38 *TERT* promoter mutant cell lines from 16 cancer types. For each cell line, *B1* expression is normalized to *GUSB* expression and plotted relative to siNon-Targeting control. Each point represents one cell line tested in biological triplicate.
D. Diagram of the proposed *B1* negative feedback loop.
E. Effect of B1LKO on total *B1* expression relative to control knockout in 3 cell lines. *B1* expression normalized to *GUSB* expression and plotted relative to control knockout value. The results are a mean + SD of two or three independent experiments.
F. GABPA occupancy at the *B1* promoter in control knockout or B1LKO clones in 3 cell lines. Each clone was subjected to ChIP for IgG or GABPA. The results are a mean + SD of two independent experiments.
G. GABPA occupancy of the *B1* promoter in A-375 parental cells or an A-375 B1X2KO clone with stable integration of *TERT*, *B1S*, or *B1L*. The results are a mean + SD of at least two independent experiments.
H. (Top) Diagram of experiment and proposed hypothesis. (Bottom) Immunoblot of B1S and B1L expression in a U-251 B1LKO clone with stable integration of an empty vector or *B1L* (#1 and #2 are independent transductions of the *B1L* expression construct) that was treated with siNon-targeting or siGABPA.
I. Immunoblot of two B1LKO clones each for A-375 and UM-UC-3 that have stable integration of an empty vector or *B1L* that was untreated or treated with siNon-targeting or siGABPA.
J. Effect of B1S or B1L overexpression on *B2* expression in B1KO UM-UC-3 cells. *B2* expression normalized to *GUSB* expression and plotted relative to control knockout values.

(A, E-G, J), Two-tailed, unpaired Student's *t*-test. (C), Linear mixed-effects model. **P* < 0.05, ***P* < 0.01, ****P* < 0.001, ns, no significance.

4.3 Supplemental Figures

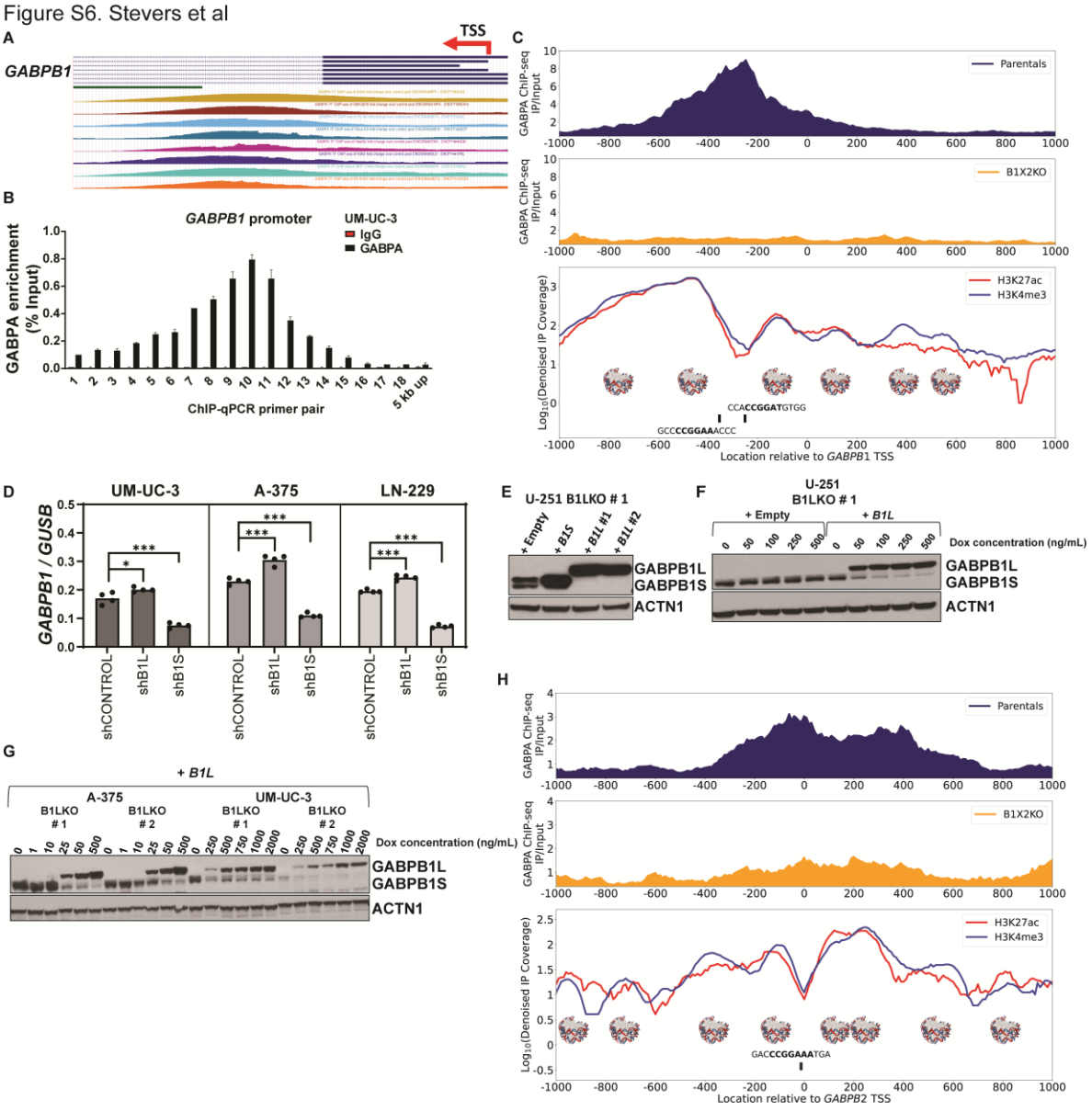

Fig. S6. GABP negatively regulates the *B1* and *B2* promoters via direct binding. (Figure caption continued on the next page.)

(Figure caption continued from the previous page.)

A. Encyclopedia of DNA Elements (ENCODE) GABPA ChIP-seq data showing GABPA enrichment at the *B1* promoter.
B. Quantitative ChIP-qPCR tiled throughout the *B1* promoter in the parental UM-UC-3 cell line. ChIP was conducted using either an IgG control or GABPA antibody. Primer pairs numbered 1 through 18 are tiled from left (3' of *B1* exon 1) to right (body of *B1* exon 1) as shown in subfigure A.
C. GABPA binds nucleosome-free linker DNA in the *B1* promoter. GABPA ChIP-seq data in A-375 cells are shown for parental (top) and the *TERT* rescued B1X2KO clone 4 (middle). IP and input samples were individually normalized by total sequencing depth before calculating the fold change. Nucleosome occupancy was inferred from denoised histone modification ChIP-seq data in the bottom panel (Methods). Bars represent the GABPA binding motifs within the ChIP-seq peak. Nucleosome images were taken from the Protein Data Bank (PDB) with image ID 6JR1.
D. Total *B1* expression in cell lines with stable integration of a mirE-based shRNA targeting controls, *B1L*, or *B1S*. *B1* expression is normalized to *GUSB* expression and presented as a mean where each point represents an independent shRNA.
E. Immunoblot of B1S and B1L expression in a U-251 B1LKO clone following transduction and stable expression of ectopic B1S or B1L (*B1L* #1 and *B1L* #2 are independent transductions of the *B1L* expression construct).
F. Immunoblot of one B1LKO clone for U-251 that has stable integration of a doxycycline inducible expression vector of *B1L*. Cells were treated with the stated doxycycline concentration for 48 hours and lysates collected.
G. Immunoblot of two separate B1LKO clones for A-375 and UM-UC-3 that have stable integration of a doxycycline inducible expression vector of *B1L*. Cells were treated with the stated doxycycline concentration for 48 hours and lysates collected.
H. GABPA binds nucleosome-free linker DNA in the *B2* promoter. GABPA ChIP-seq data in A-375 cells are shown for parental (top) and the *TERT* rescued B1X2KO clone 4 (middle). IP and input samples were individually normalized by total sequencing depth before calculating the fold change. Nucleosome occupancy was inferred from denoised histone modification ChIP-seq data in the bottom panel (Methods). Bars represent the GABPA binding motifs within the ChIP-seq peak. Nucleosome images were taken from the Protein Data Bank (PDB) with image ID 6JR1.

(D), Two-tailed, unpaired Student's *t*-test. $*P < 0.05$, $**P < 0.01$, $***P < 0.001$, ns, no significance. (E-G) ACTN1 is the loading control in this experiment.

Chapter 5: Reversing immortality phenotypes and epigenotypes

5.1 Results

The reduced *TERT* expression upon *B1* knockout in the bladder and melanoma cell lines suggests that, beyond B2 tetramers, other ETS factors cannot maintain sufficient *TERT* expression to prevent telomere shortening and enable replicative immortality. We attempted to generate *B1* knockouts in two *TERT* promoter mutant GBM cancer cell lines, U-251 and LN-229, in which we successfully generated *B1L* knockouts; however, among hundreds of clones with B1 editing, none had complete knockout. In contrast, *B1* knockout clones were readily generated from GBM cells with a wildtype *TERT* promoter, suggesting *B1* is dispensable in the *TERT* promoter wildtype, but not mutant, GBM cells. We therefore monitored the bladder cancer and melanoma *B1* knockout clones longitudinally to determine if they lose replicative immortality. Strikingly, 12 of the 14 melanoma knockout clones and 4 of the 11 bladder cancer knockout clones arrested growth within the first 24 days following genotyping (**Fig. 5A**) in agreement with time to arrest following telomerase targeting[62,63]. In stark contrast, all 8 of the *B1* knockout clones of a *TERT* promoter wildtype GBM cell line, and every *B1L* knockout clone in *TERT* promoter mutant bladder cancer, melanoma, and GBM cells expanded normally (**Fig. 5A, S7A-B**). Prior to growth arrest, each *TERT* promoter mutant *B1* knockout clone that we could assess had shortened telomeres (**Fig. 5B**).

A single melanoma *B1* knockout clone temporarily outgrew the others, although it arrested 40 days from gene editing (**Fig. 5C**). During this time course, we observed a significant number of late apoptotic cells (**Fig. S7C**), suggesting telomere shortening was associated with apoptosis[64,65]. A residual, non-expanding population of cells remained following the apoptotic phase. After an additional 20 days, most cells were senescent

(**Fig. 5D**). While senescence may be driven by telomere shortening, there were too few cells remaining to assess telomere length. During clone expansion, progressive telomere shortening was significant (**Fig. 5E**). At day 40, stable expression of *TERT* itself, or *B1L* or *B1S*—which reactivated endogenous *TERT* expression (**Fig. 5F**)—rescued the knockout clone from telomere shortening (**Fig. 5E**) and restored a population doubling rate nearly identical to the parental and control knockout cells (**Fig. 5C**). These observations, including all three rescues, were validated in a second clone with knockout of *B1* function (**Fig. S7D-J**). The apoptosis and senescence cannot be attributed entirely to dysregulation of other GABP-regulated genes, because *TERT* itself restores normal cell proliferation.

In *TERT* promoter mutant tumor cells, the wildtype allele is silenced and marked by histone H3 lysine-27 trimethylation (H3K27me3), while the mutant and transcriptionally active allele loses H3K27me3 and gains H3K4me3[23,28,66]. The expandable cultures of rescue clones offer an opportunity to investigate the consequences of GABP loss and reconstitution on the promoter regulation and epigenotype. In the absence of *B1*, GABPA occupancy significantly decreased (**Fig. S7K-L**), and the mutant promoter was remodeled to a more repressed state, gaining H3K27me3 (B1X2KO + *TERT*) (**Fig. 5G, S7M**). While reintroduction of either *B1L* or *B1S* restored GABPA occupancy (**Fig. S7N**), reactivated *TERT* expression (**Fig. 5F**), and increased *TERT* promoter H3K4me3 (**Fig. 5G**), only reintroduction of *B1L* decreased H3K27me3 (**Fig. 5G**). The original telomere length was restored or increased by all three rescues (**Fig. 5E**). In summary, B1S dimers and B1L tetramers can rescue *TERT* expression after complete *B1* elimination; however, only the tetramer restores the original epigenetically active state.

The apoptosis and senescence in the *B1* knockout cells suggest reprogramming that is specific to the *TERT* promoter mutant cancer cells. Like melanoma, the seven bladder cancer *B1* knockout clones also exhibited slowed growth and shortening telomeres (**Fig. 5H-I**), with two clones arresting growth completely. To gain insight into transcriptional changes occurring in each of these cancer types, we conducted RNA sequencing and differential gene expression analysis on the 18 *B1* knockout clones and 6 control knockout clones. Analysis of the melanoma *B1* knockout clones, including those that did and did not expand beyond day 24 post gene editing, revealed that *TERT* is among the most significantly downregulated genes (**Fig. 3D-E, S5D**). All *B1* knockout melanoma cells had significant upregulation of p53 and apoptosis pathway genes and significantly downregulated E2F target genes and G2-M checkpoint genes (**Fig. 5J; S7O-P**), suggesting the clones experienced a similar terminal phenotype. Interestingly, the bladder cancer *B1* knockout clones, which have more strongly upregulated *B2*, expressed a similar transcriptional program but with a weaker upregulation of p53 pathway genes and a greater downregulation of E2F target genes and G2-M checkpoint genes (**Fig. 5K; S7Q-R**). These results may contribute to the terminal fate differences between the *B1* knockout clones in melanoma versus bladder cancer cells.

In summary, elimination of both dimer and tetramer components can overcome the intrinsic resistance to *TERT* reduction. However, in a few cases, the paralogous tetramer component is upregulated to a level that, while not sufficient to restore original *TERT* expression levels or the original doubling rate, is sufficient to escape a terminal fate. Therefore, a strategy to reverse tumor cell immortality should simultaneously target all three GABP complexes.

5.2 Main Figures

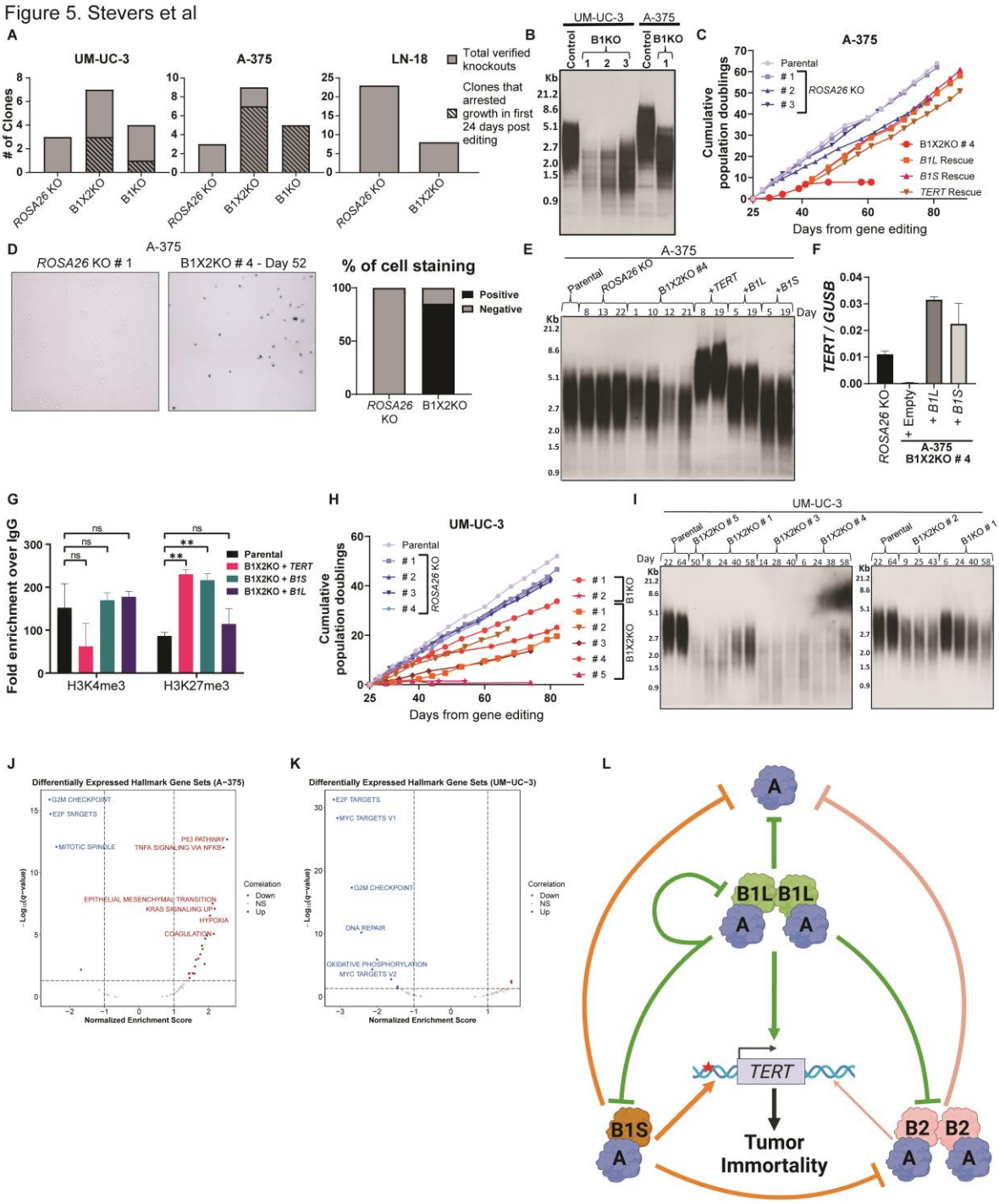

Fig. 5. Targeting total B1 restores epigenetic repression, reduces *TERT*, and shortens telomeres, leading to cancer cell death or senescence. (Figure caption continued on the next page.)

(Figure caption continued from the previous page.)

A. Knockout clones were monitored from time of genotyping and their capability to expand past day 24 post editing was recorded.
B. Terminal restriction fragment analysis (TRF) assay conducted on parental cells (control) and B1KO clones for UM-UC-3 and A-375 at 30-34 days after genotyping.
C. Population doublings of A-375 parental cells, control knockout clones, and B1X2KO clone 4. Recording began at 24 days post gene editing. Nearing 40 days post gene editing, the B1X2KO clone started undergoing catastrophic phenotypes. The growth rate of the B1X2KO clone was restored to parental levels with ectopic expression of B1S, B1L, or TERT.
D. Senescence was assessed through senescence associated Beta-Galactosidase staining of the A-375 B1X2KO clone 4 at day 52 and an A-375 control knockout clone. Images of a representative field (left) with quantification and average staining indicated for 10 fields (right).
E. Time course analysis of telomere length (TRF assay) of A-375 parental cells and A-375 B1X2KO clone 4 with or without rescues. Timepoints for rescued cells indicate number of days from rescue.
F. *TERT* expression in A-375 B1X2KO clone 4 stably transduced with empty vector, *B1L*, or *B1S* as compared to a control knockout clone. *TERT* expression is normalized to *GUSB* expression.
G. *TERT* promoter epigenetic state in A-375 parental and B1X2KO clone 4 with each rescue. Results are mean + SD of two independent experiments.
H. Population doublings of UM-UC-3 *B1* knockout clones, control knockout clones, and the parental cell line. Recording began at 24 days post gene editing.
I. Time course analysis of telomere length (TRF assay) of UM-UC-3 parental cells and B1X2KO clones.
J. Top differentially expressed Hallmark gene sets from gene set enrichment analysis comparing all A-375 *B1* knockout cells (9 clones) to controls (parental and 3 *ROSA26* KO). Gene sets with a q-value < 0.05 and an absolute normalized enrichment score > 1 are colored and those with an absolute normalized enrichment score > 2 are labeled.
K. Top differentially expressed Hallmark gene sets from gene set enrichment analysis comparing all UM-UC-3 *B1* knockout cells (9 clones) to controls (parental and 3 *ROSA26* KO). Gene sets with a q-value < 0.05 and an absolute normalized enrichment score > 1 are colored and those with an absolute normalized enrichment score > 2 are labeled.
L. A proposed model of negatively autoregulating GABP complexes and their relative activation level of the mutant *TERT* promoter.

(G), Two-tailed, unpaired Student's *t*-test. **P* < 0.05, ***P* < 0.01, ****P* < 0.001, ns, no significance.

5.3 Supplemental Figures

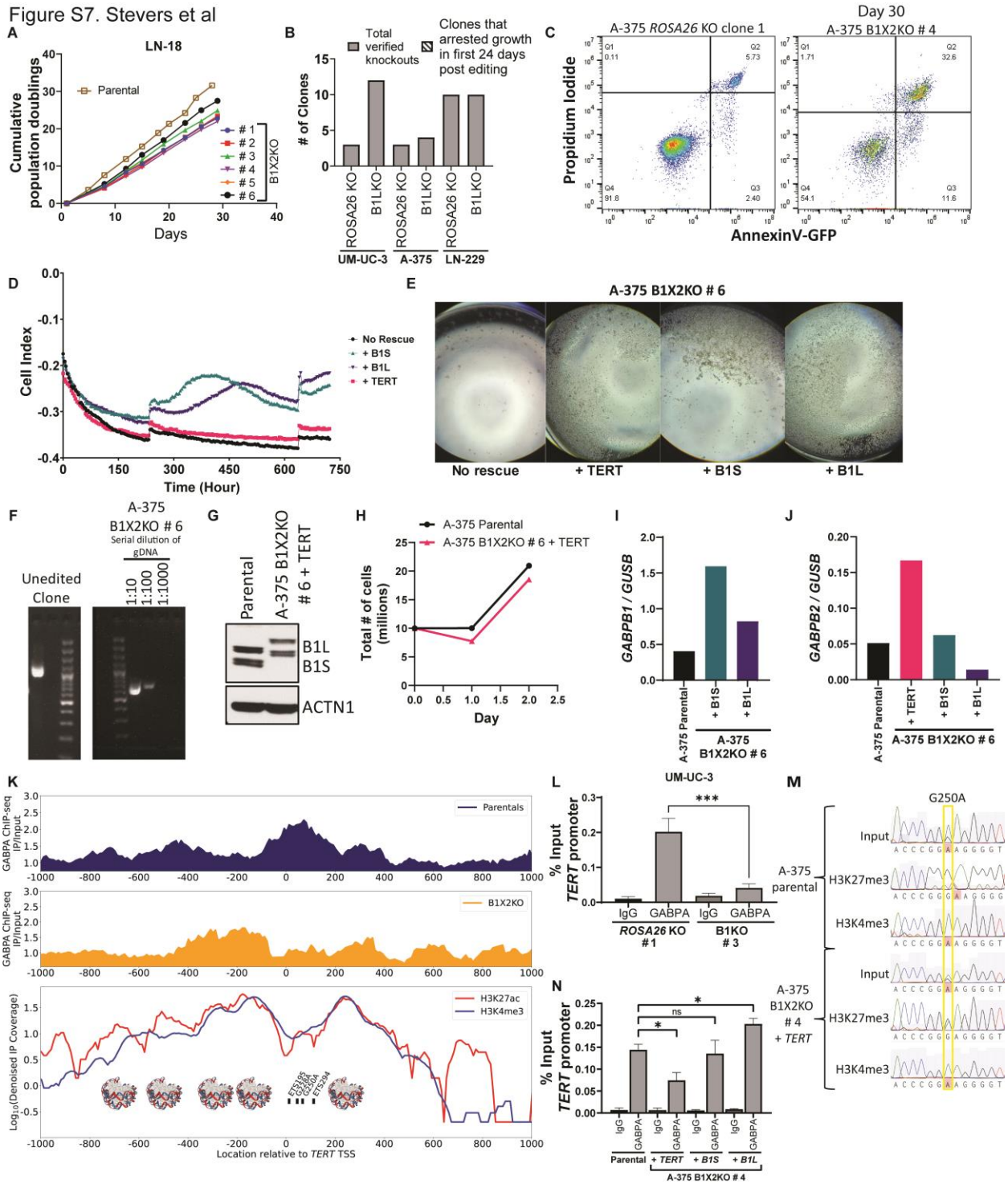

Fig. S7. Phenotypic, molecular, and expression program effects of *B1* knockout

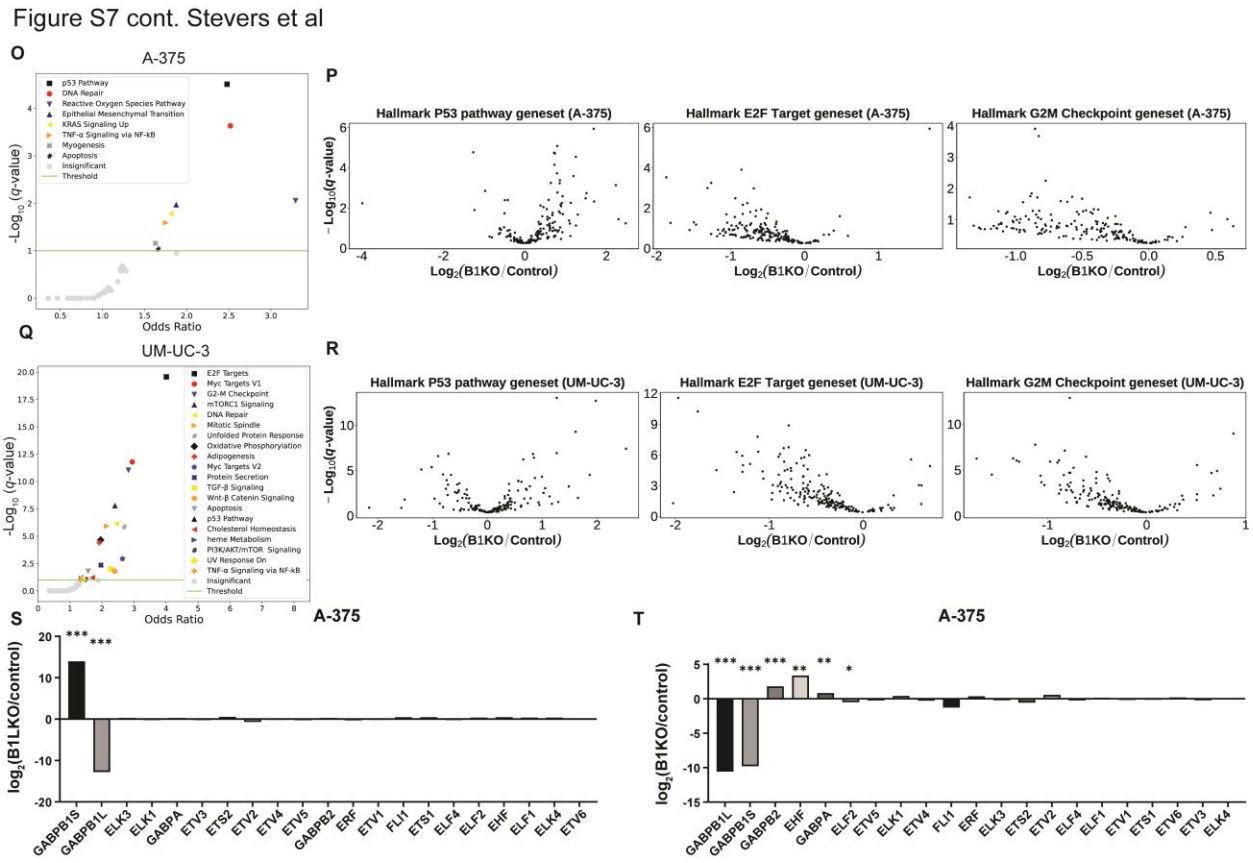

Fig. S7 (cont). Phenotypic, molecular, and expression program effects of *B1* knockout

A. Population doublings of 6 representative LN-18 B1X2KO clones across time demonstrates *B1* knockout has little if any effect on the growth of these *TERT* promoter wildtype GBM clones.
B. Knockout clones were monitored from time of genotyping and their capability to expand, defined as reaching 80-90% confluency in a 6 well dish, past day 24 post editing was recorded.
C. Apoptosis analysis via Annexin V and propidium iodide staining of the A-375 control knockout clone and the A-375 B1X2KO clone 4 at day 30 of the time course.
D. xCELLigence time course growth data of each of non-rescued and rescued A-375 B1X2KO # 6.
E. Bright field image of a replica plate of the cells in panel D at day 40.
F. PCR genotyping of the non-rescued A-375 B1X2KO # 6 showing no detectable wildtype allele as compared to an unedited clone.
G. Immunoblot of B1S and B1L expression in A-375 parental and B1X2KO # 6 + TERT showing one *B1* allele was structurally rearranged and inactivated in B1X2KO # 6. ACTN1 is the loading control in this experiment.
H. Growth rate of B1X2KO # 6 + TERT compared to A-375 parental.
I. Validation of B1 overexpression in A-375 B1X2KO # 6 stably transduced with B1S or B1L compared to A-375 parental. *B1* expression is normalized to *GUSB* expression.

(Figure caption continued on the next page)

(Figure caption continued from the previous page)

J. *B2* expression in A-375 B1X2KO # 6 + TERT cells is elevated compared to A-375 parental cells indicating the rearranged allele is a loss of function. Additionally, overexpression of B1S or B1L suppress *B2*. *B2* expression is normalized to *GUSB* expression.

K. GABPA binds nucleosome-free linker DNA in the mutant *TERT* promoter. GABPA ChIP-seq data in A-375 cells are shown for parental (top) and the *TERT* rescued B1X2KO clone 4 (middle). IP and input samples were individually normalized by total sequencing depth before calculating the fold change. Nucleosome occupancy was inferred from denoised histone modification ChIP-seq data in the bottom panel (Methods). Bars represent the locations of the native ETS-binding motifs and the GABPA binding motifs created by *TERT* promoter mutations. Nucleosome images were taken from the Protein Data Bank (PDB) with image ID 6JR1.

L. Quantitative ChIP-qPCR for GABPA occupancy at the *TERT* promoter in control knockout or B1KO UM-UC-3 cells. Each clone was subjected to ChIP for IgG or GABPA. The results are a mean + SD of three independent experiments.

M. ChIP-PCR Sanger sequencing of the *TERT* promoter conducted on total chromatin from A-375 parental cells and the A-375 B1X2KO #4 + *TERT* cells or chromatin that was subjected to ChIP for H3K27me3 or H3K4me3.

N. GABPA occupancy of the *TERT* promoter in A-375 parental cells or an A-375 B1X2KO clone with stable integration of *TERT*, *B1S*, or *B1L*. The results are a mean + SD of at least two independent experiments.

O. Top differentially expressed Hallmark gene sets from gene ontology analysis comparing A-375 *B1* knockout cells to controls. Functional terms with a *q*-value < 0.05 were reported.

P. Differential expression analysis of Hallmark gene sets (P53 pathway, E2F Targets, and G2M checkpoint) in A-375 *B1* knockout cells compared to controls.

Q. Top differentially expressed Hallmark gene sets from gene ontology analysis comparing UM-UC-3 *B1* knockout cells to controls. Functional terms with a *q*-value < 0.05 were reported.

R. Differential expression analysis of Hallmark gene sets (P53 pathway, E2F Targets, and G2M checkpoint) in UM-UC-3 *B1* knockout cells compared to controls.

S. Differential expression analysis of the detectable ETS factors in RNA seq from A-375 comparing 4 controls and 2 *B1L* knockout clones.

T. Differential expression analysis of the detectable ETS factors in RNA seq from A-375 comparing 4 controls and 9 *B1* knockout clones.

(L, N), Two-tailed, unpaired Student's *t*-test. **P* < 0.05, ***P* < 0.01, ****P* < 0.001, ns, no significance.

Chapter 6: AI-assisted design of a bioPROTAC to degrade GABPA

6.1 Results

Transcription factors have historically been viewed as undruggable. Breakthroughs in the design of proteolysis-targeting chimera (PROTACs) and their biologic equivalents, termed bioPROTACs, offer a new approach toward this therapeutic goal[67]. PROTACs are a class of small molecules composed of a ligand for a protein of interest, a linker, and a ligand for an E3 ubiquitin ligase. They induce ubiquitination and subsequent proteasomal degradation of the target protein by holding it in close proximity to a specific E3 ubiquitin ligase[67]. BioPROTACs achieve the same goal, for example, through a fusion of an E3 ubiquitin ligase with a protein-binding domain.

Recent innovations in machine learning algorithms trained for protein structure prediction and protein-protein interaction are revolutionizing biology and offer rapid predictions that can be tested experimentally. We utilized a combination of *in silico* protein-protein interaction modeling via AlphaFold[47,68,69] and experimental validation to iterate through and identify the minimal portion of the B1 ankyrin repeats capable of interacting with GABPA (B1DN10) (**Fig. S8A-B**). We then designed a GABPA-specific bioPROTAC, a GABPA degrader, by fusing B1DN10, a flexible polypeptide linker, and an E3 ubiquitin ligase binding domain-specifically, the CUL3-binding BTB domain of SPOP (**Fig. 6A-B, S8A**)[70-72]. Lentiviral transduction into GBM cell lines reduced total GABPA protein levels in all cell lines and decreased *TERT* expression in cells with the promoter mutation (**Fig. 6C-D**). Moreover, the GABPA degrader significantly reduced GABPA bound to the *TERT* promoter, increased the presence of H3K27me3, and decreased H3K4me3 (**Fig. 6E**). It also led to upregulation of *B1* and *B2* (**Fig. S8C**), and a decrease of GABPA occupancy and an increase of H3K4me3 at the *B1* promoter (**Fig. S8D**),

reinforcing our discovery of these two negative feedback loops within the network of autosuppression. Interestingly, we also observed an upregulation of *GABPA* mRNA, illuminating yet another level of autoregulation, GABP complexes that negatively regulate the *GABPA* promoter (**Fig. S8C**). Given that this third feedback loop is observable only following GABPA protein degradation, multiple GABP complexes may be capable of repressing the *GABPA* promoter. Indeed, GABPA remains bound to its promoter in B1KO cells, likely in complex with B2 (**Fig. S8E, 5L**).

A time course of tumor cells expressing the GABPA degrader revealed telomere shortening in *TERT* promoter mutant GBM cells (**Fig. 6F**) and a transcriptional reprogramming similar to B1KO cells (**Fig. S8F**). Telomerase targeting is effective in slowing growth of GBM in cases of low tumor burden, such as post-surgical resection[15]. Importantly, the degrader significantly reduced tumor growth and improved the overall survival of mice bearing an orthotopic xenograft of *TERT* promoter mutant GBM cells that were pre-transduced *in vitro* (**Fig. 6G-H, S8G**). Using magnetic resonance imaging of metabolism as a non-invasive biomarker of therapuetic response to *TERT* reduction[73,74], we observed *TERT* effects in GBM cells expressing the GABPA degrader *in vivo* (**Fig. 6I**)[73,74].

6.2 Main Figures

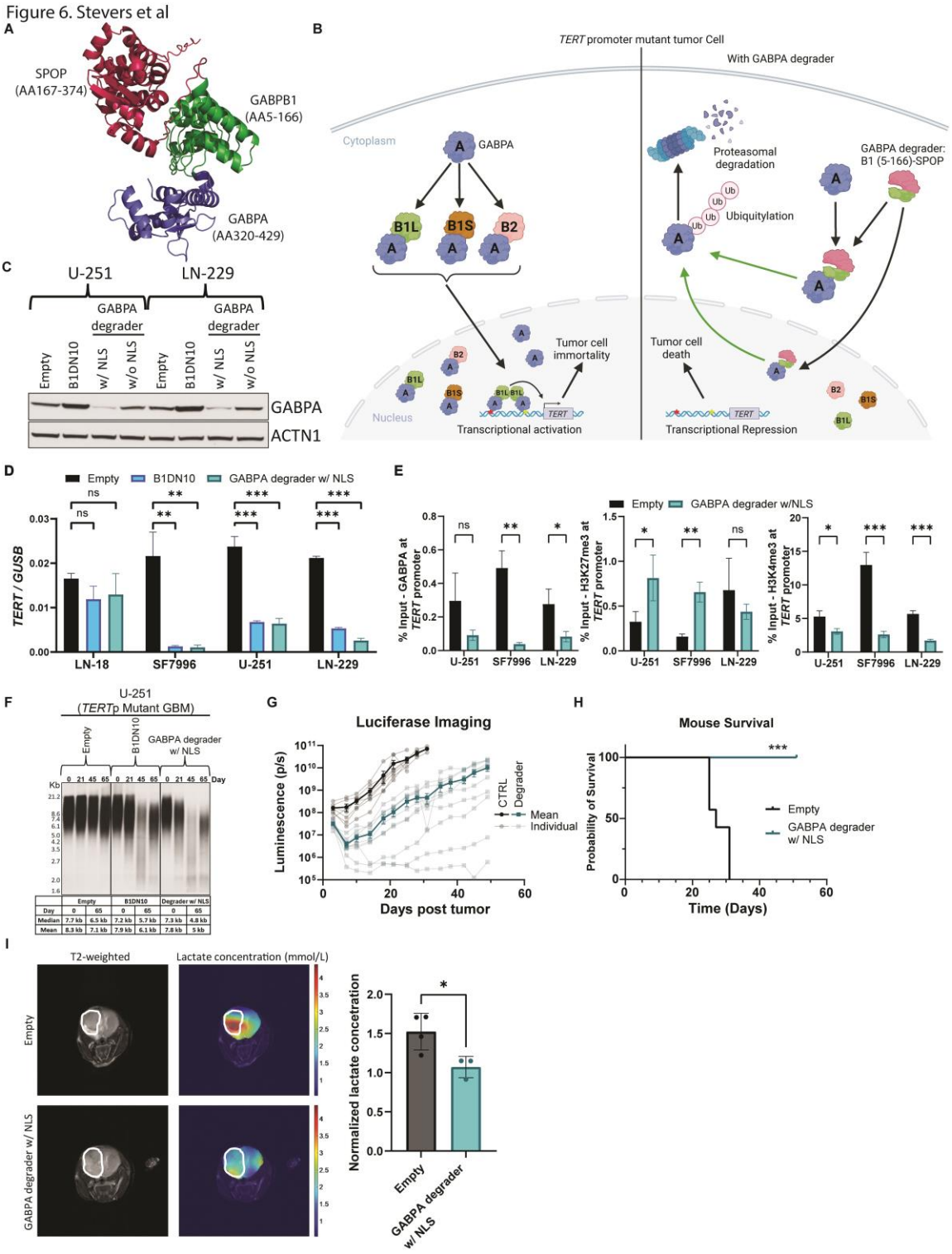

Fig. 6. AI-assisted design and testing of a GABPA degrader *in vitro* and *in vivo.* (Figure caption continued on the next page.)

(Figure caption continued from the previous page.)

A. AlphaFold v2.3.2 prediction of the GABPA degrader interacting with GABPA. The portion of GABPA used for this prediction is the human equivalent of the murine residues present in the partial GABP crystal structure (PDB#1AWC).
B. The GABPA degrader mechanism of action.
C. Immunoblot of GABPA expression in U-251 and LN-229 cells transduced with empty vector, the minimal B1 ankyrin repeats (B1DN10), or the GABPA degrader with or without the NLS.
D. Effect of GABPA degrader on *TERT* expression in GBM cell lines. *TERT* expression normalized to *GUSB* expression. The results are a mean + SD of three independent experiments.
E. GABPA, H3K27me3, and H3K4me3 occupancy at the *TERT* promoter in empty vector control or GABPA degrader transduced cells. The results are a mean + SD of three independent experiments.
F. Time course analysis of telomere length (TRF assay) of U-251 cells transduced with empty vector, the minimal B1 ankyrin repeats (B1DN10), or the GABPA degrader with or without the NLS.
G. Average and individual luminescence values of mice bearing orthotopic xenografts of U-251 cells that were transduced with empty vector (n=7) or with GABPA degrader (n=10). Data is presented as mean +/- SEM.
H. Kaplan-Meier survival curve of mice bearing orthotopic xenografts of U-251 cells that were transduced with empty vector (n=7) or with GABPA degrader (n=10).
I. (Left) Effect of the GABPA degrader on ^{2}H-lactate production from [U-^{2}H]-pyruvate in mice bearing orthotopic xenografts of U-251 cells pre-transduced with empty vector (n = 4) or with GABPA degrader (n = 3) and (right) quantification of these metabolites.

(D-E, I), Two-tailed, unpaired Student's *t*-test. (H), Log-rank (Mantel-Cox) test. **P* < 0.05, ***P* < 0.01, ****P* < 0.001, ns, no significance.

6.3 Supplemental Figures

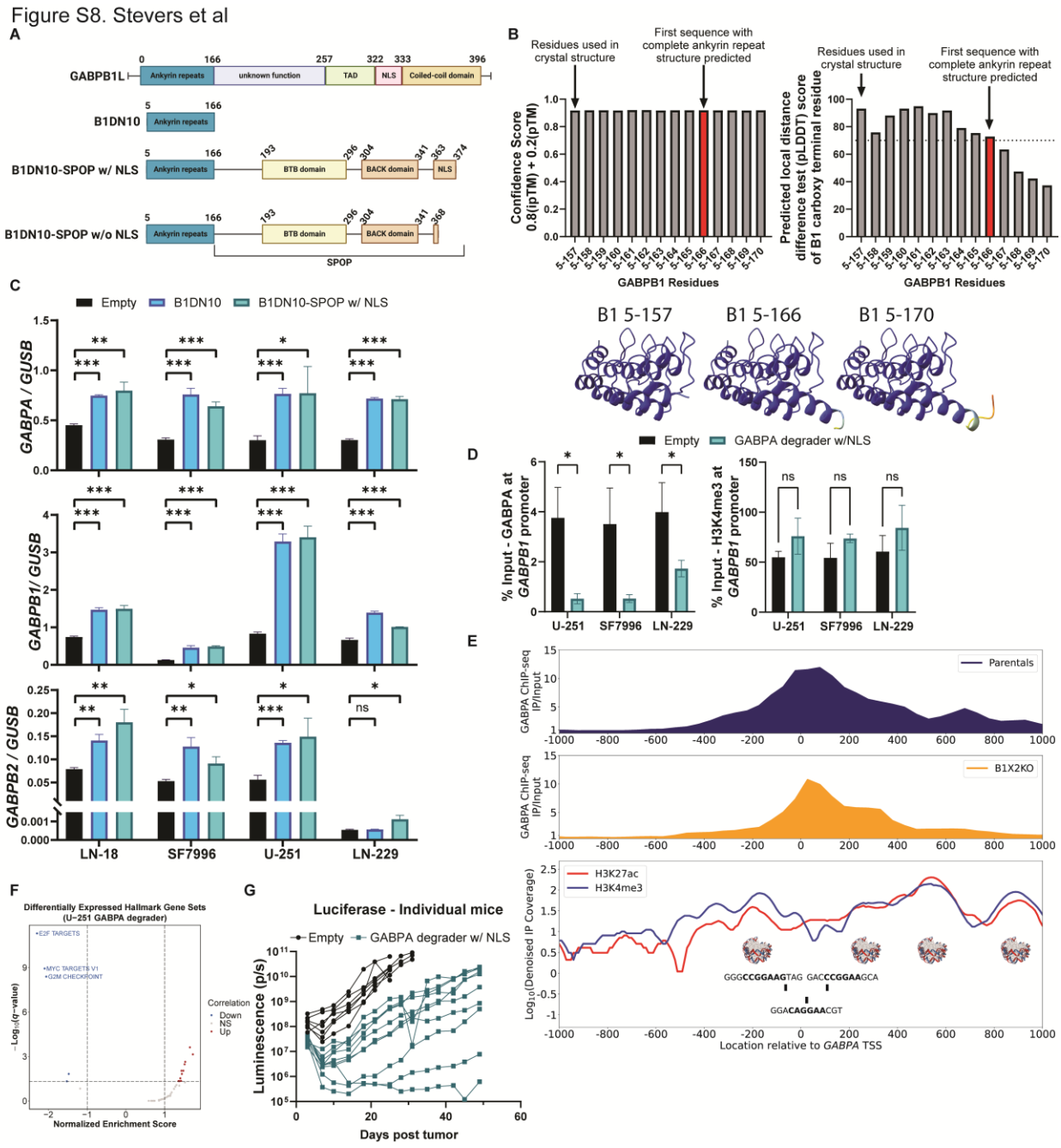

Fig. S8. Design and characterization of a GABPA degrader. (Figure caption continued on the next page.)

(Figure caption continued from the previous page.)

A. Schematic of the GABPA degrader design.
B. Results of AlphaFold2 predictions: (left) confidence score of the structure, (right) pLDDT score of the carboxy terminal residue for each B1 variant, and (bottom) three B1 variants with pLDDT score overlaid. B1DN10 (B1 5-166) is highlighted in red.
C. Effect of GABPA degrader on *GABPA*, *B1*, and *B2* expression in GBM cell lines. The expression of each gene is normalized to *GUSB* expression. The results are a mean + SD of three independent experiments.
D. GABPA and H3K4me3 occupancy at the *B1* promoter in empty vector control or GABPA degrader transduced cells. The results are a mean + SD of three independent experiments.
E. GABPA binds nucleosome-free linker DNA in the *GABPA* promoter. GABPA ChIP-seq data in A-375 cells are shown for parental (top) and the *TERT* rescued B1X2KO clone 4 (middle). IP and input samples were individually normalized by total sequencing depth before calculating the fold change. Nucleosome occupancy was inferred from denoised histone modification ChIP-seq data in the bottom panel (Methods). Bars represent the GABPA binding motifs within the ChIP-seq peak. Nucleosome images were taken from the Protein Data Bank (PDB) with image ID 6JR1.
F. Top differentially expressed Hallmark gene sets from gene set enrichment analysis comparing U-251 transduced with the GABPA degrader to U-251 cells transduced with an empty vector. Gene sets with a *q*-value < 0.05 and an absolute normalized enrichment score > 1 are colored and those with an absolute normalized enrichment score > 2 are labeled.
G. Individual luminescence values of mice bearing orthotopic xenografts of U-251 cells that were pre-transduced with empty vector (n=7) or with GABPA degrader (n=10).

(C, D), Two-tailed, unpaired Student's *t*-test. **P* < 0.05, ***P* < 0.01, ****P* < 0.001, ns, no significance.

Chapter 7: Conclusion

GABP reawakens the *TERT* promoter in cancer cells with diverse genetic and epigenetic landscapes, six different point mutations, recurrent duplications of wildtype sequence[26], adult and pediatric cancers, both sexes, and in cell lines from patients with different ethnicities. This raises the fundamental question of why, among all ETS factors, the GABP tetramer recruitment is so critical to immortalize tumor cells, strongly and specifically influencing which genetic alterations of *TERT* are positively selected for during early tumor evolution. GABP is the only ETS factor that can form multimeric complexes able to bind tandem ETS motifs[45,51,75]. Consequently, only the GABP tetramer benefits from avidity[76]. Avidity increases the binding affinity of GABP tetramers by up to 10-fold as compared to GABP dimers[50], and stabilizes tetramer DNA interactions once bound[51]. The occurrence of a *de novo* ETS motif at multiples of full helical spacings from the native ETS site, created by single or double point mutation (**Fig. 1B**)[23] or tandem duplication[26], and the necessity of both ETS motifs for the enhanced *TERT* promoter activity (**Fig. 1C**) further underscore the importance of this feature of the tetramer in mutant *TERT* promoter reactivation. ETS family members ELF1, ELF2, and ETV6 can bind a mutant *TERT* promoter oligonucleotide bait in a cell-free system, however, they are sterically precluded upon addition of the GABP tetramer[20]. In the absence of the tetramer or both the tetramer and dimer in tumor cells, we found no evidence of altered ETS factor expression or productive binding by factors other than B2. Furthermore, the GABP tetramer can initiate RNA Polymerase II-mediated transcription at TATA-less promoters like the mutant *TERT* promoter[77,78]. Together, these unique structural and biochemical features of the tetramer may provide the underlying selective advantage of the six ETS-generating *TERT* promoter mutations, as well as tandem duplications[23,26].

In the absence of competition from B1L tetramers, other ETS transcription factors have an opportunity to bind and activate the mutant *TERT* promoter, but they do not. Instead, B1S dimers maintain *TERT* expression following elimination of B1L tetramers, and B2 tetramers weakly maintain expression in the absence of B1 tetramers and dimers. If avidity explains in part why the B1L tetramer is the primary activator, it is surprising that elevated levels of B1S dimer(s) maintain *TERT* expression at a similar level. However, the energy barrier(s) to initial *TERT* promoter activation from a tightly repressed chromatin state may be different and higher than for maintenance. Investigations of GABP-mediated activation of other promoters with tandem ETS motifs revealed that the stronger ETS motif in a tandem pair is responsible for nearly all of the activation[79]. Therefore, one possibility is that B1S dimers bind to the stronger *de novo* ETS motif (CCGGAA compared to the native ETS GCGGAA), or both motifs, to maintain *TERT* expression in the absence of the B1L tetramer, although this remains to be determined. Conversely, the lack of the stronger *de novo* ETS site in the wildtype *TERT* promoter may explain why GABP binding is cancer specific. B1S dimers can occupy tandem ETS sites like B1L tetramers; however, approximately 3 to 10-fold more dimer is necessary[50], and this level is attained following B1L reduction. This extensive data on compensation by alternative GABP complexes, via release from autosuppression, support the revision of our prior conclusions that targeting the B1L tetramer alone would be sufficient for reversing *TERT* expression. We conclude that targeting the B1L tetramer concurrently with the B1S dimer, or all three complexes via GABPA degradation, is required to reverse expression from the mutant *TERT* promoter and thereby impact tumor cell immortality.

Millions of cancer patients are diagnosed annually with tumors that depend on a *TERT* promoter mutation to achieve and maintain cellular immortality, the reversal of which is an unfulfilled holy grail of cancer therapy[80]. Our results suggest that among all ETS factors, only the GABP tetramer rewires transcriptional regulation of *TERT* in a tumor-specific manner, attracting GABP interacting partners such as ASL[81] and opening chromatin to enable native regulators such as MYC to bind[82]. Presumably, upregulated GABP dimer(s) would maintain *TERT* after tetramer targeting in most tumor types. We therefore hypothesized that common elements and interfaces among GABP tetramers and dimer complexes may offer new therapeutic opportunities to simultaneously target activation and intrinsic resistance across a spectrum of cancers. Transcription factors are challenging targets; however, advances in tumor specific delivery of engineered proteins via retroviral replicating vectors[83] and other viruses may allow us to exploit the evolutionarily optimized binding domains present in multimeric proteins. This is exemplified by the B1 dominant negative - GABPA-specific degrader presented here. Unique aspects of GABP complex regulation also could be explored for this purpose including upstream regulators of GABP subunit expression[25,29], post-translational modifications that regulate GABP nuclear transport[59,84], complex formation[85], and DNA binding and transactivation activity[59,85-88]. Additionally, GABP may recruit or enable binding of other mutant promoter-specific regulators with targetable enzymatic activity or domains[81,89-92]. Further exploration into the ability of the GABP tetramer to relax the proposed G-quadruplex structure of the mutant *TERT* promoter[23,93,94] may also uncover targetable features. Solving the structure of the GABP complex bound to the mutant *TERT* promoter and better understanding the C-terminal residues of GABPA (AA 316-

454) that interact with the GABPB ankyrin repeats could allow for structure-based design of small molecule inhibitors with wide cancer applicability[47,51]. Interaction between experimentalists and AI platforms such as AlphaFold2[68,69,95] and RoseTTaFold2[96] may accelerate this process.

Chapter 8: Materials and Methods

Cell Lines

Cell lines were cultured in their respective media and supplements as listed in **table 2**. All cell lines were maintained at 37 °C in a humidified incubator with 5% CO_2. Cell culture medium was changed every 3-5 days depending on cell density. For routine passage, cells were split at a ratio of 1:3-10 when they reached 80% to 90% confluence. Cell lines were authenticated by short tandem repeat (STR) analysis at the University of California Berkeley Sequencing Facility and confirmed to be Mycoplasma free by PCR using a previously published method[26,97,98]. Doxycycline inducible cells were treated every 48 hours with doxycycline (Sigma, solubilized in water) unless otherwise noted. When many cell lines are used for a figure (Pan-cancer studies) abbreviations for the respective cancer type are used, the definitions for these abbreviations are as follows: BLCA = Bladder Urothelial Carcinoma, GBM = Glioblastoma multiforme, LGG = Brain Lower Grade Glioma, THCA = Thyroid carcinoma, SKCM = Skin Cutaneous Melanoma, LIHC = Liver hepatocellular carcinoma, HNSC = Head and Neck squamous cell carcinoma, KIRC = Kidney renal clear cell carcinoma, MB = Medulloblastoma, OV = Ovarian serous cystadenocarcinoma, Lung = LUSC (Lung squamous cell carcinoma); MESO (Mesothelioma); LUAD (Lung adenocarcinoma), COAD/READ = Colon adenocarcinoma/Rectum adenocarcinoma, BRCA = Breast invasive carcinoma, MNG = Meningioma. Abbreviations are based upon cancer cell line origin and placement within TCGA category, except for MNG (Meningioma).

TERT promoter genotyping

Cell lines were genotyped for *TERT* promoter mutation status using Phusion Green High-Fidelity DNA Polymerase (Thermo Scientific, #F-534L) with GC buffer and 5% DMSO. Cycling conditions were an initial step of 98 °C for 1 minute, followed by 31 cycles of 98 °C for 10 seconds, 70 °C for 15 seconds, and 72 °C for 30 seconds, with a final elongation step of 72 °C for 5 minutes. PCR primer sequences were designed with tails incorporating M13 primer sequences and are listed in **table 3**. Samples were submitted for Sanger sequencing (GENEWIZ) with the following sequencing primers M13 (forward: 5'-GTAAAACGACGGCCAG-3'; reverse: 5'-CAGGAAACAGCTATGAC-3'). A list of genotypes for all cell lines is provided in **table 2**.

Reverse Transcription Quantitative PCR (RT-qPCR)

Total RNA was purified using the Quick-RNA Microprep (Zymo Research, #R1051) or Miniprep (Zymo Research, #R1058) kits. Briefly, 1000 ng of Dnase-treated RNA was converted to cDNA using the iScript cDNA Synthesis Kit (BioRad, #1708891). This cDNA was then diluted 1:5 using nuclease free water, and 2 µl of this diluted cDNA was used for qPCR reactions alongside standard curves for each target gene. Reverse transcription quantitative polymerase chain reaction (RT-qPCR) was performed using POWER SYBR Green Master Mix (Applied Biosystems, #4367659). All samples were run in technical triplicate using the QuantStudio 5 (Thermo Scientific) and all gene expression data were normalized to *GUSB* mRNA. The amplification protocol is as follows: 50 °C for 2 minutes, 95 °C for 10 minutes, followed by 40 cycles of 95 °C for 15 s, and 60 °C for 60 s. Dissociation curves were performed to confirm specific product amplification. RT-qPCR

standards for each gene were generated from a mixture of human cDNA via end-point RT-PCR then gel purification, using the appropriate primer pair. Gradient PCR reactions were performed with the C1000 Touch Thermal cycler (Bio-Rad) to determine the optimal annealing temperature for each primer set and to validate a lack of non-specific products. Primer sequences are listed in **table 3**. Primer sequences corresponding to each gene for the mRNA expression analysis were designed using NCBI Primer Blast[99] or selected from those previously reported in the literature.

Pan-Cancer siRNA and RT-qPCR gene expression analysis

Cell lines were seeded at a density of 2,000 or 5,000 cells per well in a 96-well plate in 100 uL of their respective media (antibiotic free). Each cell line was plated such that there were three replicates per density and per siRNA pool. Twenty-four hours post-seeding cells were transfected with 0.1 µl of DharmaFECT 1 reagent (Horizon, #T-2001-02) and their respective siRNA pools (Dharmacon siGENOME SMARTpool) at a final concentration of 30 nM (siNon-Targeting control (#D-001206-13-05), siGABPA (#M-011662-01-0005), siGABPB1 (#M-013083-01-0005), and siGABPB2 (#M-016074-00-0005); see **table 3** for further information). At 72 hours post-transfection, the two different seeding densities were inspected for % confluency and the plating closest to 70-90% confluent were lysed, cDNA generated, cDNA diluted ½ with nuclease-free ultrapure H_2O, and qPCR performed with standards to measure gene expression (primer sequences in **table 3**) by the POWER SYBR Green Cells-to-Ct kit (Invitrogen, #4402954). Each cell line replicate (each seeded well) was measured via two qPCR technical replicates. Relative target expression compared to siNon-Targeting following target knockdown was

assessed via linear mixed-effect models. Results from the statistical analysis are presented per cell line and per cancer type in **table 1**.

Production of Lentiviral Particles and *In Vitro* Lentiviral Transduction

Replication-deficient lentivirus was produced by transient transfection of psPAX2 (Addgene; 12260), pDM2G (Addgene: 12259) and transfer plasmid into HEK293T cells. Viral supernatant was collected at 48 hours and filtered through a 0.22 micron PES membrane filter. Select cell lines were transduced with serially diluted viral supernatant supplemented with polybrene (EMD Millipore, #TR-1003-G) to a final concentration of 4 µg/mL, followed by antibiotic selection for functional titration. Cells were expanded from the viral dilution well that resulted in approximately 30% survival following antibiotic selection.

GABPA Chromatin Immunoprecipitation (ChIP)-qPCR

ChIP for GABPA was performed using the Zymo-Spin ChIP Kit (Zymo Research, #D5210) according to manufacturer's instructions and recommendations unless indicated otherwise. Cell lines were seeded at a density of 10 million cells per 15 cm dish in triplicate. Twenty-four hours after seeded one 15 cm dish was counted and viability confirmed to be greater than 90%. Cells were fixed with a final concentration of 1% methanol-free formaldehyde (Pierce, #PI28908) for 9 minutes and neutralized with glycine added to a final concentration of 0.125 M for 5 minutes then scraped into cold PBS containing 0.5% BSA, 1mM Phenylmethylsulfonyl fluoride (PMSF) (Thermo Scientific, #36978), and 1X Halt Protease Inhibitor Cocktail (Thermo Scientific, #78428).

Fixed cells were washed once and then cell pellets were flash frozen on dry ice then stored at -80 ºC until chromatin shearing. Chromatin was sonicated with the Covaris S2 Focused Ultrasonicator for 8 minutes to achieve a size range of 200-1000 bp. Four immunoprecipitations were prepared per cell line, each containing 14-20 µg of chromatin and 4 µg of one of the following antibodies per reaction: anti-GABPA #1 (Invitrogen, #PA5-27735, RRID:AB_2545211), anti-GABPA #2 (Proteintech, #21542-1-AP, RRID:AB_10858481), normal rabbit Immunoglobulin G (IgG) control #1 (Cell Signaling, #2729, RRID:AB_1031062), and normal rabbit IgG control #2 (Proteintech, #30000-0-AP, RRID:AB_2819035). Enrichment at the *TERT* promoter was determined via qPCR, with technical triplicates for each biological replicate, on the QuantStudio 5 (Thermo Scientific) with the KAPA SYBR FAST qPCR Master Mix (2X) Kit (Roche, #KK4621) using the following amplification protocol: 50 °C for 2 minutes, 95 °C for 3 minutes, followed by 40 cycles of 95 °C for 3 s, and 69 °C for 60 s. Dissociation curves were performed to confirm specific product amplification. Primers (**table 3**) were designed in silico using NCBI PrimerBlast then empirically tested with gradient annealing temperatures to determine optimum temperature. Percent Input was calculated via the following formula: % Input = 100*2^ ((Ct [10% Input] - $Log_2(10)$) - Ct [ChIP]). Fold enrichment over IgG was calculated via the following formula: %Input[GABPA] / %Input[IgG]. PCR amplification for Sanger analysis of allelic bias for the pan cancer *TERT* promoter mutant cell lines was conducted using 2 uL of the GABPA ChIP DNA for a given cell line and the PCR conducted as described in the *TERT* promoter genotyping section above.

ChIP-seq

Sample preparation for ChIP-seq was conducted as listed above with the following modifications: samples were sonicated for 6 minutes, to isolate sufficient material for sequencing library preparation a total of five GABPA IP's using the Invitrogen GABPA antibody (Cat. #PA5-27735, RRID:AB_2545211). Following chromatin isolation libraries were prepared as follows. 10-20 ng of ChIP or Input DNA was used to construct ChIP-seq libraries with KAPA Hyper Prep Kit (Cat. KK8502). Briefly, after the end repair and A-tailing reaction, the DNA was ligated with unique dual-indexed adapters (KAPA UDI Adapters KK8727). Adapter-ligated libraries were amplified for 8 cycles with HiFi Polymerase. Libraries then underwent a post-amplification SPRI cleanup with KAPA cleanup beads (0.8X bead-based cleanup). Following this cleanup, a double-sided size selection was performed. The first size cut is to exclude the unwanted large library molecules by adding 0.6X beads and keeping the supernatant, then the second cut was to clear up small molecules by adding 0.2X beads to the supernatant from the first size cut. Then library size and quality were checked with Agilent Bioanalyzer profiling. Finally, libraries were quantified with qPCR (KAPA Library Quant kit KK 4824) before pooling for sequencing on the Illumina Nova-Seq 6000 with a S4 flow cell and 150 bp paired-end reads.

Histone ChIP

Chromatin immunoprecipitation and qPCR for histone marks was performed using Active Motif High Sensitivity ChIP Kit (Active Motif, #53040) per kit specifications with antibodies to H3K4me3 (Cell Signaling Technologies, #9751) and H3K27me3 (Active

Motif, #39055). Chromatin shearing was performed using a Diagenode Bioruptor (Diagenode, #UCD-200) for 70 minutes at intervals of 30 seconds on, 90 seconds off for a total shearing time of 17.5 minutes. qPCR for the *TERT* promoter was performed as previously described [23].

Molecular Cloning, Plasmid Constructs and RNA Interference

Table 3 contains a list of all siRNAs, plasmids, and sgRNAs. Mutated ORFs were ordered from TWIST BioSciences as clonal NGS verified fragments or as non-clonal fragments and verified by Sanger sequencing after cloning. All molecular cloning was verified via Sanger sequencing. Plasmids were transfected with either X-tremeGENE HP (Roche, #6366244001) or Lipofectamine 3000 (Invitrogen, #L3000001), according to the manufacturer's instructions, depending on the transfection efficiency of the chosen cell line.

Vectors, and microRNA-adapted short hairpin RNA cloning and screening

The constitutive lentiviral vector, N174-MCS-puro (addgene #81068), was modified into a robust RNAi system (microRNA-adapted short hairpin RNA) through a sequential cloning process to contain a single CMV promoter driving expression of the TurboGFP-miR-E-IRES-puro transcript. The lenti-RNAi system employed a single CMV promoter and IRES to achieve a homogonous population of cells with efficient knockdown following transduction and puromycin selection. First, a synthetic double stranded DNA fragment was designed to include the EF1a core promoter and GFP-miR-E RNAi system [100] with modifications to replace eGFP with TurboGFP for improved fluorescent

capabilities. The EF1a core promoter/Intron1 was replaced with only EF1a core promoter to remove the 2 XhoI restriction sites present in Intron 1, which are required for cloning of miR-E shRNAs. Next, the N174-MCS-puro vector was digested with BsuI15I and MluI to remove the EF1a core promoter/Intron1 and MCS. The TurboGFP-miR-E synthetic DNA fragment was ordered from IDT as a gBlock and reconstituted with 10 mM Tris-HCl (pH 8.0). 0.1 mM EDTA then digested with FastDigest Bsu15I (ThermoFisher, #FD0143) and FastDigest MluI (ThermoFisher, #FD0564) to generate compatible sticky ends for ligation into the N174-puro backbone. The N174-EF1a-core-TurboGFP-miR-E-puro vector was then digested with FastDigest Bsu15I and FastDigest XmaJI (ThermoFisher, #FD1564) to remove the EF1a core promoter. The EF1a core promoter was first introduced followed by subsequent cloning of other promoters for comparison of knockdown efficiency. Next, the pCMV6-Neo vector (Origene Cat# PCMV6NEO) was digested with FastDigest Bsu15I and FastDigest XmaJI to release the CMV enhancer/promoter for ligation into the N174 - TurboGFP-miR-E-puro backbone. Finally, N174-CMV-GFP-miR-E-puro vector was digested with FastDigest MluI and FastDigest CpoI (ThermoFisher, #FD0744) to remove the PGK promoter for replacement with an IRES. Tet-pLKO-puro (Addgene #21915) was digested with FastDigest MluI and FastDigest CpoI to release the IRES for ligation into N174-CMV-GFP-mirE-puro backbone, generating the final vector, N174-CMV-TurboGFP-miR-E-IRES-puro, for cloning of miR-E shRNAs.

The miR-E shRNAs were designed using the online portal Splash RNA[101] (http://splashrna.mskcc.org/) with advanced settings changed to 6 predictions per gene and the input consisting of either the refseq ID or FASTA mRNA sequence. The output miR-E shRNA sequences (see **table 3**) were ordered from IDT as 97 base single stranded

DNA oligonucleotides and reconstituted at 100 µM concentrations with 10 mM Tris-HCl (pH 8.0). 0.1 mM EDTA. The 100 µM oligonucleotides were diluted 1:3000 in water and used as the template in PCR with Phusion HF polymerase (ThermoFisher, #F534L) in a 20 µl reaction containing GC buffer, 5% DMSO and the following primers from Pelossof et al: Xhol_de_novo_miRE_F GAACTCGAGAAGGTATATTGCTGTTGACAGTGAGCG and EcoRI_de_novo_miRE_R TCTCGAATTCTAGCCCCTTGAAGTCCGAGGCAGTAGGC[101]. PCR cycling conditions included an initial denaturation at 98 °C for 1 minute, 30 cycles of 98 °C for 10 seconds, 60 °C 15 seconds and 72 °C for 20 seconds, and a final extension at 72 °C for 5 minutes. The resulting 125 bp amplicons were resolved on a 2% agarose gel then purified with Zymoclean Gel DNA Recovery Kit (Zymo Research, #D4001) and eluted in a final volume of 40 µl. The gel purified amplicons were digested in 40 µl reactions with FastDigest EcoRI (ThermoFisher, #FD0274) and FastDigest Xhol (ThermoFisher, #FD0695) for 30 minutes at 37 °C. The digested amplicons were purified with the DNA Clean and Concentrator Kit (Zymo Research, #D4033) and eluted in a final volume of 50 µl. These purified amplicons were diluted 1:4 with water in a final volume of 200 µl and 1 µl was used for ligation with 25 ng of FastDigest EcoRI and FastDigest Xhol digested N174-CMV-GFP-miR-E-IRES-pur backbone. All vectors were verified by Sanger sequencing. Initially 3-6 miR-E shRNAs were designed per mRNA or isoform and cloned into N174-CMV-GFP-miR-E-IRES-puro. Next these shRNAs were screened for functional performance to identify those with the best knockdown efficiency. To achieve this, replication-deficient lentivirus was produced by transient transfection of psPAX2 (Addgene #12260), pMD2.G (Addgene #12259), and transfer plasmid (N174-CMV-GFP-miR-E-IRES-puro-shRNA) into HEK293T cells with

Lipofectamine 2000 reagent (Invitrogen, #11668027) according to the manufacturer's instructions. Viral supernatants were collected 48 hr post-infection and passed through a 0.2-micron PES membrane filter. Functional titration was performed by transduction of three cell lines with serially diluted virus in the presence of polybrene at a final concentration of 4 µg/mL (EMD Millipore, #TR-1003-G) for 6 hours followed by puromycin (Gibco, #A1113803) selection for 48 hours post-transduction. Transduced cells were then expanded from the well with at least 30% cell survival in the presence of puromycin (1 µg/mL). Cells were then grown in the absence of puromycin for at least 3 days prior to lysis for RNA isolation. Gene expression analysis was determined as outlined above in the reverse transcription quantitative PCR section. Knockdown efficiency was determined for each shRNA relative to multiple control shRNAs.

Antisense Oligonucleotide (ASO) mediated knockdown

2′-O-methoxy-ethyl (2′-MOE) ASOs with phosphorothioate (PS) modifications throughout the backbone were ordered from IDT (see **table 3**). ASOs were resuspended at 100 µM with sterile, UltraPure DNase/RNase-Free distilled water (ThermoFisher Scientific, #10977015). For transfection of cells in 96-well plates: Cell lines were seeded in biological triplicates at a density of 2,000 to 3,000 cells per well, depending on cell line, in 100 µL of their respective media (antibiotic free). Twenty-four hours post-seeding cells were transfected by adding 20 µL reaction containing serum free media, 0.1 µl of DharmaFECT 1 reagent (Horizon, #T-2001-02), and their respective ASO to achieve desired final concentration. 72 hours post-transfection, cells were lysed, cDNA generated, cDNA diluted 1:2 with UltraPure DNase/RNase-Free distilled water, and qPCR performed

with standards to measure gene expression (primer sequences in **table 3**) by the POWER SYBR Green Cells-to-Ct kit (Invitrogen, #4402954). Each cell line replicate was measured via two qPCR technical replicates.

For transfection of cells in 6-well plates: Cells were seeded at a density of 75,000 to 80,000 cells per well, depending on cell line, in 2 mL of their respective media (antibiotic free). Twenty-four hours post-seeding cells were transfected by adding 400 µL reaction containing serum free media, 2.0 µl of DharmaFECT 1 reagent (Horizon, #T-2001-02), and their respective ASO to achieve desired final concentration. Seventy-two hours post-transfection, protein lysates were collected as described in the western blot section of methods.

siRNA mediated knockdown in 6 well plates

Cells were seeded at a density of 75,000 to 80,000 cells per well, depending on the cell line, in 2 mL of their respective media (antibiotic free). Twenty-four hours post-seeding cells were transfected by adding 400 µL reaction containing serum free media, 2.0 µl of DharmaFECT 1 reagent (Horizon, #T-2001-02), and their respective siRNA pools at a final concentration of 30 nM. Seventy-two hours post-transfection, protein lysates were collected as described in the western blot section of methods.

Western Blot

Whole cell protein extracts were prepared with Mammalian Protein Extraction Reagent (M-PER) (Thermo Scientific, #78501) supplemented with 1X Halt Protease and Phosphatase Inhibitor Cocktail (Thermo Scientific, #78440) and 0.2 units/mL final of

Turbo Nuclease (Sigma, #T4330-50KU) and incubated on ice for 10 minutes followed by centrifugation at 4 °C for 10 minutes at 16,000 *g*, and finally isolation of the supernatant. Protein concentration was determined by the BCA protein assay (Pierce, #23225). Equal amounts of protein (20-50 µg) were fractionated on 10% Bis-Tris SDS-polyacrylamide gel electrophoresis gels (Invitrogen, #NPO315BOX) and transferred to PVDF membranes (Bio-Rad, #1620177). Membranes were stained with Ponceau S to confirm efficient transfer and equal loading. Membranes were then blocked with 5% nonfat dry milk (Bio-Rad, #1706404) in 1x Tris-buffered saline Tween-20 (TBST) (Pierce, #28360) for 1 hour at room temperature, while rocking. The membranes were incubated with primary antibodies in 5% nonfat dry milk in TBST at 4 °C overnight followed by incubation with secondary antibody in 5% nonfat dry milk in TBST for 1 hour at room temperature. Primary antibodies are listed in **table 4**. Enhanced chemiluminescence (Thermo Scientific, #32109) was used for protein detection. Alpha-actinin served as the loading control for each experiment.

Luciferase Promoter Reporter Assay

Promoters were either generated by PCR amplification from human genomic DNA or synthesized as double stranded DNA fragments (Twist Bioscience) and cloned into the pGL4.10 Firefly reporter plasmid. Transfection of reporter plasmid was carried out with ViaFect transfection reagent (Promega, #E4981). Briefly, cells were seeded at a density of 6,000 cells per well in 100 µl of antibiotic free media in a 96-well clear bottom white polystyrene microplate (Corning, #3610) with 4-6 wells (biological replicates) per condition. Twenty-four hours post-seeding, cells were transfected with 90 ng pGL4.10

plasmid (Firefly experimental promoter), 9 ng pGL4.74 plasmid (Renilla control promoter), and 0.3 µl of ViaFect transfection reagent in 10 µl of Opti-MEM serum free media (Gibco, #31985062). Twenty-four hours post transfection, Firefly luciferase activity was measured by using the Dual-Luciferase Reporter assay system (Promega, #E1910) on the Promega GloMax 96 well microplate luminometer and normalized against Renilla luciferase activity then presented in arbitrary units. When luciferase assays were conducted following siRNA-mediated knockdowns, cells were first plated at 2,000-3,000 cells per well in 100 µl of antibiotic free media in a 96-well plate with 4-6 wells (biological replicates) per condition, siRNA transfection conducted at 24-hours post seeding, luciferase plasmids transfected at 72-hours post seeding, and luciferase assay performed at 96-hours post seeding/72-hours following siRNA transfection.

Terminal Restriction Fragment Sothern Blotting (TRF Southern Blotting)

Assay conducted using the Millipore Sigma/Roche TeloTAGGG telomere length assay kit (Millipore Sigma, cat #12209136001) according to manufacturer's instructions and recommendations. Average telomere length was calculated using the Web-based Analyser of the Length of Telomeres (WALTER)[102].

CRISPR Gene Knockout

CRISPR-mediated knockouts were performed as previously described[103]. Single guide RNAs (sgRNAs) were designed using the Genetic Perturbation Platform Web Portal (https://portals.broadinstitute.org/gpp/public/) and the highest scoring guide RNAs were then cloned into PX458 (Cas9 expressing plasmid, Addgene #48138) and combinations

of guide RNAs were empirically tested in HEK293T cells for their cutting efficiency. Finally, gRNAs were transfected into cells and clonal cells were isolated with fluorescence-activated cell sorting (FACS) (Sony SH800 or FACSAria3) followed by plating of GFP positive cells into 96-well dishes for clonal growth. Cells were replica plated for clonal expansion and genotyping. DNA was isolated from clones with Lucigen Corporation QuickExtract DNA extraction solution 1.0 (FisherScientific, #NC9904870). Genotyping was performed with primer pairs listed in **table 3**. Primers were designed with NCBI Primer-BLAST then empirically tested by gradient end-point PCR to optimize the specificity and sensitivity.

Beta-Galactosidase Assay

The assay was conducted using the Cell Signaling Technologies Senescence beta galactosidase staining kit (Cell Signaling, cat #9860) according to manufacturer's instructions and recommendations.

Growth curves

Time course growth measurements were conducted by seeding cells at known densities and collecting and counting cells when they reach 80% confluency, or they were collected and counted 72 or 96 hours post seeding if they did not expand rapidly enough to reach 80% confluency. Two independent samplings and cell counts were obtained via the Countess 2 Automated Cell Counter (ThermoFisher Scientific, #AMQAX1000), an average was taken and the total cell number determined. The following equation was

used to determine the number of population doublings from seeding to counting for every passage:

Population Doublings = $\log_2$(total cell number at collection / number of cells seeded)

For xCELLigence growth monitoring, the A-375 B1X2KO clone # 6 was split from a 24 well plate and equally seeded into 5 wells of a 96 well xCELLigence plate and 5 wells of a standard tissue culture 96 well plate. There were five conditions on each plate: untransduced, transduced with a TERT expression vector, B1S expression vector, or a B1L expression vector. Growth was monitored for 720 hours with media replaced every 168 hours.

Annexin V Apoptosis Assay

The assay was conducted using the Life Technologies Alexa Fluor 488 Annexin V/Dead staining kit (Life Technologies, cat #V13241) according to manufacturer's instructions and recommendations.

Statistical Analyses

The design for individual experiments is described above or in figure legends. For testing significance, two-tailed, unpaired Student's *t*-tests were used for RT-qPCR, luciferase assays, and ChIP-qPCR to compare differences between means of two groups. For comparisons among three or more conditions, global significance was determined via a one-way ANOVA. If significance was reached, individual comparisons were tested via two-tailed, unpaired Student's *t*-tests. For experiments involving large panels of cell lines, linear mixed-effects models were used to assess the association between experimental

readout (i.e., gene expression) and treatment (i.e., control vs. target gene knockdown), taking both technical and biological replicates into account. Mixed effects modeling was selected to account for the multiple aspects of each experiment with treatment and technical replicates as fixed effects, cell line replicates as a random intercept to account for within-cell line-replicate correlation, and experimental readout as the dependent variable[104]. As this was an exploratory analysis, no correction was made for multiple comparisons. Analyses were performed in R v4.0.2 using the lme function in the nlme library[105]. One-way ANOVA and Student's *t*-test was performed using GraphPad Prism statistical software (GraphPad Software, Inc). We define technical replicates as repeat measurements of a static sample (i.e., cell protein lysate, cDNA sample, etc.), biological replicates as physically distinct samples (i.e., each well of a well plate with a subsampling of a parental cell line, etc.), and experimental replicates as repeats of entire experimental protocols utilizing samples unique to the experimental replicate.

Analysis of pan-cancer RNA-seq expression

Normalized RNA-sequencing data from The Cancer Genome Atlas (TCGA) was downloaded in the form of RNA-Seq by Expectation Maximization (RSEM) calculated transcripts per million (TPM) values from the Broad Institute's Genome Data Analysis Center (GDAC) Firehose. We analyzed the gene expression of glioblastoma (GBM, *n*=613), low-grade glioma (LGG, *n*=516), bladder urothelial carcinoma (BLCA, *n*=412), thyroid carcinoma (THCA, *n*=503), skin cutaneous melanoma (SKCM, *n*=470), liver hepatocellular carcinoma (LIHC, *n*=377), head and neck squamous cell carcinoma

(HNSC, *n*=528), kidney renal clear cell carcinoma (KIRC, *n*=537), ovarian serous cystadenocarcinoma (OV, *n*=602), lung squamous cell carcinoma (LUSC, *n*=504), colon adenocarcinoma (COAD, *n*=460), rectum adenocarcinoma (READ, *n*=171), breast invasive carcinoma (BRCA, *n*=1098). A pseudo-count of 1 was added to the RSEM calculated TPM values and then these values were $\log_2$-transformed within their independent disease subgroup. The $\log_2$-transformed values of each gene was averaged across all subgroup samples to obtain disease-type-specific gene expression. Analysis and visualization of normalized pan-cancer RNA-sequencing data were conducted with R 4.1.2 and pheatmap version 1.0.12.

Analysis of Cancer Cell Line Encyclopedia (CCLE) RNA-seq expression

RNA-sequencing data for CCLE cell lines (Expression_22Q2_Public), in the form of RSEM calculated TPM values that have been $\log_2$ transformed with a pseudo-count of 1, was downloaded from the Dependency Map (DepMap) portal. We analyzed the gene expression of glioblastoma (GBM, *n*=48), low-grade glioma (LGG, *n*=16), bladder urothelial carcinoma (BLCA, *n*=37), thyroid carcinoma (THCA, *n*=14), skin cutaneous melanoma (SKCM, *n*=83), liver hepatocellular carcinoma (LIHC, *n*=22), head and neck squamous cell carcinoma (HNSC, *n*=56), kidney renal clear cell carcinoma (KIRC, *n*=33), ovarian serous cystadenocarcinoma (OV, *n*=65), non-small cell lung cancer (NSCLC, *n*=135), colon adenocarcinoma (COAD, *n*=72), breast invasive carcinoma (BRCA, *n*=61), meningioma (MNG, *n*=3), mesothelioma (MESO, *n*=20), medulloblastoma (MB, *n*=8). Gene expression for each gene was averaged within each tumor type to obtain disease-

type-specific gene expression. Analysis and visualization of RNA-sequencing data were conducted with R 4.2.1 and pheatmap version 1.0.12.

Analysis of AACR GENIE data

AACR GENIE v15.0 data was accessed via cBioportal and data sets for glioblastoma, melanoma, bladder cancer, and hepatocellular carcinoma generated with the following "Sequence Assay ID" were downloaded for analysis as they contain most of the TERT promoter mutation data in the database: "MSK-IMPACT468 or MSK-IMPACT505 or MSK-IMPACT410 or UCSF-IDTV5-TO or MSK-IMPACT341 or DFCI-ONCOPANEL-3 or DFCI-ONCOPANEL-3.1 or UCSF-NIMV4-TO or UCSF-NIMV4-TN or UCSF-IDTV5-TN or VHIO-300 or WAKE-CLINICAL-T7 or WAKE-CLINICAL-DX1 or DUKE-F1-DX1 or DUKE-F1-T7 or COLU-CSTP-V1 or YALE-OCP-V3 or UHN-OCA-V3 or UHN-TSO500-V1." All patients without a mutation called in the TERT promoter were assumed to be TERT promoter wildtype.

Determination of GABPA binding sites genome-wide

Paired-end ChIP-seq reads were mapped to the human genome (GRCh38) using bowtie2 (version 2.4.2)[106]. Mapped reads were filtered using the view command in samtools (version 1.12) with the options -h -F 4 -q 10 [107]. Reads mapped to the same genomic coordinates were deduplicated using the markdup command in samtools with the option -r. Peak calling for deduplicated reads was determined using the callpeak command in MACS2 (version 2.2.5) with a *q*-value threshold of 0.05 [108,109].

RNA isolation, RNA-Sequencing, and sequence analysis

RNA was isolated with the Qiagen AllPrep DNA/RNA/miRNA Universal Kit (Cat.80224) according to manufacturer's protocol. Following agilent profiling for quality control and qubit for quantification, 300 ng good quality RNA (RIN>7) was used for construction of RNA-seq libraries with KAPA Stranded mRNA-Seq Kit (Cat. KK8421). Briefly, mRNA was captured and fragmented to 200-300 bp before 1st strand cDNA synthesis. Second strand cDNA synthesis coverts cDNA:RNA hybrid to dsDNA while marking the 2nd strand with dUTP. After A-tailing repair, dscDNA was ligated with adapters with unique indexes. Adapter-ligated libraries were then amplified by PCR, cleaned up and quantified before pooled for sequencing on the Illumina Nova-Seq 6000 with a S4 flow cell and 150 bp paired-end reads.

Quantification of gene expression

Paired-end RNA-seq reads were mapped to the human genome (GRCh38) using HISAT2 (version 2.2.1) [110]. Mapped reads were filtered using the view command in samtools (version 1.12) with the options -h -F 4 -q 10. Reads mapped to the same genomic coordinates were deduplicated using the markdup command in samtools with the option -r [107]. To prevent ambiguous mapping between overlapping isoforms in B1KO, B1X2KO, B1LKO, and parental samples, custom reference transcriptomes were constructed, reflecting the isoforms present in each of the engineered samples. Reads from each of the B1KO, B1X2KO, B1LKO, and parental samples were thus mapped to their corresponding reference transcriptomes. Gene expression quantified both in terms of raw counts and TPM were determined using StringTie2 (version 2.1.1) using the

options -e -A [111]. Expression levels for samples with multiple technical replicates were determined by taking the average of gene abundance across replicates.

Differential gene expression

Differential gene expression analysis was performed using the DESeq2 package (version 1.34.0), where raw read counts of samples averaged over technical replicates were used as inputs[112]. For the two-group (knockout vs. control) analysis, genes were filtered out if the number of samples with counts per million (CPM) values greater than 1 was less than the number of samples in the smaller group. After filtering, normalized counts were fit to a negative-binomial distribution with a design matrix separating the m samples into two groups. Samples with a within-group Cook's distance greater than the 95% quantile of the *F*-distribution $F(2, m-2)$ were determined to be outliers and were replaced by the trimmed mean of the m samples, discarding the bottom 20% and top 20%, if the group contained 7 or more samples[113]. After replacing outliers of normalized counts with the trimmed mean, the normalized counts were refit to a negative binomial distribution, using the argument, fitType="local". A threshold of 0.05 for the *q*-values was used to determine differentially expressed (DE) genes (**table 5**)[109].

Gene ontology analysis

The EnrichR web tool was used to perform gene ontology (GO) analysis to determine the functional enrichment of gene sets that show significant DE between knockouts and parental cells[114-116]. All DE genes were used in the analysis. GO terms were selected from the Molecular Signatures Database (MSigDB) Hallmark gene

sets[117,118]. Functional terms enriched compared to the control set of all human genes with *q*-value < 0.05 were reported (**table 6**)[119].

Gene set enrichment analysis

Pre-ranked gene set enrichment analysis (GSEA)[117] was carried out by ranking genes with the product of their fold-change sign and the -log10(adjusted P value). Gene sets with a *q*-value < 0.05 and |normalized enrichment score| > 1 were considered enriched. Functional terms enriched compared to the control set of all human genes with *q*-value < 0.05 were reported (**table 6**).

Prediction of nucleosome occupancy

Nucleosome occupancy was predicted from H3K27ac and H3K4me3 histone modification ChIP-seq datasets in the A-375 cell line (SRR5660627 and SRR5660629 in the Sequence Read Archive)[120]. Paired-end ChIP-seq reads were mapped to the human genome (GRCh38) using bowtie2 (version 2.4.2). Mapped reads were filtered using the view command in samtools (version 1.12) with the options -h -F 4 -q 10. Nucleosome occupancy was determined with the NPS package (version 1.3.2), using default parameters and using only filtered paired-end reads[121].

Structure of the convolutional neural network (CNN) for learning GABPA binding patterns

A CNN binary classifier was designed to predict whether a given 101 bp-long sequence belongs to a GABPA ChIP-seq peak. One-hot encoded arrays of size 101×4

were used as CNN inputs, each array representing a 101 bp-long sequence, with the rows corresponding to the nucleotide positions in the sequence and the columns encoding the presence or absence of a particular nucleotide. The first layer of the CNN generated another 101×4 array representing the reverse complement of the input sequence and concatenated the reverse complement array with the original array, creating a 101×8 array. The resulting 101×8 array was passed through a convolution layer with 8 convolutional filters of size 8×4 and stride 1×4. The convolutional layer output was passed through a max pooling layer of size 6×2 and a dropout layer of dropout rate 0.2 to reduce overfitting. The dropout layer output was further passed through a fully connected layer with 50 neurons using a rectified linear unit (ReLu) activation. The output of the fully connected layer was passed through a final layer consisting of a single neuron with a sigmoid activation, yielding a final output value between 0 and 1. The greater the output, the more likely for the input sequence to be from a peak region. The CNN was constructed using the Python package Keras https://keras.io.

CNN training

The CNN was trained as a binary classifier to predict whether a given sequence belongs to a GABPA ChIP-seq peak. The dataset used to train the CNN consisted of 101 bp-long sequences centered at the summits of the GABPA parental ChIP-seq peaks. A corresponding negative control set was constructed by randomly permuting the nucleotides in each sequence. The full dataset was divided into 80% training, 10% validation, and 10% test sets. The CNN was trained on the training set. Training was

terminated when there was no improvement in the binary cross-entropy loss on the validation set for 10 consecutive epochs, and the CNN model at the epoch with the lowest validation loss was considered for further analysis. The classification accuracy was determined using the test set. The CNN was trained using the binary cross-entropy loss function and the stochastic gradient descent optimizer with Nesterov momentum of 0.9, initial learning rate of 10^{-3}, and decay factor of 10^{-6}.

Identifying salient sequence features learned by the CNN in GABPA ChIP-seq peaks

After the CNN was trained, MaxEnt, a deep neural network interpretation method based on Markov Chain Monte Carlo (MCMC) sampling, was used to determine the important subsequences learned by the CNN in classifying a sequence as being bound by GABP[122]. In MaxEnt, inputs were initialized using sequences in the test set with a CNN prediction output greater than 0.95. Next, random bases from the input sequences were iteratively mutated, where in the i^{th} iteration step of MCMC sampling, the i^{th} proposed sequence is generated by mutating 4 random bases of the sequence from the previous step into 4 random nucleotides. The MCMC acceptance probability of the proposed sequence was determined by the similarity between the CNN prediction values of the proposed sequence and the previous sequence; the less important the mutated bases in the CNN prediction, the more similar the CNN prediction output of the proposed sequence to that of the previous sequence, thereby yielding a high acceptance probability for proposals that average out unimportant subsequences.

For each input sequence, we initiated 1000 independent Markov chains, and after a large number of MCMC steps, the simulated sequences from the last step were averaged over all chains, resulting in a position-specific score matrix (PSSM). To determine the number of iterations, we first define K_j as the Kullback-Leibler (KL) divergence of the nucleotide frequency at base j from the uniform nucleotide distribution and define K_{max} as the maximum possible KL divergence from the uniform nucleotide distribution. Iteration stops if $\underset{j}{\text{med}}\, K_j < 0.05 \times K_{max}$. Important sub-sequences were defined as bases that are within a 3bp window of a base j satisfying $K_j > 0.9 \times K_{max}$.

Constructing a GABPA binding motif based on sequences from localized regions

A consensus GABPA motif was constructed using the PSSMs from the MaxEnt method, as follows: The PSSMs encode sequence motifs having varying length and orientations. To filter out PSSMs that were too short or too long, the distribution of the PSSM lengths was fitted to a normal distribution. Denoting the mean and the standard deviation of the normal distribution as μ and σ, respectively, PSSMs with a length outside the 2σ range of the fitted normal distribution were filtered out. To align the PSSMs after filtering, we attempted gap-free alignment of every pair of PSSMs and their reverse complements under the constraint that at least 6 bps must overlap. For every possible combination of alignment configurations, we averaged the position-wise Jensen-Shannon (JS) divergence across the overlapping bases. Two PSSMs were considered to be aligned if their relative configuration minimized the JS divergence between the PSSMs. Defining $D\left(PSSM_i, PSSM_j\right)$ as the minimum JS divergence between $PSSM_i$ and $PSSM_j$, we

chose a central PSSM, $PSSM_c$, such that $PSSM_c = \underset{PSSM \in S}{\operatorname{argmin}} \sum_j D(PSSM, PSSM_j)$, where $S = \{PSSM | length(PSSM) < \mu\}$. All PSSMs were aligned with respect to $PSSM_c$ and averaged position wise to yield the GABPA motif learned by the CNN.

AlphaFold2 structure predictions

AlphaFold v2.3.2 and its reference databases were installed. To determine the minimal portion of B1 for use as a binding protein for GABPA, iterative single residue extensions (from amino acid 157 to 170) of the carboxy end of the human B1 equivalent of the sequence used for the murine crystal structure (B1 amino acids 5-157) were modeled in multimer mode with amino acids 320-429 of the human GABPA (the human equivalent of the GABPA residues used to generate the murine crystal structure of GABP)[47]. The sequence that was predicted to complete the ankyrin repeat domain of the human B1 (determined by inspecting predicted structures) as well as had a high predicted confidence score and high per residue pLDDT was selected. For **figure S7B**: the top-ranking models for B1 5-157, B1 5-166, and B1 5-170 were visualized with pLDDT scores overlaid via ChimeraX. FASTA files were generated containing the sequence of the GABPA degrader and of the amino acids 320-429 of the human GABPA. AlphaFold was run in multimer mode with default options and the highest rank resulting pdb file was visualized using Pymol. Image was exported with settings “ray 5000,5000” and “png image,dpi=2400”.

ChIP-qPCR for the GABPA degrader samples

ChIP for the GABPA degrader expressing cell lines was performed using the Cell Signaling SimpleChIP Plus Sonciation kit (cat # 56383). Experiments were conducted according to manufacturer specifications, with the following notes. Cell lines were seeded at a density of 10 million cells per 15 cm dish in triplicate. Twenty-four hours after seeded one 15 cm dish was counted and viability confirmed to be greater than 90%. Cells were fixed with a final concentration of 1% methanol-free formaldehyde (Pierce, #PI28908) for 9 minutes and neutralized with glycine added according to the cell signaling protocol. Chromatin was sonicated with the Covaris S2 Focused Ultrasonicator for 8 minutes to achieve a size range of 200-1000 bp. Immunoprecipitations were conducted with 15 ug of sheared chromatin and with one of the following antibodies: 2.66 ug of anti-GABPA (Invitrogen, #PA5-27735, RRID:AB_2545211), 10 uL of anti-H3K4me3 (Cell Signaling, #9751S, RRID: AB_2616028), 6 uL of anti-H3K27me3 (Active Motif, #39155, RRID: AB_2561020), or 4 uL (4 ug) normal rabbit IgG control (Cell Signaling, #2729, RRID:AB_1031062). qPCR was conducted as noted previously.

Orthotopic Tumor Model

All experiments used 6- to 7-week-old female athymic nu/nu mice NU/J (Homozygous for Foxn1^{nu} mice (JAX, 002019). Animals were handled in the Animal Facility at UCSF, per an Institutional Animal Care and Use Committee-approved protocol. Luciferase positive U-251 cells were generated via transduction with a 3rd generation self-inactivating replication defective lentivirus (pRRL-sin) with the luciferase gene driven by a CMV promoter. 4x10^5 U251 cells stably expressing firefly luciferase transduced

with either an empty lentiviral vector (n=7 mice) or a lentiviral vector encoding the GABPA degrader (n =10 mice) were stereotactically implanted in a total volume of 4 µl into the right frontal cortex (mediolateral [ML]: 1.5 mm, anteroposterior [AP]: 1 mm, and dorsoventral [DV]: -3.5 mm, relative to bregma)[27]. Tumor progression was evaluated by luminescence emission on a Xenogen IVIS Spectrum 10 min after an i.p. injection of 150 mg/kg D-luciferin (Revvity, 122799) prepared according to the manufacturer's instructions. The radiance signal (p/s) was used to generate all tumor growth data, with results presented as mean±SEM.

Magnetic Resonance Imaging

Animal studies were conducted in accordance with UCSF Institutional Animal Care and Use Committee guidelines. SCID mice were intracranially injected with 3 x 10^5 U-251 cells expressing an empty vector or the GABPA degrader as described before[73]. All magnetic resonance (MR) studies were performed on a Bruker 3T preclinical horizontal MR scanner. Axial T2-weighted images were acquired using a spin echo TurboRARE sequence (TE/TR = 64/3484ms, FOV = 30 × 30mm^2, 256 × 256, slice thickness = 1.5mm, NA = 6). Tumors were contoured manually, and volume calculated as the sum of the areas multiplied by slice thickness[73]. Once tumors reached a volume of 87±18.6mm^3 ^{2}H-MR studies were performed using a 16 mm ^{2}H surface coil. Following intravenous injection of a bolus of [U-^{2}H]-pyruvate (450mg/kg), a two-dimensional (2D) chemical shift imaging (CSI) sequence with a temporal resolution of 8min 26s (TE/TR = 1.04/263.617ms, FOV = 30 x 30mm^3, 128 points, 512.82kHz spectral width, NA = 30, nominal voxel size = 112.5 mL) was used to collect spatial localized metabolic signals.

Data were analyzed using in-house Matlab codes as described before[73]. The concentration of ^{2}H-lactate was quantified in a 10.99mm^{3} volume from tumor and contralateral normal brain. All experiments were performed on a minimum of three samples (n = 4 control and n=3 GABPA degrader) and results presented as mean±SD.

Prediction of ASO hybridization to *GABPB1* transcripts

Prediction of ASO hybridization to regions in the *GABPB1* isoforms was conducted using the default parameters of the RNAplex package in the ViennaRNA suite (v2.4.14)[123-125]. Hybridization affinities were determined by calculating the hybridization energies (kcal/mol) of the ASO to 25 bp-long sliding windows across *GABPB1* mRNA isoforms. An individual window was declared as containing a potential off-target hybridization site if the maximum absolute energy value $|E|$, corresponding to the optimal hybridization configuration with minimum free energy, in that window was within the upper 5% of $|E|$ values in *GABPB1* isoforms and if the window did not contain any bases of the designated ASO on-target site.

Data and materials availability:

Processed differential gene expression analysis via DESeq2 are available in supplementary **table S5**. Pre-processed RNA-seq and ChIP-seq data are deposited at Gene Expression Omnibus (https://www.ncbi.nlm.nih.gov/geo/) under accession GSE224166. All other data are available in the main text or the supplementary materials. Please contact the corresponding author for any other materials.

Chapter 9: Tables

Table 1 - Pan cancer siRNA statistics: Pan-cancer cell lines siRNA experiment statistics by cell line.
p values from comparison of each siRNA treatment to siNon-targeting within each cell line via linear mixed-effects models.

		TERT expression		
Cancer type	Cell line	siGABPA vs siNon-targeting	siGABPB1 vs siNon-targeting	siGABPB2 vs siNon-targeting
BLCA	5637	0	0	0.7811
BLCA	TCCSUP	0	0	0
BLCA	UM-UC-3	0	0	0
BLCA	HT-1376	0	0	0.0055
BLCA	639-V	0	0	0.6774
GBM	LN-229	0	0	0.9973
GBM	U-251	0	0.7596	0.0022
THCA	SW 579	0.0001	0.3664	0.0038
THCA	MDA-T120	0	0	0.5736
THCA	MDA-T32	0	0	0.6766
THCA	MDA-T85	0	0	0
SKCM	A-375	0	0	0.0006
SKCM	SK-MEL-2	0	0	0.0134
SKCM	SK-MEL-5	0	0	0.047
SKCM	WM-266-4	0	0	0.0189
SKCM	SK-MEL-24	0	0.0001	0.1022
SKCM	WM793B	0	0	0.7575
SKCM	SK-MEL-28	0	0	0.0379
SKCM	COLO 829	0	0	0.1991
LIHC	SNU-475	0	0	0
LIHC	SNU-423	0	0	0.3643
LIHC	Huh-7	0	0	0.4595
LIHC	SNU-398	0	0	0.0591
HNSC	Cal-33	0	0.0012	0
HNSC	CAL 27	0	0.0108	0
HNSC	PE/CA-PJ49	0.0802	0	0
KIRC	786-O	0	0	0
MB	Daoy	0	0	0
OV	ES-2	0	0	0
OV	RMG-I	0	0	0.0045
OV	VOA-10816	0	0	0
MESO	NCI-H2052	0	0	0.8744
LUAD	NCI-H1435	0	0	0.0174
LUSC	CALU-1	0	0	0
COAD/READ	MDST8	0.0001	0.0016	0

		TERT expression		
Cancer type	Cell line	siGABPA vs siNon-targeting	siGABPB1 vs siNon-targeting	siGABPB2 vs siNon-targeting
BRCA	MDA-MB-231	0	0	0.0001
MNG	CH157-MN	0	0	0.0189
LGG	SF10417	0.0015	0.6325	0

Table 1 (cont.) - Pan cancer siRNA statistics:

		GABPA expression		
Cancer type	Cell line	siGABPA vs siNon-targeting	siGABPB1 vs siNon-targeting	siGABPB2 vs siNon-targeting
BLCA	5637	0	0.0173	0.0124
BLCA	TCCSUP	0	0.8297	0.0891
BLCA	UM-UC-3	0	0	0.3634
BLCA	HT-1376	0	0.2215	0.0077
BLCA	639-V	0.0001	0	0.5539
GBM	LN-229	0	0.0001	0
GBM	U-251	0	0.1444	0.3855
THCA	SW 579	0	0.3525	0.468
THCA	MDA-T120	0	0	0
THCA	MDA-T32	0	0.0825	0
THCA	MDA-T85	0	0	0.0007
SKCM	A-375	0	0.0003	0.0212
SKCM	SK-MEL-2	0	0	0.1494
SKCM	SK-MEL-5	0	0	0.9277
SKCM	WM-266-4	0	0	0.727
SKCM	SK-MEL-24	0	0	0.0114
SKCM	WM793B	0	0.0194	0.0401
SKCM	SK-MEL-28	0	0	0.1938
SKCM	COLO 829	0	0	0.0176
LIHC	SNU-475	0	0	0
LIHC	SNU-423	0	0.554	0.0005
LIHC	Huh-7	0.0001	0	0.0757
LIHC	SNU-398	0	0	0.261
HNSC	Cal-33	0	0.0214	0.6797
HNSC	CAL 27	0	0	0.0058
HNSC	PE/CA-PJ49	0	0.001	0
KIRC	786-O	0	0	0
MB	Daoy	0	0	0.0003
OV	ES-2	0	0.0038	0.1702
OV	RMG-I	0	0	0.4345
OV	VOA-10816	0	0.0005	0.7669
MESO	NCI-H2052	0	0.0572	0.205
LUAD	NCI-H1435	0	0	0.0773
LUSC	CALU-1	0	0.5107	0.2357
COAD/READ	MDST8	0	0	0.0931
BRCA	MDA-MB-231	0	0	0.0313

		GABPA expression		
Cancer type	Cell line	siGABPA vs siNon-targeting	siGABPB1 vs siNon-targeting	siGABPB2 vs siNon-targeting
MNG	CH157-MN	0.0044	0.0002	0.2642
LGG	SF10417	0	0	0.079

Table 1 (cont.) - Pan cancer siRNA statistics:

		GABPB1 expression		
Cancer type	Cell line	siGABPA vs siNon-targeting	siGABPB1 vs siNon-targeting	siGABPB2 vs siNon-targeting
BLCA	5637	0	0.0001	0.0416
BLCA	TCCSUP	0	0	0.2003
BLCA	UM-UC-3	0	0	0.4284
BLCA	HT-1376	0	0	0.0003
BLCA	639-V	0	0	0.022
GBM	LN-229	0	0	0.0865
GBM	U-251	0	0.6405	0.2072
THCA	SW 579	0	0.0715	0.7402
THCA	MDA-T120	0	0	0.0064
THCA	MDA-T32	0	0	0.0969
THCA	MDA-T85	0	0	0.0919
SKCM	A-375	0	0.0002	0.181
SKCM	SK-MEL-2	0	0.0004	0.5685
SKCM	SK-MEL-5	0	0	0.6687
SKCM	WM-266-4	0	0.002	0.3184
SKCM	SK-MEL-24	0	0	0.5629
SKCM	WM793B	0	0	0.3224
SKCM	SK-MEL-28	0	0	0.0881
SKCM	COLO 829	0	0	0.2121
LIHC	SNU-475	0	0	0
LIHC	SNU-423	0	0	0.0002
LIHC	Huh-7	0	0	0.2069
LIHC	SNU-398	0	0	0.0492
HNSC	Cal-33	0	0	0.6597
HNSC	CAL 27	0	0	0.0043
HNSC	PE/CA-PJ49	0.0009	0	0.8815
KIRC	786-O	0	0	0
MB	Daoy	0	0.0006	0.0073
OV	ES-2	0	0	0.9687

		GABPB1 expression		
Cancer type	Cell line	siGABPA vs siNon-targeting	siGABPB1 vs siNon-targeting	siGABPB2 vs siNon-targeting
OV	RMG-I	0	0.0002	0.5527
OV	VOA-10816	0	0	0.168
MESO	NCI-H2052	0	0	0.3462
LUAD	NCI-H1435	0	0	0.407
LUSC	CALU-1	0	0	0.4825
COAD/READ	MDST8	0	0.0039	0.0897
BRCA	MDA-MB-231	0	0	0.4291
MNG	CH157-MN	0	0	0.0511
LGG	SF10417	0	0.0022	0.3614

Table 1 (cont.) - Pan cancer siRNA statistics:

p values from comparison of each siRNA treatment to siNon-targeting within each cancer type via linear mixed-effects models.

	TERT expression		
Cancer type	siGABPA vs siNon-targeting	siGABPB1 vs siNon-targeting	siGABPB2 vs siNon-targeting
BLCA	0	0	0.8883
GBM	0	0.0005	0.2131
THCA	0	0	0.6681
SKCM	0	0	0.0027
LIHC	0	0	0.6627
HNSC	0	0.067	0
KIRC	0	0	0
MB	0	0	0
OV	0	0	0
MESO	0	0	0.8744
LUAD	0	0	0.0174
LUSC	0	0	0
COAD/READ	0.0001	0.0016	0
BRCA	0	0	0.0001
MNG	0	0	0.0189
LGG	0.0015	0.6325	0

Table 1 (cont.) - Pan cancer siRNA statistics:

	GABPA expression		
Cancer type	siGABPA vs siNon-targeting	siGABPB1 vs siNon-targeting	siGABPB2 vs siNon-targeting
BLCA	0	0	0.7978
GBM	0	0.1795	0.0041
THCA	0	0.0012	0.278
SKCM	0	0	0.1067
LIHC	0	0	0.5367
HNSC	0	0.0405	0.0061
KIRC	0	0	0
MB	0	0	0.0003
OV	0	0	0.3127
MESO	0	0.0572	0.205
LUAD	0	0	0.0773
LUSC	0	0.5107	0.2357
COAD/READ	0	0	0.0931
BRCA	0	0	0.0313
MNG	0.0044	0.0002	0.2642
LGG	0	0	0.079

	GABPB1 expression		
Cancer type	siGABPA vs siNon-targeting	siGABPB1 vs siNon-targeting	siGABPB2 vs siNon-targeting
BLCA	0	0	0.886
GBM	0	0.4943	0.7821
THCA	0	0	0.8425
SKCM	0	0	0.8558
LIHC	0	0	0.385
HNSC	0	0	0.382
KIRC	0.0009	0	0
MB	0	0.0006	0.0073
OV	0	0	0.3371
MESO	0	0	0.3462
LUAD	0	0	0.407
LUSC	0	0	0.4825
COAD/READ	0	0.0039	0.0897
BRCA	0	0	0.4291
MNG	0	0	0.0511
LGG	0	0.0022	0.3614

Table 1 (cont.) - Pan cancer siRNA statistics:

	GABPB2 expression		
Cancer type	siGABPA vs siNon-targeting	siGABPB1 vs siNon-targeting	siGABPB2 vs siNon-targeting
BLCA	0	0	0
GBM	0.2625	0	0.0936
THCA	0	0.0008	0
SKCM	0	0	0
LIHC	0	0	0.0007
HNSC	0	0.0005	0.0001
KIRC	0	0.0145	0
MB	0	0	0.0159
OV	0	0	0
MESO	0.0006	0.7757	0
LUAD	0	0	0
LUSC	0	0.4517	0
COAD/READ	0.0011	0.0138	0
BRCA	0.0005	0	0
MNG	0	0.0001	0
LGG	0	0	0

p values from comparison of each siRNA treatment to siNon-targeting within each *TERT*p mutation via linear mixed-effects models.

	TERT expression
	siGABPA vs siNon-targeting
G228A	0
G250A	0
GG242/243AA	0
T161G	0
G228T	0
GG228/229AA	0

Table 2 – Cell line information: Pan-cancer culture conditions, STR results, *TERT* promoter genotyping compared to expected, and usage in ChIP-qPCR and siRNA-qPCR.

Cell Line Name	Basal Media	Additional Supplements	Gender	Ethnicity
5637	RPMI-1640	10% FBS, 1X Pen/Strep	Male	Asian
253J-BV	DMEM	10% FBS, 1X Pen/Strep	Male	Caucasian
639-V	DMEM	10% FBS, 1X Pen/Strep	Male	Caucasian
769-P	RPMI-1640	10% FBS, 1X Pen/Strep	Female	Caucasian
786-O	RPMI-1640	10% FBS, 1X Pen/Strep	Male	Caucasian
A-375	RPMI-1640	10% FBS, 1X Pen/Strep	Female	Caucasian
BICR-6	DMEM	10% FBS, 1X Pen/Strep	Male	Caucasian
Cal 27	DMEM	10% FBS, 1X Pen/Strep	Male	Caucasian
Cal-33	DMEM	10% FBS, 1X Pen/Strep	Male	Caucasian
CALU-1	M5A	10% FBS, 1X Pen/Strep	Male	Caucasian
CH157-MN	EMEM	10% FBS, 1X Pen/Strep	Female	
COLO-829	RPMI-1640	10% FBS, 1X Pen/Strep	Male	Caucasian
Daoy	EMEM	10% FBS, 1X Pen/Strep	Male	Caucasian
DI-98	EMEM	10% FBS, 1X Pen/Strep		
ES-2	M5A	10% FBS, 1X Pen/Strep	Female	Caucasian
Fadu	DMEM	10% FBS, 1X Pen/Strep	Male	Caucasian
HCT116	M5A	10% FBS, 1X Pen/Strep	Male	Caucasian
HT-1376	EMEM	10% FBS, 1X Pen/Strep	Female	Caucasian
Huh-7	DMEM	10% FBS, 1X Pen/Strep	Male	Asian
LN-18	DMEM:F12	10% FBS, 1X Pen/Strep	Male	Caucasian
LN-229	DMEM:F12	10% FBS, 1X Pen/Strep	Female	Caucasian
MDA-MB-231	RPMI-1640	10% FBS, 1X Pen/Strep	Female	Caucasian
MDA-MB-453	RPMI-1640	10% FBS, 1X Pen/Strep	Female	Caucasian
MDA-T120	RPMI-1640	10% FBS, 1X NEAA, 1X Pen/Strep	Female	
MDA-T32	RPMI-1640	10% FBS, 1X NEAA, 1X Pen/Strep	Male	Caucasian
MDA-T41	RPMI-1640	10% FBS, 1X NEAA, 1X Pen/Strep	Male	Caucasian
MDA-T85	RPMI-1640	10% FBS, 1X NEAA, 1X Pen/Strep	Male	Hispanic
MDST8	DMEM	10% FBS, 1X Pen/Strep		Caucasian
NCI-H1299	RPMI-1640	10% FBS, 1X Pen/Strep	Male	Caucasian
NCI-H1435	RPMI-1640	5% FBS, 1X Pen/Strep	Female	Caucasian
NCI-H2052	RPMI-1640	10% FBS, 1X Pen/Strep	Male	Caucasian
PE/CA-PJ49	DMEM	10% FBS, 1X Pen/Strep	Male	Caucasian

Cell Line Name	Basal Media	Additional Supplements	Gender	Ethnicity
RMG-I	RPMI-1640	5% FBS, 1X Pen/Strep	Female	Asian
RMG-II	RPMI-1640	5% FBS, 1X Pen/Strep	Female	Asian
RPMI 2650	EMEM	10% FBS, 1X Pen/Strep	Male	
RPMI-7951	EMEM	10% FBS, 1X NEAA, 1X Pen/Strep	Female	Caucasian
SF10417	Neurocult NS-A (STEMCELL Technologies Cat. #05751)	N-2 supplement (Invitrogen Cat. #17502048), B-27 supplement minus vitamin A (Invitrogen Cat. #12587010), 1% P/S, 1% glutamine, and 1% sodium pyruvate,20 ng/mL EGF (Peprotech Cat. #AF-100-15), bFGF (Peprotech Cat. #AF-100-18B), and PDGF-AA (Peprotech Cat. #AF-100-13A).		
SK-MEL-2	EMEM	10% FBS, 1X NEAA, 1X Pen/Strep	Male	Caucasian
SK-MEL-24	EMEM	10% FBS, 1X NEAA, 1X Pen/Strep	Male	Caucasian
SK-MEL-28	EMEM	10% FBS, 1X NEAA, 1X Pen/Strep	Male	Caucasian
SK-MEL-5	EMEM	10% FBS, 1X Pen/Strep	Female	Caucasian
SNU-182	RPMI-1640	10% FBS, 1X Pen/Strep	Male	Asian
SNU-387	RPMI-1640	10% FBS, 1X Pen/Strep	Female	Asian
SNU-398	RPMI-1640	10% FBS, 1X Pen/Strep	Male	Asian
SNU-423	RPMI-1640	10% FBS, 1X Pen/Strep	Male	Asian
SNU-475	RPMI-1640	10% FBS, 1X Pen/Strep	Male	Asian
SW 579	RPMI-1640	10% FBS, 1X Pen/Strep	Male	Caucasian
TCCSUP	EMEM	10% FBS, 1X Pen/Strep	Female	Caucasian
U-251 MG (KO)	DMEM:F12	10% FBS, 1X Pen/Strep	Male	Caucasian
UM-UC-3	EMEM	10% FBS, 1X Pen/Strep	Male	Caucasian
VOA-10816	M199/MCDB105	5% FBS, 1X Pen/Strep	Female	#N/A
VOA-4841	M199/MCDB105	5% FBS, 1X Pen/Strep	Female	#N/A
WM-266-4	EMEM	10% FBS, 1X NEAA, 1X Pen/Strep	Female	#N/A
WM793B	DMEM	10% FBS, 1X Pen/Strep	Male	Caucasian
293T	DMEM	10% FBS, 1X Pen/Strep		

Table 2 (cont.) – Cell line information:

Cell Line Name	age	Expected TERTp Mutation	TERTp Sanger Sequencing Results
5637	68	5.1295228.G.A	5.1295228.G.A
253J-BV	53	Wildtype	Wildtype
639-V	69	5.1295228.G.A	5.1295228.G.A
769-P	63	Wildtype	Wildtype
786-O	58	5.1295228.G.A	5.1295228.G.A
A-375	54	5.1295250.G.A	5.1295250.G.A
BICR-6	0	Wildtype	Wildtype
Cal 27	56	5.1295228.G.A	5.1295228.G.A
Cal-33	69	5.1295228.G.A	5.1295228.G.A
CALU-1	47	5.1295228.G.A	homozygous 5.1295228.G.A
CH157-MN	41	5.1295228.G.A	Homozygous 5.1295228.G.A
COLO-829	45	5.1295228-1295229.GG.AA	5.1295228-1295229.GG.AA
Daoy	4	5.1295228.G.A	5.1295228.G.A
DI-98		Wildtype	Wildtype
ES-2	47	5.1295242-1295243.GG.AA	5.1295242-1295243.GG.AA
Fadu	56	Wildtype	Wildtype
HCT116	48	Wildtype	Wildtype
HT-1376	58	5.1295228.G.A	5.1295228.G.A
Huh-7	57	5.1295228.G.A	5.1295228.G.A
LN-18	65	Wildtype	Wildtype
LN-229	60	5.1295228.G.A	5.1295228.G.A
MDA-MB-231	51	5.1295228.G.A	5.1295228.G.A
MDA-MB-453	48	Wildtype	Wildtype
MDA-T120	72	5.1295228.G.A	5.1295228.G.A
MDA-T32	74	5.1295228.G.A	5.1295228.G.A
MDA-T41	74	Wildtype	Wildtype
MDA-T85	61	5.1295228.G.A	5.1295228.G.A
MDST8		5.1295250.G.A	homozygous 5.1295250.G.A
NCI-H1299	43	Wildtype	Wildtype
NCI-H1435	35	5.1295228.G.T	5.1295228.G.T
NCI-H2052	65	5.1295228.G.A	5.1295228.G.A
PE/CA-PJ49	57	5.1295250.G.A	5.1295250.G.A
RMG-I	34	5.1295228.G.A	5.1295228.G.A
RMG-II	53	Wildtype	Wildtype
RPMI 2650	52	Wildtype	Wildtype

Cell Line Name	age	Expected TERTp Mutation	TERTp Sanger Sequencing Results
RPMI-7951	18	5.1295242-1295243.GG.AA	5.1295242-1295243.GG.AA
SF10417	#N/A	5.1295228.G.A	5.1295228.G.A
SK-MEL-2	60	5.1295250.G.A	5.1295250.G.A
SK-MEL-24	67	5.1295228.G.A	5.1295228.G.A
SK-MEL-28	51	5.1295161.T.G	5.1295161.T.G
SK-MEL-5	24	5.1295242-1295243.GG.AA	5.1295242-1295243.GG.AA
SNU-182	24	Wildtype	Wildtype
SNU-387	41	5.1295228.G.A	5.1295228.G.A
SNU-398	42	5.1295228.G.A	5.1295228.G.A
SNU-423	40	5.1295228.G.A	5.1295228.G.A
SNU-475	43	5.1295228.G.A	5.1295228.G.A
SW 579	59	5.1295228.G.A	5.1295228.G.A
TCCSUP	67	5.1295228.G.A	5.1295228.G.A
U-251 MG (KO)	75	5.1295228.G.A	5.1295228.G.A
UM-UC-3	0	5.1295228.G.A	5.1295228.G.A
VOA-10816	#N/A	5.1295228.G.A	5.1295228.G.A
VOA-4841	#N/A	Wildtype	Wildtype
WM-266-4	55	5.1295250.G.A	5.1295250.G.A
WM793B	37	5.1295228.G.A	5.1295228.G.A
293T			

Table 2 (cont.) – Cell line information:

Cell Line Name	Source	Cancer
5637	UCSF, Felix Feng lab	Bladder
253J-BV	UCSF, Felix Feng lab	Bladder
639-V	UCSF, Felix Feng lab	Bladder
769-P	UCSF Cell Line Repository	Kidney
786-O	UCB Cell Line Repository	Kidney
A-375	UCSF, Robert Judson lab	Melanoma
BICR-6	UCSF, Jennifer Grandis lab	Head and Neck
Cal 27	UCSF, Jennifer Grandis lab	Head and Neck
Cal-33	UCSF, Jennifer Grandis lab	Head and Neck
CALU-1	ATCC	Lung
CH157-MN	UCSF, David Raleigh lab	Meningioma
COLO-829	ATCC	Melanoma

Cell Line Name	Source	Cancer
Daoy	UCSF Cell Line Repository	Embryonal Tumor
DI-98	UCSF, David Raleigh lab	Meningioma
ES-2	UCSF Cell Line Repository	Ovarian
Fadu	UCSF, Jennifer Grandis (Hua Li)	Head and Neck
HCT116	UCSF Cell Line Repository	Colorectal
HT-1376	UCSF, Felix Feng (Jonathan Chou)	Bladder
Huh-7	UCSF, John Gordan	Liver
LN-18	UCSF, Costello Lab	Glioma
LN-229	UCSF, Costello Lab	Glioma
MDA-MB-231	UCSF Cell Line Repository	Breast
MDA-MB-453	UCSF Cell Line Repository	Breast
MDA-T120	ATCC	Thyroid
MDA-T32	ATCC	Thyroid
MDA-T41	ATCC	Thyroid
MDA-T85	ATCC	Thyroid
MDST8	ECACC via Sigma	Colorectal
NCI-H1299	UCB Cell Line Repository	Lung
NCI-H1435	ATCC	Lung
NCI-H2052	ATCC	Lung
PE/CA-PJ49	UCSF, Jennifer Grandis lab	Head and Neck
RMG-I	UCSF, Alan Ashworth lab	Ovarian
RMG-II	BCC, David Huntsman lab	Ovarian
RPMI 2650	UCSF Cell Line Repository	Head and Neck
RPMI-7951	UCSF Cell Line Repository	Melanoma
SF10417	UCSF, Costello Lab	Glioma
SK-MEL-2	UCSF, Robert Judson lab	Melanoma
SK-MEL-24	UCSF Cell Line Repository	Melanoma
SK-MEL-28	UCSF Cell Line Repository	Melanoma
SK-MEL-5	UCSF, Robert Judson lab	Melanoma
SNU-182	UCSF, John Gordan lab	Liver
SNU-387	UCSF, John Gordan lab	Liver
SNU-398	UCSF, John Gordan lab	Liver
SNU-423	UCSF, John Gordan lab	Liver
SNU-475	UCSF, John Gordan lab	Liver
SW 579	UCSF Cell Line Repository	Thyroid
TCCSUP	UCSF, Felix Feng lab	Bladder
U-251 MG (KO)	UCSF, Costello Lab	Glioma
UM-UC-3	UCSF, Felix Feng lab	Bladder

Cell Line Name	Source	Cancer
VOA-10816	BCC, David Huntsman lab	Ovarian
VOA-4841	BCC, David Huntsman lab	Ovarian
WM-266-4	UCSF Cell Line Repository	Melanoma
WM793B	UCSF, Robert Judson lab	Melanoma
293T		

Table 2 (cont.) – Cell line information:

Cell Line Name	STR % Match Reference	Used for ChIP-qPCR?	Used for siRNA and RT-qPCR?
5637	100	Yes	Yes
253J-BV	100	Yes	No
639-V	80	Yes	Yes
769-P	100	Yes	No
786-O	100	Yes	Yes
A-375	100	Yes	Yes
BICR-6	95.6	Yes	No
Cal 27	100	Yes	Yes
Cal-33	96.6	Yes	Yes
CALU-1	100	Yes	Yes
CH157-MN	No Reference Profile	Yes	Yes
COLO-829	100	Yes	Yes
Daoy	94	Yes	Yes
DI-98	No Reference Profile	Yes	No
ES-2	100	Yes	Yes
Fadu	100	Yes	No
HCT116	100	Yes	No
HT-1376	100	Yes	Yes
Huh-7	100	Yes	Yes
LN-18	100	Yes	No
LN-229	96	Yes	Yes
MDA-MB-231	100	Yes	Yes
MDA-MB-453	100	Yes	No
MDA-T120	100	Yes	Yes
MDA-T32	ATCC	Yes	Yes
MDA-T41	ATCC	Yes	No
MDA-T85	ATCC	Yes	Yes
MDST8	100	Yes	Yes

Cell Line Name	STR % Match Reference	Used for ChIP-qPCR?	Used for siRNA and RT-qPCR?
NCI-H1299	94	Yes	No
NCI-H1435	ATCC	Yes	Yes
NCI-H2052	100	Yes	Yes
PE/CA-PJ49	100	Yes	Yes
RMG-I	96	Yes	Yes
RMG-II	100	Yes	No
RPMI 2650	100	Yes	No
RPMI-7951	96.2	Yes	No
SF10417	No Reference Profile	Yes	Yes
SK-MEL-2	96.9	Yes	Yes
SK-MEL-24	93.7	No	Yes
SK-MEL-28	83.8	Yes	Yes
SK-MEL-5	96.7	Yes	Yes
SNU-182	100	Yes	No
SNU-387	100	Yes	No
SNU-398	100	Yes	Yes
SNU-423	96	Yes	Yes
SNU-475	100	Yes	Yes
SW 579	88	Yes	Yes
TCCSUP	100	Yes	Yes
U-251 MG (KO)	89.6	Yes	Yes
UM-UC-3	100	Yes	Yes
VOA-10816	96.2	Yes	Yes
VOA-4841	100	Yes	No
WM-266-4	100	Yes	Yes
WM793B	96.3	Yes	Yes
293T			

Table 2 (cont.) – Cell line information:

Basal Media Sources	Manufacturer	Catalogue #
RPMI-1640	Corning	10040CV
DMEM	Corning	10013CV
EMEM	Corning	10010CV
M5A	Corning	10050CV
DMEM:HamsF12	Corning	10090CV
M199/MCDB105		

Table 2 (cont.) – Cell line information:

Additional Media Supplements	Manufacturer	Catalogue #
FBS	Gibco	10082-147
Non-Essential Amino Acids (NEAA)		
Penicillin-Streptomycin (10,000 U/mL)	Gibco	15-140-122

Table 3 – Nucleic acids used in this study: Primers used in this study for RT-qPCR, CRISPR KO clone genotyping, ChIP-qPCR, and *TERT* promoter genotyping. siRNA, sgRNA, shRNA-mirE, and antisense oligonucleotide sequences. Plasmid sequences.

Application	Name	sequences
siRNA	siGENOME Non-Targeting siRNA Pool #1 Cat # D-001206-13-05	UAGCGACUAAACACAUCAA (Target sequence)
		UAAGGCUAUGAAGAGAUAC (Target sequence)
		AUGUAUUGGCCUGUAUUAG (Target sequence)
		AUGAACGUGAAUUGCUCAA (Target sequence)
	siGENOME Human GABPA (2551) siRNA - SMARTpool Cat # M-011662-01-0005	GAAAUUCUCUGGAGUCAUC (Target sequence)
		AGACAUCAAUGAACCAAUA (Target sequence)
		GGAAUUGAACCAAAGUUAA (Target sequence)
		GAAUUCAGCAUGACCGAUA (Target sequence)
	siGENOME Human GABPB1 (2553) siRNA - SMARTpool Cat # M-013083-01-0005	GCAAAUGGAGCUCCCUUUA (Target sequence)
		GACCGAACACCAUUACAUA (Target sequence)
		CAGCAAGUCAUCACAAUAG (Target sequence)
		GCUAAGAGACAAUGUAUCG (Target sequence)
	siGENOME Human GABPB2 (126626) siRNA - SMARTpool Cat # M-016074-00-0005	GAAGAGAAGUUGCCACUAA (Target sequence)
		AGAAUCAGGUGAAUGUUAA (Target sequence)
		GGCCAGCCAUUUAUUGUAA (Target sequence)
		GUUAACCUCGCAAGCCUUA (Target sequence)

Application	Name	sequences
sgRNA	Rosa26_upstream_topstrand	CACCGACAGCAAGTTGTCTAACCCG
	Rosa26_upstream_bottomstrand	AAACCGGGTTAGACAACTTGCTGTC
	Rosa26_downstream_topstrand	CACCGCATCAGCTGTCCTTTATATG
	Rosa26_downstream_bottomstrand	AAACATATAAAGGACAGCTGATGC
	GABPB1L_upstream_topstrand	CACCGTCTTGAACTGTACACAACAA
	GABPB1L_upstream_bottomstrand	AAACTTGTTGTGTACAGTTCAAGAC
	GABPB1L_downstream_topstrand	CACCGGTCTAGGAAATTTCAATAGG
	GABPB1L_downstream_bottomstrand	AAACCCTATTGAAATTTCCTAGACC
	GABPB1_TOTAL_upstream_topstrand	CACCGATGTTTTGTTTAGATGTCCC
	GABPB1_TOTAL_upstream_bottomstrand	AAACGGGACATCTAAACAAAACATC
	GABPB1_TOTAL_downstream_topstrand	CACCGAGAAGCTCTTCAGAAACAGC
	GABPB1_TOTAL_downstream_bottomstrand	AAACGCTGTTTCTGAAGAGCTTCTC
	GABPB1_X2_upstream_topstrand	CACCGCCCTTCAAAAGAGTGTGCTA
	GABPB1_X2_upstream_bottomstrand	AAACTAGCACACTCTTTTGAAGGGC
	GABPB1_X2_downstream_topstrand	CACCGAAAGGCCTTATAAATAGCAC
	GABPB1_X2_downstream_bottomstrand	AAACGTGCTATTTATAAGGCCTTTC
	B1S_PAS_KO_upsteam_topstrand	CACCGGTCTGTCATCTTGATAACAC
	B1S_PAS_KO_upsteam_bottomstrand	AAACGTGTTATCAAGATGACAGACC

Application	Name	sequences
	B1S_PAS_KO_downsteam_topstrand	CACCGGAGGGCTTGCTATATGTATA
	B1S_PAS_KO_downsteam_bottomstrand	AAACTATACATATAGCAAGCCCTCC

Table 3 (cont.) – Nucleic acids used in this study:

Application	Name	sequences
shRNA	shPPP1R12C_1	TTATCTCGAAAATACCTTCTCC
	shPPP1R12C_2	TTTATCTCGAAAATACCTTCTC
	shFirefly	TTAATCAGAGACTTCAGGCGGT
	shRenilla	TAGATAAGCATTATAATTCCTA
	shGABPB1L_6	TTATCAACTCATTTGGAACTGT
	shGABPB1L_7	TATACATGTAAATCTACTTGGG
	shGABPB1L_9	TTTAAATACATTTCACAACTTC
	shGABPB1L_10	TTTTAAATACATTTCACAACTT
	shGABPB1S_2	TATCAAAACAATACTGTCAGTA
	shGABPB1S_3	TGTATCAAAACAATACTGTCAG
	shGABPB1S_4	TTGAATTTATTTTGGATGACTG
	shGABPB1S_8	TTTATTTTGGATGACTGCGGCA
	shGABPB2_3	TTAACATTCACCTGATTCTGCA
	shGABPB2_4	TTGGTTGAAGAAATAAGGCTTG

Table 3 (cont.) – Nucleic acids used in this study:

Application	Name	sequences
RT-qPCR Primers	GABPA_F	AAGAACGCCTTGGGATACCCT
	GABPA_R	GTGAGGTCTATATCGGTCATGCT
	GABPB1_F	AAACGGGTGTATCTGCTGTTC
	GABPB1_R	GGCCACTACTGGAGTTTCTGAA
	GABPB1S_F	CCATGCCAGATGGACAAC
	GABPB1S_R	GCAAAGCACACCGGGTAAA
	GABPB1L_F	CGAAATAATTGAAAACCGGGTGGA
	GABPB1L_R	TCTTTCTTTAGGAGCTGCTGTCG
	GABPB2_F	AGCTCTGGAGAAAAACAATGCTG
	GABPB2_R	GCAGCCATACTCACAGGGTC
	GUSB_F	CTCATTTGGAATTTTGCCGATT
	GUSB_R	CCGAGTGAAGATCCCCTTTTTA
	TERT_F	TCACGGAGACCACGTTTCAAA
	TERT_R	TTCAAGTGCTGTCTGATTCCAAT

Table 3 (cont.) – Nucleic acids used in this study:

Application	Name	sequences
CRISPR KO genotyping primers	Rosa26_F	CATGAAAATGACAGGTGAAACTCCA
	Rosa26_R	ACCTTATGCATCACATTCACGA
	GABPB1_geno_WT_F	AGTGTCAGGACTCTCTGGGTTTGT
	GABPB1_geno_WT_R	CCATGATGTGCCCCTACACTGTC
	GABPB1_geno_KO_F	TTAGGCCAGCTTTTCTCTGC
	GABPB1_geno_KO_R	CCCATGGCTGTACCTTTGTT
	GABPB1L_F	TTCCTTGCAGTCAGAAATTAATCCA
	GABPB1L_R	TGGCTTAAGTCCAATTATCCATCT
	GABPB1_X2KO_F	TTGCTGCAAACCCTCCAGTA
	GABPB1_X2KO_R	GCCTTCCCCACAACTACCTTC
	B1S_pas_KO_F	TGATACAGAATGAAAGTGCGTAGT
	B1S_pas_KO_R	TGGTATTTTCCTTTAGTGACGTGT

Table 3 (cont.) – Nucleic acids used in this study:

Application	Name	sequences
ChIP-qPCR Primers	TERT_ChIP_F	CTGCCCCTTCACCTTCCAG
	TERT_ChIP_R	AGCGCTGCCTGAAACTCG
	GABPB1_ChIP_F	GTTACCACCGGATGTGGAAGT
	GABPB1_ChIP_R	GGAAACCCGGCGCCTTAAT
	GABPB1_promoter_tiling_F1	CGACTGGAGGTTGGCAGTG
	GABPB1_promoter_tiling_R1	CGCCCGTTCCCCTCTCC
	GABPB1_promoter_tiling_F2	GGCTTGCCGGTCCCGAG
	GABPB1_promoter_tiling_R2	TTCCTCTTTCTCCCGCCCAC
	GABPB1_promoter_tiling_F3	CTACCCGGCTTGCCGGTCC
	GABPB1_promoter_tiling_R3	CCTCTTTCTCCCGCCCACTG
	GABPB1_promoter_tiling_F4	CCCTCCTCGGCCCTAGC
	GABPB1_promoter_tiling_R4	CCACTGCCAACCTCCAGTC
	GABPB1_promoter_tiling_F5	GCACACTGCTTCTGGGAGGG
	GABPB1_promoter_tiling_R5	CGCTCGGGACCGGCAAG
	GABPB1_promoter_tiling_F6	GGCACACTGCTTCTGGGAGG
	GABPB1_promoter_tiling_R6	GCTCGGGACCGGCAAGC
	GABPB1_promoter_tiling_F7	CTCCTGGCCCCGCTTATTCC
	GABPB1_promoter_tiling_R7	CCCCTCCCAGAAGCAGTGTG
	GABPB1_promoter_tiling_F8	TCCTGGCCCCGCTTATTCC
	GABPB1_promoter_tiling_R8	CTCCCAGAAGCAGTGTGCCC
	GABPB1_promoter_tiling_F9	CCAGATCATCCCCGCGATTT
	GABPB1_promoter_tiling_R9	CGACCCCCGCGGAATAAG
	GABPB1_promoter_tiling_F10	GTTACCACCGGATGTGGAAGT
	GABPB1_promoter_tiling_R10	GGAAACCCGGCGCCTTAAT
	GABPB1_promoter_tiling_F11	GCGCTTTGTGTGTAGCGG
	GABPB1_promoter_tiling_R11	AACTTCCACATCCGGTGGTA
	GABPB1_promoter_tiling_F12	AGCTTGACTCACTCGCACAC
	GABPB1_promoter_tiling_R12	CACAGGGCGCTATTTTCCGA
	GABPB1_promoter_tiling_F13	AAAATCCTCGGGCGATGAGC
	GABPB1_promoter_tiling_R13	GGACACATGGTGTGCGAGT
	GABPB1_promoter_tiling_F14	ATTCCGCCGCTTTCTTTGTG
	GABPB1_promoter_tiling_R14	CCACTCCCTAGCTGTGTTCC
	GABPB1_promoter_tiling_F15	AACTCCTACCCACCGCAGAA
	GABPB1_promoter_tiling_R15	CACAAAGAAAGCGGCGGAAT
	GABPB1_promoter_tiling_F16	GATTCTGCTAGGCCGCACA
	GABPB1_promoter_tiling_R16	TTCTGCGGTGGGTAGGAGTT
	GABPB1_promoter_tiling_F17	ACCTCACTCGTTCCTTCCCT
	GABPB1_promoter_tiling_R17	GCAGAATCCTGGGAGACGG
	GABPB1_promoter_tiling_F18	GGATCTACGAAACATGAGGCATAA
	GABPB1_promoter_tiling_R18	AAGGAACGAGTGAGGTTCCTTTT

Table 3 (cont.) – Nucleic acids used in this study:

Application	Name	sequences
TERTp genotyping Primers	M13_TERTp_PCR_F	**GTAAAACGACGGCCAG**ACGTGGCGGAGGGACTG
	M13_TERTp_PCR_R	**CAGGAAACAGCTATGAC**AGGGCTTCCCACGTGCG
		Note: The M13 sequences are underlined, bolded, and in red.

Application	Name	sequences
Antisense Oligonucleotides	UTR1	+C*+T*+A*A*C*C*A*A*C*A*A*C*G*+A*+T*C
	Gapmer control	+T*+T*T*A*A*G*C*C*G*A*T*G*C*G*+T*T
	2'MOE Control (Scramble ASO)	/52MOErT/*/i2MOErC/*/i2MOErA/*/i2MOErC/*/i2MOErC/*/i2MOErT/*/i2MOErT/*/i2MOErC/*/i2MOErA/*/i2MOErC/*/i2MOErC/*/i2MOErC/*/i2MOErT/*/i2MOErC/*/i2MOErT/*/i2MOErC/*/i2MOErC/*/i2MOErA/*/i2MOErC/*/32MOErT/
	B1L-ASO1	/52MOErG/*/i2MOErG/*/i2MOErT/*/i2MOErA/*/i2MOErA/*/i2MOErA/*/i2MOErA/*/i2MOErG/*/i2MOErA/*/i2MOErC/*/i2MOErT/*/i2MOErC/*/i2MOErC/*/i2MOErT/*/i2MOErT/*/i2MOErA/*/i2MOErC/*/i2MOErT/*/i2MOErT/*/32MOErC/
	B1L-ASO2	/52MOErC/*/i2MOErC/*/i2MOErG/*/i2MOErG/*/i2MOErG/*/i2MOErT/*/i2MOErA/*/i2MOErA/*/i2MOErA/*/i2MOErA/*/i2MOErA/*/i2MOErG/*/i2MOErA/*/i2MOErC/*/i2MOErT/*/i2MOErC/*/i2MOErC/*/i2MOErT/*/i2MOErT/*/i2MOErA/*/32MOErC/
* = phosphorothioate (PS) modifications + = locked nucleic acid base modification /52MOEr(T,C,G,A)/ or /i2MOEr(T,C,G,A)/ or /32MOEr(T,C,G,A)/ = 2'-O-methoxy-ethyl (2'-MOE) modified nucleic acid bases		

Table 4 - Western Blot Antibodies: Antibodies used for western blot assays in this study.

Protein	Company	Cat#	Species	Primary or Secondary	Clonality	Clone	Applications tested	Conjugated	Blocking	Probe	Dilution	WB MW (kDa)	RRID
GABPB1	ProteinTech	12597-1-AP	Rabbit	Primary	Polyclonal	N/A	WB	N/A	5% Milk	5% Milk	WB 1:2000	40-50	AB_10951115
GABPA	Santa Cruz	sc-22810	Rabbit	Primary	Polyclonal	N/A	WB	N/A	5% Milk	5% Milk	WB 1:500		AB_2247389
Anti-Rabbit IgG	Cell Signaling	7074	Goat	Secondary	Polyclonal	N/A	WB	HRP	N/A	5% Milk	WB 1:2000	N/A	AB_2099233
Anti-Mouse IgG	Cell Signaling	7076	Horse	Secondary	Polyclonal	N/A	WB	HRP	N/A	5% Milk	WB 1:2000	N/A	AB_330924
α-Actinin (D6F6)	Cell Signaling	6487	Rabbit	Primary	Monoclonal	D6F6	WB	N/A	5% Milk	5% BSA	WB: 1:2000	100	AB_11179206

Chapter 10: References

1 Chin, L. *et al.* p53 Deficiency Rescues the Adverse Effects of Telomere Loss and Cooperates with Telomere Dysfunction to Accelerate Carcinogenesis. *Cell* **97**, 527-538, doi:10.1016/s0092-8674(00)80762-x (1999).

2 Kim, N. W. *et al.* Specific association of human telomerase activity with immortal cells and cancer. *Science* **266**, 2011-2015, doi:10.1126/science.7605428 (1994).

3 Saretzki, G., Sitte, N., Merkel, U., Wurm, R. E. & von Zglinicki, T. Telomere shortening triggers a p53-dependent cell cycle arrest via accumulation of G-rich single stranded DNA fragments. *Oncogene* **18**, 5148-5158, doi:10.1038/sj.onc.1202898 (1999).

4 Counter, C. M. *et al.* Telomerase activity is restored in human cells by ectopic expression of hTERT (hEST2), the catalytic subunit of telomerase. *Oncogene* **16**, 1217-1222, doi:10.1038/sj.onc.1201882 (1998).

5 Sieverling, L. *et al.* Genomic footprints of activated telomere maintenance mechanisms in cancer. *Nat Commun* **11**, 733, doi:10.1038/s41467-019-13824-9 (2020).

6 Blackburn, E. H., Greider, C. W. & Szostak, J. W. Telomeres and telomerase: the path from maize, Tetrahymena and yeast to human cancer and aging. *Nat Med* **12**, 1133-1138, doi:10.1038/nm1006-1133 (2006).

7 Bell, R. J. *et al.* Understanding TERT Promoter Mutations: A Common Path to Immortality. *Mol Cancer Res* **14**, 315-323, doi:10.1158/1541-7786.MCR-16-0003 (2016).

8 Huang, F. W. *et al.* TERT promoter mutations and monoallelic activation of TERT in cancer. *Oncogenesis* **4**, e176, doi:10.1038/oncsis.2015.39 (2015).

9 Chiba, K. *et al.* Cancer-associated TERT promoter mutations abrogate telomerase silencing. *Elife* **4**, doi:10.7554/eLife.07918 (2015).

10 Zehir, A. *et al.* Mutational landscape of metastatic cancer revealed from prospective clinical sequencing of 10,000 patients. *Nat Med* **23**, 703-713, doi:10.1038/nm.4333 (2017).

11 Huang, D. S. *et al.* Recurrent TERT promoter mutations identified in a large-scale study of multiple tumour types are associated with increased TERT expression and telomerase activation. *Eur J Cancer* **51**, 969-976, doi:10.1016/j.ejca.2015.03.010 (2015).

12 Huang, F. W. *et al.* Highly recurrent TERT promoter mutations in human melanoma. *Science* **339**, 957-959, doi:10.1126/science.1229259 (2013).

13 Meyerson, M. *et al.* hEST2, the putative human telomerase catalytic subunit gene, is up-regulated in tumor cells and during immortalization. *Cell* **90**, 785-795, doi:10.1016/s0092-8674(00)80538-3 (1997).

14 Appin, C. L. *et al.* Whole tumor analysis reveals early origin of the TERT promoter mutation and intercellular heterogeneity in TERT expression. *Neuro Oncol*, doi:10.1093/neuonc/noad231 (2023).

15 Aquilanti, E. *et al.* Telomerase inhibition is an effective therapeutic strategy in TERT promoter-mutant glioblastoma models with low tumor volume. *Neuro-Oncology*, doi:10.1093/neuonc/noad024 (2023).

16 Miki, S. *et al.* TERT promoter C228T mutation in neural progenitors confers growth advantage following telomere shortening in vivo. *Neuro Oncol* **24**, 2063-2075, doi:10.1093/neuonc/noac080 (2022).

17 Li, Y. *et al.* Non-canonical NF-kappaB signalling and ETS1/2 cooperatively drive C250T mutant TERT promoter activation. *Nat Cell Biol* **17**, 1327-1338, doi:10.1038/ncb3240 (2015).

18 Xu, X. *et al.* Structural basis for reactivating the mutant TERT promoter by cooperative binding of p52 and ETS1. *Nat Commun* **9**, 3183, doi:10.1038/s41467-018-05644-0 (2018).

19 Pierini, T. *et al.* New somatic TERT promoter variants enhance the Telomerase activity in Glioblastoma. *Acta Neuropathol Commun* **8**, 145, doi:10.1186/s40478-020-01022-4 (2020).

20 Makowski, M. M. *et al.* An interaction proteomics survey of transcription factor binding at recurrent TERT promoter mutations. *Proteomics* **16**, 417-426, doi:10.1002/pmic.201500327 (2016).

21 Thornton, C. E. M., Hao, J., Tamarapu, P. P. & Landa, I. Multiple ETS Factors Participate in the Transcriptional Control of TERT Mutant Promoter in Thyroid Cancers. *Cancers (Basel)* **14**, doi:10.3390/cancers14020357 (2022).

22 Gabler, L. *et al.* TERT expression is susceptible to BRAF and ETS-factor inhibition in BRAF(V600E)/TERT promoter double-mutated glioma. *Acta Neuropathol Com* **7**, doi:ARTN 128

10.1186/s40478-019-0775-6 (2019).

23 Bell, R. J. *et al.* Cancer. The transcription factor GABP selectively binds and activates the mutant TERT promoter in cancer. *Science* **348**, 1036-1039, doi:10.1126/science.aab0015 (2015).

24 Mancini, A. *et al.* Disruption of the beta1L Isoform of GABP Reverses Glioblastoma Replicative Immortality in a TERT Promoter Mutation-Dependent Manner. *Cancer Cell* **34**, 513-528 e518, doi:10.1016/j.ccell.2018.08.003 (2018).

25 McKinney, A. M. *et al.* GABP couples oncogene signaling to telomere regulation in TERT promoter mutant cancer. *Cell Rep* **40**, 111344, doi:10.1016/j.celrep.2022.111344 (2022).

26 Barger, C. J. *et al.* Conserved features of TERT promoter duplications reveal an activation mechanism that mimics hotspot mutations in cancer. *Nat Commun* **13**, 5430, doi:10.1038/s41467-022-33099-x (2022).

27 Amen, A. M. *et al.* Cancer-specific loss of TERT activation sensitizes glioblastoma to DNA damage. *Proc Natl Acad Sci U S A* **118**, doi:10.1073/pnas.2008772118 (2021).

28 Stern, J. L., Theodorescu, D., Vogelstein, B., Papadopoulos, N. & Cech, T. R. Mutation of the TERT promoter, switch to active chromatin, and monoallelic TERT expression in multiple cancers. *Genes Dev* **29**, 2219-2224, doi:10.1101/gad.269498.115 (2015).

29 Liu, R., Zhang, T., Zhu, G. & Xing, M. Regulation of mutant TERT by BRAF V600E/MAP kinase pathway through FOS/GABP in human cancer. *Nat Commun* **9**, 579, doi:10.1038/s41467-018-03033-1 (2018).

30 Vinagre, J. *et al.* TERT promoter mutations in pancreatic endocrine tumours are rare and mainly found in tumours from patients with hereditary syndromes. *Sci Rep* **6**, 29714, doi:10.1038/srep29714 (2016).

31 McKelvey, B. A. *et al.* Characterization of Allele-Specific Regulation of Telomerase Reverse Transcriptase in Promoter Mutant Thyroid Cancer Cell Lines. *Thyroid* **30**, 1470-1481, doi:10.1089/thy.2020.0055 (2020).

32 Guo, Y. X. *et al.* GABPA is a master regulator of luminal identity and restrains aggressive diseases in bladder cancer. *Cell Death Differ* **27**, 1862-1877, doi:10.1038/s41418-019-0466-7 (2020).

33 Hu, K., Ghandi, M. & Huang, F. W. Integrated evaluation of telomerase activation and telomere maintenance across cancer cell lines. *Elife* **10**, doi:10.7554/eLife.66198 (2021).

34 Gupta, S. *et al.* A Pan-Cancer Study of Somatic TERT Promoter Mutations and Amplification in 30,773 Tumors Profiled by Clinical Genomic Sequencing. *J Mol Diagn* **23**, 253-263, doi:10.1016/j.jmoldx.2020.11.003 (2021).

35 Yang, H. *et al.* Frequency of TERT Promoter Mutations in Real-World Analysis of 2,092 Thyroid Carcinoma Patients. *Endocrinol Metab (Seoul)* **37**, 652-663, doi:10.3803/EnM.2022.1477 (2022).

36 Hurst, C. D., Platt, F. M. & Knowles, M. A. Comprehensive mutation analysis of the TERT promoter in bladder cancer and detection of mutations in voided urine. *Eur Urol* **65**, 367-369, doi:10.1016/j.eururo.2013.08.057 (2014).

37 Allory, Y. *et al.* Telomerase reverse transcriptase promoter mutations in bladder cancer: high frequency across stages, detection in urine, and lack of association with outcome. *Eur Urol* **65**, 360-366, doi:10.1016/j.eururo.2013.08.052 (2014).

38 Horn, S. *et al.* TERT promoter mutations in familial and sporadic melanoma. *Science* **339**, 959-961, doi:10.1126/science.1230062 (2013).

39 Wei, G. H. *et al.* Genome-wide analysis of ETS-family DNA-binding in vitro and in vivo. *EMBO J* **29**, 2147-2160, doi:10.1038/emboj.2010.106 (2010).

40 Eisenberg, E. & Levanon, E. Y. Human housekeeping genes, revisited. *Trends Genet* **29**, 569-574, doi:10.1016/j.tig.2013.05.010 (2013).

41 Stern, J. L. *et al.* Mesenchymal and MAPK Expression Signatures Associate with Telomerase Promoter Mutations in Multiple Cancers. *Mol Cancer Res*, doi:10.1158/1541-7786.MCR-19-1244 (2020).

42 de la Brousse, F. C., Birkenmeier, E. H., King, D. S., Rowe, L. B. & McKnight, S. L. Molecular and genetic characterization of GABP beta. *Genes Dev* **8**, 1853-1865, doi:10.1101/gad.8.15.1853 (1994).

43 Hollenhorst, P. C., Jones, D. A. & Graves, B. J. Expression profiles frame the promoter specificity dilemma of the ETS family of transcription factors. *Nucleic Acids Res* **32**, 5693-5702, doi:10.1093/nar/gkh906 (2004).

44 Rosmarin, A. G., Resendes, K. K., Yang, Z., McMillan, J. N. & Fleming, S. L. GA-binding protein transcription factor: a review of GABP as an integrator of intracellular signaling and protein-protein interactions. *Blood Cells Mol Dis* **32**, 143-154, doi:10.1016/j.bcmd.2003.09.005 (2004).

45 Chinenov, Y., Henzl, M. & Martin, M. E. The alpha and beta subunits of the GA-binding protein form a stable heterodimer in solution. Revised model of heterotetrameric complex assembly. *J Biol Chem* **275**, 7749-7756, doi:10.1074/jbc.275.11.7749 (2000).

46 Yang, Z. F., Mott, S. & Rosmarin, A. G. The Ets transcription factor GABP is required for cell-cycle progression. *Nat Cell Biol* **9**, 339-346, doi:10.1038/ncb1548 (2007).

47 Batchelor, A. H., Piper, D. E., de la Brousse, F. C., McKnight, S. L. & Wolberger, C. The structure of GABPalpha/beta: an ETS domain- ankyrin repeat heterodimer bound to DNA. *Science* **279**, 1037-1041, doi:10.1126/science.279.5353.1037 (1998).

48 Brown, T. A. & McKnight, S. L. Specificities of protein-protein and protein-DNA interaction of GABP alpha and two newly defined ets-related proteins. *Genes Dev* **6**, 2502-2512, doi:10.1101/gad.6.12b.2502 (1992).

49 LaMarco, K., Thompson, C. C., Byers, B. P., Walton, E. M. & McKnight, S. L. Identification of Ets- and notch-related subunits in GA binding protein. *Science* **253**, 789-792, doi:10.1126/science.1876836 (1991).

50 Gugneja, S., Virbasius, J. V. & Scarpulla, R. C. Four structurally distinct, non-DNA-binding subunits of human nuclear respiratory factor 2 share a conserved transcriptional activation domain. *Mol Cell Biol* **15**, 102-111, doi:10.1128/mcb.15.1.102 (1995).

51 Thompson, C. C., Brown, T. A. & Mcknight, S. L. Convergence of Ets-Related and Notch-Related Structural Motifs in a Heteromeric DNA-Binding Complex. *Science* **253**, 762-768, doi:DOI 10.1126/science.1876833 (1991).

52 Watanabe, H. *et al.* cDNA cloning of transcription factor E4TF1 subunits with Ets and notch motifs. *Mol Cell Biol* **13**, 1385-1391, doi:10.1128/mcb.13.3.1385-1391.1993 (1993).

53 Sawa, C. *et al.* Functional domains of transcription factor hGABP beta1/E4TF1-53 required for nuclear localization and transcription activation. *Nucleic Acids Res* **24**, 4954-4961, doi:10.1093/nar/24.24.4954 (1996).

54 Graves, B. J. Inner workings of a transcription factor partnership. *Science* **279**, 1000-1002, doi:10.1126/science.279.5353.1000 (1998).

55 Yuan, X., Larsson, C. & Xu, D. Mechanisms underlying the activation of TERT transcription and telomerase activity in human cancer: old actors and new players. *Oncogene* **38**, 6172-6183, doi:10.1038/s41388-019-0872-9 (2019).

56 Lin, A., Giuliano, C. J., Sayles, N. M. & Sheltzer, J. M. CRISPR/Cas9 mutagenesis invalidates a putative cancer dependency targeted in on-going clinical trials. *Elife* **6**, doi:10.7554/eLife.24179 (2017).

57 Rowland, T. J., Dumbovic, G., Hass, E. P., Rinn, J. L. & Cech, T. R. Single-cell imaging reveals unexpected heterogeneity of telomerase reverse transcriptase expression across human cancer cell lines. *Proc Natl Acad Sci U S A* **116**, 18488-18497, doi:10.1073/pnas.1908275116 (2019).

58 Xue, H. H. *et al.* Targeting the GA binding protein beta1L isoform does not perturb lymphocyte development and function. *Mol Cell Biol* **28**, 4300-4309, doi:10.1128/MCB.01855-07 (2008).

59 Wu, H. *et al.* The Ets transcription factor GABP is a component of the hippo pathway essential for growth and antioxidant defense. *Cell Rep* **3**, 1663-1677, doi:10.1016/j.celrep.2013.04.020 (2013).

60 Jeong, B. C. *et al.* Brain-specific angiogenesis inhibitor 2 regulates VEGF through GABP that acts as a transcriptional repressor. *FEBS Lett* **580**, 669-676, doi:10.1016/j.febslet.2005.12.086 (2006).

61 Genuario, R. R. & Perry, R. P. The GA-binding protein can serve as both an activator and repressor of ribosomal protein gene transcription. *J Biol Chem* **271**, 4388-4395, doi:10.1074/jbc.271.8.4388 (1996).

62 Wang, Y. *et al.* TERT Promoter Revertant Mutation Inhibits Melanoma Growth through Intrinsic Apoptosis. *Biology (Basel)* **11**, doi:10.3390/biology11010141 (2022).

63 Wen, L. *et al.* CRISPR/Cas9-Mediated TERT Disruption in Cancer Cells. *Int J Mol Sci* **21**, doi:10.3390/ijms21020653 (2020).

64 Zhang, X., Mar, V., Zhou, W., Harrington, L. & Robinson, M. O. Telomere shortening and apoptosis in telomerase-inhibited human tumor cells. *Genes Dev* **13**, 2388-2399, doi:10.1101/gad.13.18.2388 (1999).

65 Li, X. *et al.* Programmable base editing of mutated TERT promoter inhibits brain tumour growth. *Nat Cell Biol* **22**, 282-288, doi:10.1038/s41556-020-0471-6 (2020).

66 Stern, J. L. *et al.* Allele-Specific DNA Methylation and Its Interplay with Repressive Histone Marks at Promoter-Mutant TERT Genes. *Cell Rep* **21**, 3700-3707, doi:10.1016/j.celrep.2017.12.001 (2017).

67 Bekes, M., Langley, D. R. & Crews, C. M. PROTAC targeted protein degraders: the past is prologue. *Nat Rev Drug Discov* **21**, 181-200, doi:10.1038/s41573-021-00371-6 (2022).

68 Jumper, J. *et al.* Highly accurate protein structure prediction with AlphaFold. *Nature* **596**, 583-589, doi:10.1038/s41586-021-03819-2 (2021).

69 Evans, R. *et al.* Protein complex prediction with AlphaFold-Multimer. *bioRxiv*, 2021.2010.2004.463034, doi:10.1101/2021.10.04.463034 (2022).

70 Baltz, M. R., Stephens, E. A. & DeLisa, M. P. Design and Functional Characterization of Synthetic E3 Ubiquitin Ligases for Targeted Protein Depletion. *Curr Protoc Chem Biol* **10**, 72-90, doi:10.1002/cpch.37 (2018).

71 Lim, S. *et al.* bioPROTACs as versatile modulators of intracellular therapeutic targets including proliferating cell nuclear antigen (PCNA). *Proc Natl Acad Sci U S A* **117**, 5791-5800, doi:10.1073/pnas.1920251117 (2020).

72 Maekawa, M. & Higashiyama, S. The Roles of SPOP in DNA Damage Response and DNA Replication. *Int J Mol Sci* **21**, doi:10.3390/ijms21197293 (2020).

73 Batsios, G. *et al.* Deuterium Metabolic Imaging Reports on TERT Expression and Early Response to Therapy in Cancer. *Clin Cancer Res* **28**, 3526-3536, doi:10.1158/1078-0432.CCR-21-4418 (2022).

74 Minami, N. *et al.* Imaging biomarkers of TERT or GABPB1 silencing in TERT-positive glioblastoma. *Neuro Oncol* **24**, 1898-1910, doi:10.1093/neuonc/noac112 (2022).

75 Oikawa, T. & Yamada, T. Molecular biology of the Ets family of transcription factors. *Gene* **303**, 11-34, doi:10.1016/s0378-1119(02)01156-3 (2003).

76 Fromm, L. & Burden, S. J. Synapse-specific and neuregulin-induced transcription require an ets site that binds GABPalpha/GABPbeta. *Genes Dev* **12**, 3074-3083, doi:10.1101/gad.12.19.3074 (1998).

77 Yu, M. *et al.* GA-binding protein-dependent transcription initiator elements. Effect of helical spacing between polyomavirus enhancer a factor 3(PEA3)/Ets-binding sites on initiator activity. *J Biol Chem* **272**, 29060-29067, doi:10.1074/jbc.272.46.29060 (1997).

78 Sucharov, C., Basu, A., Carter, R. S. & Avadhani, N. G. A novel transcriptional initiator activity of the GABP factor binding ets sequence repeat from the murine cytochrome c oxidase Vb gene. *Gene Expr* **5**, 93-111 (1995).

79 Genuario, R. R., Kelley, D. E. & Perry, R. P. Comparative utilization of transcription factor GABP by the promoters of ribosomal protein genes rpL30 and rpL32. *Gene Expr* **3**, 279-288 (1993).

80 Gao, J. & Pickett, H. A. Targeting telomeres: advances in telomere maintenance mechanism-specific cancer therapies. *Nat Rev Cancer* **22**, 515-532, doi:10.1038/s41568-022-00490-1 (2022).

81 Shi, Z. *et al.* Argininosuccinate lyase drives activation of mutant TERT promoter in glioblastomas. *Mol Cell* **82**, 4582-4583, doi:10.1016/j.molcel.2022.11.009 (2022).

82 Khattar, E. & Tergaonkar, V. Transcriptional Regulation of Telomerase Reverse Transcriptase (TERT) by MYC. *Front Cell Dev Biol* **5**, doi:ARTN 1

10.3389/fcell.2017.00007 (2017).

83 Collins, S. A., Shah, A. H., Ostertag, D., Kasahara, N. & Jolly, D. J. Clinical development of retroviral replicating vector Toca 511 for gene therapy of cancer. *Expert Opin Biol Ther* **21**, 1199-1214, doi:10.1080/14712598.2021.1902982 (2021).

84 Zhang, P., Zhang, H. & Wang, Y. FGFR4 promotes nuclear localization of GABP to inhibit cell apoptosis in uterine leiomyosarcoma. *Cell Tissue Res* **383**, 865-879, doi:10.1007/s00441-020-03296-5 (2021).

85 Chinenov, Y., Schmidt, T., Yang, X. Y. & Martin, M. E. Identification of redox-sensitive cysteines in GA-binding protein-alpha that regulate DNA binding and heterodimerization. *J Biol Chem* **273**, 6203-6209, doi:10.1074/jbc.273.11.6203 (1998).

86 Flory, E., Hoffmeyer, A., Smola, U., Rapp, U. R. & Bruder, J. T. Raf-1 kinase targets GA-binding protein in transcriptional regulation of the human immunodeficiency virus type 1 promoter. *J Virol* **70**, 2260-2268, doi:10.1128/JVI.70.4.2260-2268.1996 (1996).

87 Fromm, L. & Burden, S. J. Neuregulin-1-stimulated phosphorylation of GABP in skeletal muscle cells. *Biochemistry* **40**, 5306-5312, doi:10.1021/bi002649m (2001).

88 Ryu, D. *et al.* A SIRT7-dependent acetylation switch of GABPbeta1 controls mitochondrial function. *Cell Metab* **20**, 856-869, doi:10.1016/j.cmet.2014.08.001 (2014).

89 Agarwal, N. *et al.* TRIM28 is a transcriptional activator of the mutant TERT promoter in human bladder cancer. *Proc Natl Acad Sci U S A* **118**, doi:10.1073/pnas.2102423118 (2021).

90 Li, Y., Cheng, H. S., Chng, W. J. & Tergaonkar, V. Activation of mutant TERT promoter by RAS-ERK signaling is a key step in malignant progression of BRAF-

mutant human melanomas. *Proc Natl Acad Sci U S A* **113**, 14402-14407, doi:10.1073/pnas.1611106113 (2016).

91 Wu, Y. *et al.* Synergistic activation of mutant TERT promoter by Sp1 and GABPA in BRAF(V600E)-driven human cancers. *NPJ Precis Oncol* **5**, 3, doi:10.1038/s41698-020-00140-5 (2021).

92 Akincilar, S. C. *et al.* Long-Range Chromatin Interactions Drive Mutant TERT Promoter Activation. *Cancer Discov* **6**, 1276-1291, doi:10.1158/2159-8290.CD-16-0177 (2016).

93 Sharma, S. *et al.* Human telomerase is directly regulated by non-telomeric TRF2-G-quadruplex interaction. *Cell Rep* **35**, 109154, doi:10.1016/j.celrep.2021.109154 (2021).

94 Monsen, R. C. *et al.* The hTERT core promoter forms three parallel G-quadruplexes. *Nucleic Acids Res* **48**, 5720-5734, doi:10.1093/nar/gkaa107 (2020).

95 Jumper, J. *et al.* Applying and improving AlphaFold at CASP14. *Proteins* **89**, 1711-1721, doi:10.1002/prot.26257 (2021).

96 Baek, M. *et al.* Efficient and accurate prediction of protein structure using RoseTTAFold2. *bioRxiv*, 2023.2005.2024.542179, doi:10.1101/2023.05.24.542179 (2023).

97 Uphoff, C. C. & Drexler, H. G. Detecting Mycoplasma contamination in cell cultures by polymerase chain reaction. *Methods Mol Med* **88**, 319-326, doi:10.1385/1-59259-406-9:319 (2004).

98 Uphoff, C. C. & Drexler, H. G. Detecting mycoplasma contamination in cell cultures by polymerase chain reaction. *Methods Mol Biol* **731**, 93-103, doi:10.1007/978-1-61779-080-5_8 (2011).

99 Ye, J. *et al.* Primer-BLAST: a tool to design target-specific primers for polymerase chain reaction. *BMC Bioinformatics* **13**, 134, doi:10.1186/1471-2105-13-134 (2012).

100 Fellmann, C. *et al.* An optimized microRNA backbone for effective single-copy RNAi. *Cell Rep* **5**, 1704-1713, doi:10.1016/j.celrep.2013.11.020 (2013).

101 Pelossof, R. *et al.* Prediction of potent shRNAs with a sequential classification algorithm. *Nat Biotechnol* **35**, 350-353, doi:10.1038/nbt.3807 (2017).

102 Lycka, M. *et al.* WALTER: an easy way to online evaluate telomere lengths from terminal restriction fragment analysis. *BMC Bioinformatics* **22**, 145, doi:10.1186/s12859-021-04064-0 (2021).

103 Ran, F. A. *et al.* Genome engineering using the CRISPR-Cas9 system. *Nat Protoc* **8**, 2281-2308, doi:10.1038/nprot.2013.143 (2013).

104 Blainey, P., Krzywinski, M. & Altman, N. Points of significance: replication. *Nat Methods* **11**, 879-880, doi:10.1038/nmeth.3091 (2014).

105 Pinheiro, J. B., Douglas; and {R Core Team}. nlme: Linear and Nonlinear Mixed Effects Models. (2022).

106 Langmead, B. & Salzberg, S. L. Fast gapped-read alignment with Bowtie 2. *Nat Methods* **9**, 357-359, doi:10.1038/nmeth.1923 (2012).

107 Li, H. *et al.* The Sequence Alignment/Map format and SAMtools. *Bioinformatics* **25**, 2078-2079, doi:10.1093/bioinformatics/btp352 (2009).

108 Zhang, Y. *et al.* Model-based analysis of ChIP-Seq (MACS). *Genome Biol* **9**, R137, doi:10.1186/gb-2008-9-9-r137 (2008).

109 Storey, J. D. The positive false discovery rate: A Bayesian interpretation and the q-value. *Ann Stat* **31**, 2013-2035, doi:DOI 10.1214/aos/1074290335 (2003).

110 Kim, D., Paggi, J. M., Park, C., Bennett, C. & Salzberg, S. L. Graph-based genome alignment and genotyping with HISAT2 and HISAT-genotype. *Nat Biotechnol* **37**, 907-915, doi:10.1038/s41587-019-0201-4 (2019).

111 Kovaka, S. *et al.* Transcriptome assembly from long-read RNA-seq alignments with StringTie2. *Genome Biol* **20**, 278, doi:10.1186/s13059-019-1910-1 (2019).

112 Love, M. I., Huber, W. & Anders, S. Moderated estimation of fold change and dispersion for RNA-seq data with DESeq2. *Genome Biol* **15**, 550, doi:10.1186/s13059-014-0550-8 (2014).

113 Cook, R. D. Detection of Influential Observation in Linear Regression. *Technometrics* **19**, 15-18, doi:10.2307/1268249 (1977).

114 Chen, E. Y. *et al.* Enrichr: interactive and collaborative HTML5 gene list enrichment analysis tool. *BMC Bioinformatics* **14**, 128, doi:10.1186/1471-2105-14-128 (2013).

115 Kuleshov, M. V. *et al.* Enrichr: a comprehensive gene set enrichment analysis web server 2016 update. *Nucleic Acids Res* **44**, W90-97, doi:10.1093/nar/gkw377 (2016).

116 Xie, Z. *et al.* Gene Set Knowledge Discovery with Enrichr. *Curr Protoc* **1**, e90, doi:10.1002/cpz1.90 (2021).

117 Subramanian, A. *et al.* Gene set enrichment analysis: a knowledge-based approach for interpreting genome-wide expression profiles. *Proc Natl Acad Sci U S A* **102**, 15545-15550, doi:10.1073/pnas.0506580102 (2005).

118 Liberzon, A. *et al.* The Molecular Signatures Database (MSigDB) hallmark gene set collection. *Cell Syst* **1**, 417-425, doi:10.1016/j.cels.2015.12.004 (2015).

119 Benjamini, Y. & Hochberg, Y. Controlling the False Discovery Rate: A Practical and Powerful Approach to Multiple Testing. *Journal of the Royal Statistical Society. Series B (Methodological)* **57**, 289-300 (1995).

120 Joung, J. *et al.* Genome-scale activation screen identifies a lncRNA locus regulating a gene neighbourhood. *Nature* **548**, 343-346, doi:10.1038/nature23451 (2017).

121 Zhang, Y., Shin, H., Song, J. S., Lei, Y. & Liu, X. S. Identifying positioned nucleosomes with epigenetic marks in human from ChIP-Seq. *BMC Genomics* **9**, 537, doi:10.1186/1471-2164-9-537 (2008).

122 Finnegan, A. & Song, J. S. Maximum entropy methods for extracting the learned features of deep neural networks. *PLoS Comput Biol* **13**, e1005836, doi:10.1371/journal.pcbi.1005836 (2017).

123 Lorenz, R. *et al.* ViennaRNA Package 2.0. *Algorithms Mol Biol* **6**, 26, doi:10.1186/1748-7188-6-26 (2011).

124 Tafer, H. & Hofacker, I. L. RNAplex: a fast tool for RNA-RNA interaction search. *Bioinformatics* **24**, 2657-2663, doi:10.1093/bioinformatics/btn193 (2008).

125 Mathews, D. H. *et al.* Incorporating chemical modification constraints into a dynamic programming algorithm for prediction of RNA secondary structure. *Proc Natl Acad Sci U S A* **101**, 7287-7292, doi:10.1073/pnas.0401799101 (2004).

Publishing Agreement

It is the policy of the University to encourage open access and broad distribution of all theses, dissertations, and manuscripts. The Graduate Division will facilitate the distribution of UCSF theses, dissertations, and manuscripts to the UCSF Library for open access and distribution. UCSF will make such theses, dissertations, and manuscripts accessible to the public and will take reasonable steps to preserve these works in perpetuity.

I hereby grant the non-exclusive, perpetual right to The Regents of the University of California to reproduce, publicly display, distribute, preserve, and publish copies of my thesis, dissertation, or manuscript in any form or media, now existing or later derived, including access online for teaching, research, and public service purposes.

DocuSigned by:
Nicholas Stevers
DE5BE4A317ED46B... Author Signature

11/29/2024
Date